CASE FILE COPY

NACA TN 3607

NACA TN 3607

NATIONAL ADVISORY COMMITTEE FOR AERONAUTICS

NACA TN 3607

TECHNICAL NOTE 3607

EFFECT OF THICKNESS, CAMBER, AND THICKNESS DISTRIBUTION ON AIRFOIL CHARACTERISTICS AT MACH NUMBERS UP TO 1.0

By Bernard N. Daley and Richard S. Dick

Langley Aeronautical Laboratory
Langley Field, Va.

Washington
March 1956

REPRODUCED BY
NATIONAL TECHNICAL
INFORMATION SERVICE
U. S. DEPARTMENT OF COMMERCE
SPRINGFIELD, VA. 22161

77

NOTICE

THIS DOCUMENT HAS BEEN REPRODUCED FROM THE BEST COPY FURNISHED US BY THE SPONSORING AGENCY. ALTHOUGH IT IS RECOGNIZED THAT CERTAIN PORTIONS ARE ILLEGIBLE, IT IS BEING RELEASED IN THE INTEREST OF MAKING AVAILABLE AS MUCH INFORMATION AS POSSIBLE.

NATIONAL ADVISORY COMMITTEE FOR AERONAUTICS

TECHNICAL NOTE 3607

EFFECT OF THICKNESS, CAMBER, AND THICKNESS DISTRIBUTION ON AIRFOIL CHARACTERISTICS AT MACH NUMBERS UP TO 1.0[1]

By Bernard N. Daley and Richard S. Dick

SUMMARY

Tests of a group of related NACA airfoil sections varying in maximum thickness, design lift coefficient, and thickness distribution have been conducted in a two-dimensional open-throat type of wind tunnel at Mach numbers of 0.3 to about 1.0 and at corresponding Reynolds numbers from 0.7×10^6 to 1.6×10^6. Normal-force, drag, and pitching-moment coefficients are presented, together with representative schlieren photographs and pressure-distribution diagrams.

The results of these tests indicate that at near-sonic speeds the maximum ratio of the normal force to drag $\left((n/d)_{max}\right)$ approaches the low values theoretically determined for a biconvex airfoil in supersonic flow; contrary to low-speed results the $(n/d)_{max}$ increased as either the thickness ratio or the camber was decreased. At all Mach numbers the normal-force coefficient for $(n/d)_{max}$ generally increased with increases in thickness ratio and camber and with forward movement of the position of maximum thickness. The trends of the data in the highest Mach number range indicated that the normal-force-curve slopes of all airfoils tested are approximately equal at Mach number 1.0, the value being about the same as at low speeds.

INTRODUCTION

Designers of aircraft and aircraft propellers have repeatedly expressed the need for airfoil-section data in the transonic speed range. Almost all section data in the subsonic speed range have been obtained from closed-throat tunnels which inherently limit the speed range of the tests to Mach numbers less than the choking value, generally about 0.9. Airfoil force characteristics measured at Mach numbers near the choking value are influenced an undetermined amount by the flow distortion associated with this choking limitation. Furthermore,

---

[1]Supersedes recently declassified NACA Research Memorandum L52G31a by Bernard N. Daley and Richard S. Dick, 1952.

the correction applied to the closed-throat data for the effect of the tunnel boundary is fundamentally a low-speed correction which has been extended to high-speed conditions by the Prandtl-Glauert factor. Since this factor is strictly applicable only at subcritical Mach numbers, the applicability of the correction at higher Mach numbers is questionable.

One method of extending the subsonic speed range of two-dimensional experimental tests is the utilization of the open-jet principal to eliminate the choking limitations. This scheme permits the streamlines around the model to curve somewhat more than in purely two-dimensional flow and presents some difficulty in measurement of the stream Mach number, but the only large correction required for the data is applicable to the angle of attack. This correction is theoretically defined only at low speeds; but, since all the force characteristics of an airfoil can be obtained simultaneously at the same effective or nominal angle of attack, the lack of the correction should affect only those data in which angle of attack is used as a variable or as a parameter. Although the use of the open-jet principle is subject to these disadvantages, its use appeared to be a logical first step toward the attainment of experimental data near Mach number 1.0. The flow boundaries in the Langley rectangular high-speed tunnel were therefore extensively revised to produce a two-dimensional open-throat-type tunnel, now designated as the Langley 4- by 19-inch semiopen tunnel. This method was used by Ferri (ref. 1) in obtaining airfoil data at Mach numbers up to 0.94 and Reynolds numbers up to 4.2×10^5.

In the present investigation, a group of related airfoil sections varying in maximum thickness, camber, and thickness distribution were tested for the purpose of determining the effects of these variables on the flow and force characteristics of airfoils at Mach numbers up to 1.0 and at Reynolds numbers up to 1.6×10^6. The results of these tests are presented herein. When the results of high-speed airfoil tests in a semiopen tunnel such as the Langley 4- by 19-inch semiopen tunnel or the tunnel used in reference 1 are compared with airfoil data from closed-throat tunnels, certain characteristic discrepancies are noted. In particular, the airfoil force coefficients at supercritical speeds tend to change more rapidly with Mach number in a closed-throat tunnel. It is unfortunately impossible at present to determine definitely which type of tunnel produces the more nearly correct results. Comparisons of the present results with transonic airfoil data derived from transonic wing tests in free air and in a large slotted tunnel are included in this report, and these comparisons lend support to the validity of the present data. However, until more conclusive evidence becomes available, all high-speed airfoil data should be used with some caution.

SYMBOLS

A	aspect ratio of wing
c	airfoil chord
c_d	section drag coefficient
c_{d_o}	section drag coefficient at zero lift
c_m	section pitching-moment coefficient, about quarter chord
c_n	section normal-force coefficient
c_{l_i}	design section lift coefficient (incompressible)
c_{n_α}	section normal-force-curve slope, uncorrected, $\partial c_n / \partial \alpha_{test}$
h	test-section height
H	test-section total pressure
M	test-section Mach number (determined from a calibration using the average pressure in the chambers above and below the model as a reference)
M_{dr}	test-section Mach number at drag rise $\left(\frac{dc_d}{dM} = 0.1\right)$
M_{fb}	test-section Mach number at force break $\left(\frac{dc_n}{dM} = 0\right)$
M_l	local Mach number
n/d	section normal-force—drag ratio
$(n/d)_{max}$	maximum section normal-force—drag ratio
P	pressure coefficient, $\frac{p_l - p}{q}$
P_c	critical pressure coefficient, $\frac{0.528H - p}{q}$

p	test-section static pressure
p_l	local static pressure
p_{ref}	static pressure used as reference for calibration
q	test-section dynamic pressure
R	Reynolds number, based on 4-inch chord
t	airfoil maximum thickness
x_{cp}	location of center of pressure, chords behind leading edge
α_{test}	section angle of attack, uncorrected
α_c	section angle of attack, corrected for jet deflection (as calculated for incompressible flow)

APPARATUS AND TESTS

Wind Tunnel

General description.- The tests were conducted in the Langley 4- by 19-inch semiopen tunnel, an induction tunnel which is shown in figure 1. The parallel plates or side walls form fixed boundaries to the flow in the plane of figure 1(b). The test section of the tunnel is sealed from the atmosphere, but the flow over the top and bottom of the test section is not restrained by fixed boundaries. An external duct connects the upper with the lower chamber. For two-dimensional models this arrangement results in an essentially open-throat tunnel which is not subject to the usual choking limitations of a closed-throat tunnel. An adjustable choking device, which controlled the tunnel mass flow by varying the minimum area of the stream, was installed in the exit cone. Since the power available was always sufficient to maintain the speed of sound at the minimum area of the stream, the choking device stabilized the flow and was used to fix the test-section Mach number at any desired value from 0.3 to about 1.0. Reynolds numbers up to about 1.6×10^6 were obtained.

Mach number distributions in tunnel.- Figure 2 shows that the Mach number is reasonably uniform across the 19-inch dimension of the tunnel. Uniform longitudinal Mach number distributions, however, are more difficult to obtain. Figure 3(a) shows that the Mach number variation along the test region in the empty tunnel varies up to ±2.5 percent of the free-stream Mach number.

The effect of the model on the flow in the tunnel is also shown in figure 3. (In this figure the local Mach number at the 24-inch station is the same with or without the model installed.) The model restrains the flow along the tunnel longitudinal axis and greatly reduces the maximum Mach number obtainable within the region bounded by the nozzle blocks (fig. 3(a)) and along the edges of the jet (fig. 3(b)). In the regions above or below the model location and near the edges of the open jet, the distributions without model are relatively flat.

Calibrations.- Calibrations of the tunnel velocity were obtained (fig. 4) by using as references the average pressure in the chambers above and below the model; also, as a separate calibration, the pressure at the 24-inch station was used (fig. 4). The upstream orifice (24-inch station) provides no indication of the expansion existing at the lips of the nozzle (with the model in place). Therefore, the maximum Mach number indicated by this method is low. (See fig. 3(a).) The calibration based on the average chamber pressure includes the effect of expansion near the lips of the nozzle and is more regular and less critical than the one based on the upstream orifice (24-inch station). (See fig. 4.) The average chamber pressure has been used, therefore, as a reference for calibration in this investigation. The stream Mach number, as determined by the pressure in the tunnel chambers, may be influenced by two opposing effects: an increase in velocity due to the model and the decrease in velocity near the lips of the exit cone. The amount by which these effects influence the stream Mach number is not known, but it is not expected to be large.

Exit-cone size.- Exploratory tests were made to determine the effect of exit-cone opening on the tunnel flow. Figure 4 shows that, although the exit-cone opening did not exert a large influence on the tunnel calibration, it did affect the highest obtainable Mach number. When the exit-cone opening was as small as $19\frac{3}{4}$ inches, the highest test Mach number was 0.935. The exit-cone opening required to prevent a reduction in the maximum test Mach number was larger than the opening at the exit of the nozzle $\left(19\frac{1}{4}\text{ in.}\right)$ because of the flow mixing along the 8-inch length of free boundaries. When an airfoil was tested, an additional increase in exit-cone opening was required because of the model wake. Tests with models indicated that a minimum exit-cone opening of $20\frac{3}{4}$ inches was required so that the highest speed range of the tunnel could be utilized. This value has been used for the data in the remainder of this paper.

Jet-boundary effects.- Aerodynamic data from this type of wind tunnel are subject to corrections similar to those of an open jet. References 2 and 3 show that the only important correction to the airfoil forces in an

open jet is the jet deflection or angle-of-attack correction. The Langley 4- by 19-inch semiopen tunnel is a modified open-throat-type wind tunnel, since the exit cone provides some restraint to the jet deflection. The corrected angle of attack (in degrees) for this specific configuration with equal pressures in the chambers above and below the model can be calculated by reference 4 to be $\alpha_c = \alpha_{test} - 1.85c_n$ for incompressible flow. No methods have been devised to extend this correction to Mach numbers near 1.0, but some indication that the magnitude of the correction does not change greatly at high Mach numbers is given under the section "Comparisons With Other Data." For the purpose of consistency, however, all data presented in this paper are uncorrected unless otherwise specified. The values of angle of attack presented herein, therefore, are nominal only. The values of normal-force-curve slope presented herein are also uncorrected and should not be used quantitatively, but they should be qualitatively correct in their variations with airfoil shape parameter, normal-force coefficient, and Mach number. Since all the aerodynamic forces were measured simultaneously at the same effective angle of attack, the validity of all other data presented herein (that is, all data which are presented without reference to angle of attack) and the conclusions drawn should not be affected by neglecting the corrections.

Effect of duct size and humidity.- The tests of all the airfoils were not conducted with external ducts of the same size. An external duct having a minimum area of 5.5 square inches was used for the original tests. After these tests showed that equal pressures in the chambers above and below the model could not be maintained at high angles of attack, the minimum duct area was increased to 52 square inches to insure pressure equalization. Limited investigations to determine the effect of duct size on the aerodynamic characteristics have been made and the results of one of these tests are presented in figure 5. The disagreements shown in this figure between the data of the different duct sizes are the largest found in any of the tests. For this particular comparison, a considerable amount of the difference between the data of the two duct sizes appears to be due to a difference in Mach number and effective angle of attack, but this was not consistently found in other comparisons.

At zero angle of attack (fig. 5), where no flow occurs through the duct and a change in duct size should not affect the airfoil characteristics, differences in drag coefficient may be observed in the Mach number range above the drag rise. It is believed that these differences are due to differences in relative humidity. Evidence was found that condensation shocks in the flow which have the effect of increasing the normal-to-chord extent of the shock loss are possible when the stagnation relative humidity is as low as 25 percent. Since it was not generally possible to test at relative humidities much less than 20 percent, some of the drag coefficients in the highest Mach number range may be

subject to condensation effects. The differences in drag coefficient shown at the higher speeds for all lifting conditions in figure 5 are therefore not necessarily due to the effect of duct size. No evidence was found that the stagnation relative humidity had appreciable effects on the lift and moment coefficients. The duct size used for each airfoil is indicated in the basic data plots where the data are plotted as a function of Mach number. Whenever a comparison of airfoil data is made to show the effects of change of airfoil maximum thickness, design lift coefficient, or thickness distribution, the duct size is the same.

Comparisons with other data.- No other two-dimensional data are available at Mach numbers approaching 1.0 with which to compare the data presented herein; however, an attempt to verify the data from the Langley 4- by 19-inch semiopen tunnel was made at somewhat lower speeds by comparing the data presented herein with those obtained from other two-dimensional facilities. Points of agreement could be found in these comparisons; but simultaneous agreement of all forces was not found, either between the data of the 4- by 19-inch tunnel and those from any other facility or between the data from any two of these other facilities. Comprehensive quantitative comparisons are therefore omitted.

Several figures have been prepared by using the meager available data to provide a qualitative indication of the value of the data presented herein, particularly at the high Mach numbers. The variation of the zero-lift drag with Mach number obtained in the 4- by 19-inch tunnel for several symmetrical airfoils is compared in figure 6 with data obtained by the falling-body method (refs. 5 to 7) and with data from a two-dimensional closed-throat tunnel for which $\frac{c}{h} = 0.133$. (See ref. 8.) NACA 64A-series airfoils having infinite aspect ratio were used in the 4- by 19-inch-tunnel tests, whereas NACA 65-series airfoils having an aspect ratio of 7.6 were used in the falling-body tests and NACA 64-series airfoils having infinite aspect ratio were used in the closed-throat-tunnel tests (shown to the choking Mach number). The drag data from the 4- by 19-inch tunnel are lower than those from the closed-throat tunnel at high Mach numbers. This difference could result from three possible effects: the lack of sufficient restraint to the flow along the free boundaries of the open tunnel, the influence of the choking limitations in the closed-throat tunnel, and the questionable nature of the closed-throat-tunnel corrections at high Mach numbers. The drag data from the 4- by 19-inch tunnel are higher than those obtained by the falling-body method. At a Mach number beyond the drag rise, the Mach number increment between the drag curves of the NACA 65_1-012 wing ($A = 7.6$) tested by the falling-body method and the NACA 64A012 airfoil ($A = \infty$) tested in the 4- by 19-inch tunnel is approximately the same as that which would be expected for this change in aspect ratio from the results of reference 9; for airfoils of lesser thickness, this increment decreases, as would be expected. Since the data of references 5 to 7 should correspond closely

to conditions of unrestrained flow, it appears, therefore, that the variation of drag coefficient with Mach number as obtained in the Langley 4- by 19-inch semiopen tunnel is approximately correct.

Chordwise pressure distributions have been obtained at various spanwise stations on the wing of the X-1 airplane in flight tests conducted at the NACA High-Speed Flight Station at Edwards, Calif., and on a $\frac{1}{4}$-scale model of the X-1 airplane in the Langley 16-foot transonic tunnel. These data for spanwise stations 49 or 64 percent of the semispan from airplane center line are compared at equal lift coefficients (fig. 7) and excellent agreement is obtained. For purposes of comparison with these data, the same airfoil section, the NACA 65-110, was tested in the Langley 4- by 19-inch semiopen tunnel. The angle of attack of the 4- by 19-inch-tunnel data (for figs. 7 and 8 only) has been corrected for jet deflection (as calculated for incompressible flow) and is compared with 16-foot-tunnel data (uncorrected for downwash) at corresponding angles of attack. Although a comparison of two- and three-dimensional data at high subsonic Mach numbers is complicated by unknown effects of tip relief and fuselage velocity field, some significant points can be observed. The pressure distributions from the two sources (fig. 7) are in good agreement over the forward portion of the profile at all Mach numbers. This similarity of the forward portions of the pressure distributions provides an indication that the calculated incompressible correction to angle of attack is of the proper order at these Mach numbers. At Mach numbers of 0.85 and 0.90, the pressure distributions over the rear of the airfoil are similar for both tests, except that the rapid pressure rises associated with the shock phenomenon on the upper and lower surfaces are somewhat more rearward on the wing than on the airfoil and it appears that little or no separation occurs on the wing forward of the shock wave. These differences are magnified as the Mach number is increased from 0.90 to 0.95, in which range the data for the three-dimensional case are very sensitive to changes in Mach number. These differences may be the result of three-dimensional effects or differences in Reynolds number, that of the 16-foot-tunnel tests being approximately three times those of the present tests. At a Mach number of 1.0, good agreement between the two- and three-dimensional data is observed, the shock wave being near the trailing edge for both configurations.

A similar comparison for normal-force and pitching-moment coefficients is presented in figure 8. Good agreement is shown between the 16-foot-tunnel data and the 4- by 19-inch-tunnel data up to a Mach number of 0.90. At somewhat higher Mach numbers the three-dimensional data indicate larger normal-force coefficients and more negative moment coefficients than the two-dimensional data. At $M = 1.0$, the two-dimensional force data are again in good agreement with the three-dimensional data. Although the differences shown at Mach numbers of 0.925 and 0.95 appear

to be due to a difference in indicated Mach number, it should not be concluded that a Mach number error exists in either group of data because of the possible large influences of fuselage shock, tip relief, and Reynolds number on the wing pressure distribution in this speed range.

Models

Aerodynamic data for airfoils are presented herein to show the following effects:

Thickness	Camber	Thickness distribution
NACA 64A004	NACA 64A006	NACA 63A009
NACA 64A006	NACA 64A206	NACA 64A009
NACA 64A009	NACA 64A506	NACA 65A009
NACA 64A012		NACA 16-009

Ordinates for these airfoils are given in table I and a comparison of the profiles is made in figure 9. (See ref. 10 for the development of the 6A-series airfoils.) All models had 4-inch chords and completely spanned the 4-inch dimension of the tunnel. Static-pressure orifices having diameters of 0.0135 inch were drilled normal to the surface near the mid-span station at chordwise locations shown in figure 9.

Tests

All static-pressure orifices were connected to a recording manometer so that the distribution of pressures could be obtained. Normal-force and pitching-moment coefficients for some of the airfoils were obtained with the NACA electrical pressure integrator (model B) connected to the same pressure orifices. (See ref. 11 for description of this instrument.) Corresponding data for the other airfoils were computed directly from manometer records of the airfoil-surface pressures. Drag coefficients were computed by the method of reference 12, with the pressures measured in a total-pressure survey downstream of the model. The angle-of-attack range for most airfoils extended from the angle corresponding to zero lift to 8°. For some of the airfoils, normal-force and moment data were obtained at angles of attack of 10° and 12°. Tests were conducted through a Mach number range from 0.30 to approximately 1.00, with a corresponding Reynolds number range from 0.7×10^{6} to 1.6×10^{6}.

PRESENTATION OF RESULTS

The basic force characteristics of all airfoils tested are presented as a function of Mach number in figure 10 by using uncorrected angle of attack, α_{test}, as a parameter (see section entitled "Jet-Boundary Effects"). These data are analyzed with reference to normal-force coefficient in figures 11 to 13, drag coefficient in figures 14 to 17, moment coefficient in figures 18 to 22, the transonic similarity rules in figure 23, and flow characteristics in figures 24 to 26.

Several of the figures have been presented in the form of a modified "carpet." For the carpets in figures 11, 14, 19, and 21, the scales for α_{test}, c_d, c_m, and x_{cp}, respectively, are correctly oriented only for that Mach number specified in the scale identification. For any other Mach number presented, these scales must be shifted so that the zero for the scale is on the coordinate which is labeled with the selected Mach number.

DISCUSSION

Normal-Force Coefficient

Normal-force-coefficient data for each of the airfoils are shown in figures 10 and 11. In order to facilitate the analysis of these data, the normal-force-curve slope $\left(c_{n_\alpha}\right)$ is plotted as a function of Mach number in figure 12 for several values of normal-force coefficient. As previously discussed, the values of angle of attack of these data have not been corrected for jet deflection. The omission of this correction causes the values of normal-force-curve slope presented to be too low, but these values should be qualitatively correct in their variations with airfoil shape parameter, normal-force coefficient, and Mach number.

The effect of change in airfoil-thickness ratio on c_{n_α} is illustrated in figure 12. At the lower speeds c_{n_α} does not appear to be affected by change in airfoil thickness or normal-force coefficient. As the Mach number is increased, c_{n_α} of all the airfoils increases. The peak value of c_{n_α} and the Mach number corresponding to the peak value are progressively higher as the airfoil thickness decreases. In addition, the Mach number range through which the values of c_{n_α} for the thin airfoils are higher than those of the thick airfoils increases as the normal-force coefficient increases. The values of c_{n_α} at high Mach numbers for all of the airfoils generally increased as the normal-force coefficient increased; this was particularly noticeable for the 12-percent-thick airfoil, which exhibited a large loss in c_{n_α} at zero lift.

An increase in design lift coefficient causes an increase in the normal-force coefficient attained at zero angle of attack for all Mach numbers (fig. 11(b)). The normal-force coefficient attained at $\alpha_{test} = 0^{\circ}$ increases with Mach number up to $M = 0.9$ for $c_{l_i} = 0.2$ or to $M = 0.8$ for $c_{l_i} = 0.5$, and decreases progressively with further increase in Mach number (figs. 10(d), 10(e), 10(f), and 11(b)). The effect of change in airfoil design lift coefficient on c_{n_α} (fig. 12) is irregular at low Mach numbers, probably because of the curvature of the normal-force curves of the NACA 64A206 airfoil (fig. 11(b)). In the Mach number range near 0.87, the airfoil having the highest camber produced the lowest value of c_{n_α}, but at Mach numbers of 0.95 and above the airfoil having the highest camber produced the highest value of c_{n_α}.

The effect of change in airfoil thickness distribution on c_{n_α} is shown in figure 12. Except for localized differences at Mach numbers from 0.90 to 0.95, there appears to be little systematic variation of c_{n_α} with normal-force coefficient or thickness distribution for the 6A-series airfoils. Where differences can be observed in the low-speed range, however, the 65A airfoil generally has the lowest values of c_{n_α}. The 16-series airfoil has a lower value of c_{n_α} than the 6A-series airfoils, except at the highest Mach numbers or at the highest normal-force-coefficients. At low normal-force coefficients the change in c_{n_α} through the Mach number range is less for the 16-series airfoil than for the 6A-series airfoils, but at a normal-force coefficient of 0.4 there is little difference between the data of the various airfoils.

The trends in c_{n_α} in the highest Mach number range indicate that the values of c_{n_α} of all airfoils tested will be essentially equal at a Mach number of 1.0, the value being about the same as at low speeds and only slightly affected by normal-force coefficient (fig. 12). At high Mach numbers the effect on c_{n_α} produced by the change in airfoil thickness was the largest of any profile parameter within the ranges investigated, and the change in thickness distribution produced the smallest effect.

The Mach number for normal-force break (fig. 13) generally decreases with increase in normal-force coefficient. At any particular normal-force coefficient, an increase in airfoil thickness or design lift coefficient decreases the Mach number for normal-force break, whereas thickness distribution has little effect.

Drag Coefficient

Drag-coefficient data obtained by the wake-survey method are presented in figures 10 and 14 for the various airfoils. The velocity field of the model extends approximately to the tunnel boundary at the highest Mach number presented; but, since the local Mach numbers experienced at the tunnel boundary never exceed 1.05 for any data presented herein, very little shock loss is experienced in this region and the effect on the drag coefficients is negligible. (The irregularities observed in the data for the 64A506 airfoil at Mach numbers above 0.9 are believed to be the result of condensation shocks.) The omission of the angle-of-attack correction due to jet deflection (previously discussed) does not influence the data presented in this section since angle of attack is not used as a parameter or variable.

Figures 15 and 16 illustrate the effects of change in airfoil section, normal-force coefficient, and Mach number on n/d. Figures 15(a) and 16 show that $(n/d)_{max}$ and the c_n at $(n/d)_{max}$ increase as the thickness ratio increases for Mach numbers of 0.75 and lower; the thicker airfoils maintain their superiority at the highest normal-force coefficients investigated (fig. 15(a)), but at low normal-force coefficients little difference can be noted between the n/d values for airfoils of different thicknesses. Throughout the normal-force-coefficient range, the values of n/d undergo a reduction at some Mach number above 0.70; the Mach number at which this reduction in n/d occurs increases as the airfoil thickness decreases. At Mach numbers of 0.9 and above, n/d at any normal-force coefficient increases as the thickness ratio decreases.

For the cambered airfoils (figs. 15(b) and 16), $(n/d)_{max}$ and the c_n for $(n/d)_{max}$ increase with design lift coefficient at Mach numbers up to about 0.75, the c_n for $(n/d)_{max}$ being always somewhat greater than the design lift coefficient. In this speed range the NACA 64A206 airfoil generally had the highest value of n/d at low normal-force coefficients (fig. 15(b)), but at higher normal-force coefficients the NACA 64A506 airfoil had the highest n/d. These effects of changes in design lift coefficient on n/d in this speed range are in agreement with those pointed out in reference 13. A decrease in $(n/d)_{max}$ occurs for all airfoils at some Mach number above 0.70, the largest decrease occurring for the airfoil having the highest design lift coefficient $\left(c_{l_i} = 0.5\right)$. At Mach numbers of about 0.85 and above, the NACA 64A506 airfoil has a lower value of n/d than those airfoils having less camber, this undesirable feature occurring throughout the normal-force-coefficient range investigated.

At Mach numbers less than 0.75, the effect of change in thickness distribution on the 6A-series airfoils (figs. 15(c) and 16) was to reduce progressively $(n/d)_{max}$ and the c_n for $(n/d)_{max}$ as the location of maximum thickness was moved rearward. The differences between the values of n/d for the airfoils of this series, however, are generally not large over the whole normal-force-coefficient range (fig. 15(c)). The values of n/d at moderate normal-force coefficients, of $(n/d)_{max}$, and of c_n for $(n/d)_{max}$ were generally lower for the 16-series airfoils than for the 6A-series airfoils at Mach numbers less than 0.80. At higher Mach numbers, all airfoils indicate a rapid decrease in the value of n/d as the Mach number increases. This decrease occurs at $M \approx 0.85$ for the 16-series airfoil and at $M \approx 0.80$ for the 6A-series airfoils and thus causes the 16-series airfoil to have the higher values of n/d in the Mach number range near 0.85. At Mach numbers above 0.90, thickness distribution has little effect on n/d.

Generally, the effect on n/d produced by the change in airfoil thickness or design lift coefficient (within the range of airfoil parameters investigated) was much larger than that produced by the change in thickness distribution. At high Mach numbers, $(n/d)_{max}$ generally increases with a decrease in thickness and design lift coefficient (a reversal of the low-speed results) and decreases rapidly with increasing Mach number. The values of $(n/d)_{max}$ for the airfoils at $M \approx 0.97$ closely approach the theoretical values for a biconvex airfoil in supersonic flow computed by the method of reference 14 (fig. 15(d)). At Mach numbers somewhat greater than 0.8, the c_n for $(n/d)_{max}$ for all airfoils tested increases with Mach number (fig. 16). The c_n for $(n/d)_{max}$ increases with airfoil thickness, design lift coefficient, and with forward movement of the location of maximum thickness at all Mach numbers. This increase in c_n for $(n/d)_{max}$ is associated primarily with a reduction of the rate of change of c_d with c_n (fig. 14), rather than with an increase in the zero-lift-drag coefficient.

A related effect is shown in figure 14(a) in which the dotted lines indicate $c_{d_o} + c_n \sin \alpha$, where $c_n \sin \alpha$ is drag coefficient due to lift when the resultant of the lift component and the drag due to lift component is assumed to be normal to the chord; in this figure a horizontal line originating at the drag coefficient for zero lift indicates the drag when this resultant is normal to stream direction (drag due to lift equals zero, as predicted by potential-flow theory). These conditions have been referred to as zero leading-edge suction and full leading-edge suction, respectively, but for supercritical flows the change in pressure over the rear part of an airfoil that occurs with change in lift coefficient can have a stronger effect on drag due to

lift than changes in the suction forces near the leading edge. In the lower c_n range, an increase in Mach number increases the measured drag increment due to lift except at the highest Mach numbers on the thick airfoils. A decrease in airfoil thickness also increases the drag increment due to lift (in the lower c_n range) except at Mach numbers between 0.85 and 0.95. An analysis has shown that the conditions which bring about these variations are very complex because of the unpredictable nature of the flow when shock and separation are present.

The drag-rise Mach number of the various airfoils is presented in figure 17. This parameter is presented and discussed only in the normal-force-coefficient range where low values of the low-speed-drag coefficient are obtained and the significance of the drag-rise Mach number as an indication of airfoil performance is not impaired by flow separation. The highest drag-rise Mach number occurred at zero lift for the symmetrical airfoils, as expected, and at normal-force coefficients approaching the design value for the cambered airfoils. The maximum drag-rise Mach number increased with a decrease in thickness and design lift coefficient but was little influenced by changes in location of maximum thickness of the 6A-series airfoils. The 16-009 airfoil had higher values of the drag-rise Mach number than the 6A-series airfoils of comparable thickness throughout the normal-force-coefficient range.

Moment Coefficient

The basic data in figure 10 have been cross-plotted in figure 18 to show the effect of Mach number on c_m for the various airfoils at several normal-force coefficients. The omission of the angle-of-attack correction due to jet deflection (previously discussed) does not influence the data presented in this section since angle of attack is not used as a parameter or variable. The effect of increase in c_n for symmetrical airfoils from zero to some positive value is to cause large variations in the moment coefficient to occur at high Mach numbers (fig. 18). With the exception of the 16-009 airfoil, the effect of increasing the normal-force coefficient from 0.2 to 0.4 is small.

Little effect of thickness on the moment coefficient is observed for lifting conditions at Mach numbers less than 0.8. Above this speed, the thickest airfoil experiences a rapid increase in climbing moment, followed by an equally rapid decrease, while the thinnest airfoil experiences only an increase in diving moment, which is less rapid and occurs at a somewhat higher Mach number than on the thick airfoil. For intermediate thicknesses the moment trends experienced with change in Mach number tend to fall somewhere between these two extremes. This change in variation of c_m with Mach number is caused by the differences in flow over the rear portion of airfoils of different thicknesses;

as will be pointed out later, the thick airfoils experience reversals in loading over the rear portion, while the thin airfoils have relatively high loadings near the trailing edge. The effect of increasing the design lift coefficient of the 6-percent-thick airfoils was to cause a negative shift in moment coefficient without greatly affecting the trends with Mach number. Changes in the thickness distribution had little effect on the 6A-series airfoils, but changing the profile to the 16-series airfoil eliminated the abrupt pitch-up tendency at high Mach numbers and changed the character of the curve throughout the Mach number range investigated.

Most airfoils tested were neutrally stable or slightly unstable in the lower Mach number range (figs. 19 and 20), the NACA 16-series airfoil being most unstable. Except for the thicker airfoils near zero lift, all airfoils tested become stable in the higher speed range. Large changes in the stability parameter $\partial c_m/\partial c_n$ are observed, however, at these higher Mach numbers. Because of the large abrupt changes in c_n and c_m with Mach number in this speed range, it is often difficult to define exactly the stability parameter.

Although the stability parameter is erratic in its variations, the chordwise location of the center of pressure (x_{cp}) behaves in a more regular fashion (figs. 21 and 22). All of the 6A-series airfoils showed an initial rearward shift in x_{cp} with Mach number at Mach numbers around 0.8 to 0.9. This rearward shift with Mach number is continued to the highest speeds tested for the 4-percent-thick airfoil and is little affected by changes in normal-force coefficient. For the thicker sections, however, this initial rearward shift is followed by a forward shift and for the thickest airfoils an additional reversal occurs which returns x_{cp} to approximately its low-speed value. These variations in x_{cp} for the thickest airfoils are reduced as the normal-force coefficient is increased. An increase in design lift coefficient resulted in a rearward shift of x_{cp}, as expected. A rearward shift was also caused by increasing the Mach number for these 6-percent-thick cambered airfoils. The effect of an increase in normal-force coefficient was to produce a forward shift in x_{cp}, which would be expected at low speeds, and this forward shift was found to occur throughout the Mach number range. The effect of change in thickness distribution on x_{cp} was small for the 6A-series airfoils. The 16-series airfoil produced a somewhat more desirable variation of x_{cp} with Mach number, but the total change in x_{cp} through the Mach number range did not decrease with normal-force coefficient, as was the case for the 6A-series airfoils.

Correlations Made by the Transonic Similarity Law

The transonic similarity rules provide a method of correlating data from thin airfoils at Mach numbers near 1.0 in such a manner that any particular force or moment component for all airfoils of a family may be defined in two-dimensional flows by a single curve. Thus, if data from one profile are available, data for any other airfoil section having the same thickness distribution may be estimated or predicted by this rule, provided the flows are truly similar. A correlation of the experimental data of the 64A-series airfoils varying in thickness is shown in figure 23, based on the transonic similarity parameters presented in reference 15. All these airfoils correlate well on the basis of zero-lift drag coefficient. The correlation of the 4- and 6-percent-thick airfoils on the basis of drag due to lift, normal-force and pitching-moment parameters, is reasonably good at high Mach numbers. The disagreements between these results at lower Mach numbers result from dissimilar flow conditions; the flow over the 4-percent-thick airfoil separates near the leading edge at a very low angle of attack, so that the normal-force coefficient is reduced (see fig. 11(a)); whereas the flow over the 6-percent-thick airfoil remains attached over most of the surface at these low angles. The 9- or 12-percent-thick airfoils do not generally correlate with the thinner airfoils in the high Mach number range, but there is a tendency toward correlation at the highest speed shown. Some of the differences may be due to the application of the similarity rule beyond its limitations but most of the differences shown are probably due to the combination of two effects on the thick airfoils, the separation behind the shock wave over the rear of the upper surface and the rapid decrease in pressure over the lower surface with increase in Mach number; both effects tend to cause the normal-force coefficient to decrease and the moment coefficient to break in the positive direction for thick airfoils.

Flow Characteristics

The schlieren photographs and pressure distributions shown in figures 24 to 26 are representative of the flow conditions over the airfoils investigated. The pressure distributions over the airfoil surface are superimposed on the schlieren photographs so that the airfoil chord line identifies the $P = 0$ axis. The solid line represents the upper-surface distribution and the dashed line represents the lower-surface distribution. In general, the flow changes in the near-sonic speed range are similar to those frequently observed in a lower supercritical speed range; that is, the effect of increase in Mach number is to increase the local pressure over the fore part of the upper surface and cause the shock waves on both airfoil surfaces to move consistently rearward with a resulting decrease in the local pressures over the rear part of the airfoil.

For lifting conditions, the separation which occurs over the upper surface of the symmetrical airfoils at high speeds (parts (b) and (c) of figs. 24 and 26) is generally much more severe for the thicker airfoils than for the thin airfoils. This separation tends to increase the local pressure over the rear part of the upper surface. The flow generally remains attached on the lower surface, however, and produces low pressures over the lower surface near the rear part of the model and a consequent reversal in airfoil loading near the trailing edge. This reversal is particularly noticeable for the NACA 16-009 airfoil (parts (b) and (c) of fig. 26) and the NACA 64A012 airfoil (fig. 24(b)).

Two widely separated shock waves of three types are frequently observed simultaneously on the lower surface of cambered airfoils at low angles of attack (figs. 25(a) and 25(b)). Each of these separate shocks is similar in nature to shocks observed on symmetrical airfoils; they are unusual primarily in that they occur in combination on the cambered airfoils. The shock located at the leading edge (lower surface) of the highly cambered airfoil occurs because the upwash (near the leading edge) at high Mach numbers is much less than at low speeds. The leading edge of the airfoil is then effectively at a negative angle of attack and the leading-edge-flow conditions are similar to those discussed in reference 16. The lower-surface shock near the midchord of the moderately cambered airfoil appears to be associated with the basic curvature of the surface itself, since increasing the design lift coefficient eliminates this phenomenon. The third type of shock which may occur in combination with another shock is located at the trailing edge and is frequently preceded by an expansion (indicated by a dark region on the schlieren photographs). This trailing-edge expansion followed by a shock wave has been observed at supersonic speeds (ref. 17) and was attributed to a pressure difference between the upper and lower surfaces near the trailing edge which caused a turning of the flow around the trailing edge until its direction is upward relative to the free stream, followed by a deflection to the free-stream direction through a shock upon meeting the flow from the upper surface. This trailing-edge expansion with the subsequent shock was observed also at Mach numbers approaching unity on symmetrical airfoils under lifting conditions (parts (c) of figs. 24 and 26) and in some of these cases little difference in pressure coefficient between the upper and lower surfaces was indicated. This phenomenon was particularly noticeable, however, on the cambered airfoils (fig. 25), where large differences in pressure exist between the upper and lower surfaces near the trailing edge.

Large variations in the shock angle are observed at $M = 1.0$ for the various airfoils at low angles of attack, as illustrated in fig. 24(a). These variations follow the trends expected from supersonic theory, which predicts that the shock angle would be a function of the local Mach number ahead of the shock and the effective turning angle of the flow into a corner at the trailing edge. Separation of the flow, however, prohibits a more detailed analysis of this phenomenon.

CONCLUDING REMARKS

Tests of a group of related NACA airfoils, varying in thickness (64A004, 64A006, 64A009, 64A012), design lift coefficient (64A006, 64A206, 64A506), and thickness distribution (63A009, 64A009, 65A009, 16-009), have been conducted in a two-dimensional open-throat-type wind tunnel at Mach numbers from 0.3 to about 1.0 and at corresponding Reynolds numbers from 0.7×10^6 to 1.6×10^6. The angle-of-attack range of the tests extended from that for zero lift to about 10°. The only appreciable correction to these data is believed to be a jet-deflection correction to angle of attack which has not been determined for the high Mach number range. This correction, therefore, has not been applied to the data presented, but its omission is not expected to alter the following conclusions:

1. The trends of the data in the highest Mach number range indicated that the normal-force-curve slopes of all airfoils tested will be approximately equal at Mach number 1.0, the value being about the same as at low speeds and only slightly affected by normal-force coefficient.

2. At near-sonic speeds, the maximum ratio of normal force to drag approaches the low values theoretically determined for a biconvex airfoil in supersonic flows, and, in a direct reversal of the low-speed results, increases with a decrease in airfoil-thickness ratio and design lift coefficient.

3. At all Mach numbers the normal-force coefficient for maximum ratio of normal force to drag generally increases with airfoil thickness, with design lift coefficient, and with forward movement of the location of maximum thickness.

4. Except for the thicker airfoils near zero lift, all airfoils tested become stable in the higher speed range with respect to a moment center at the quarter-chord point.

Langley Aeronautical Laboratory,
National Advisory Committee for Aeronautics,
Langley Field, Va., July 31, 1952.

REFERENCES

1. Ferri, Antonio: Completed Tabulation in the United States of Tests of 24 Airfoils at High Mach Numbers (Derived From Interrupted Work at Guidonia, Italy, in the 1.31- by 1.74-Foot High-Speed Tunnel). NACA WR L-143, 1945. (Formerly NACA ACR L5E21.)

2. Goldstein, S., and Young, A. D.: The Linear Perturbation Theory of Compressible Flow, With Applications to Wind-Tunnel Interference. R. & M. No. 1909, British A.R.C., 1943.

3. Glauert, H.: Wind Tunnel Interference on Wings, Bodies and Airscrews. R. & M. No. 1566, British A.R.C., 1933.

4. Katzoff, S., Gardner, Clifford S., Diesendruck, Leo, and Eisenstadt, Bertram J.: Linear Theory of Boundary Effects in Open Wind Tunnels With Finite Jet Lengths. NACA Rep. 976, 1950. (Supersedes NACA TN 1826.)

5. Thompson, Jim Rogers, and Marschner, Bernard W.: Comparative Drag Measurements at Transonic Speeds of an NACA 65-006 Airfoil and a Symmetrical Circular-Arc Airfoil. NACA RM L6J30, 1947.

6. Mathews, Charles W., and Thompson, Jim Rogers: Drag Measurements at Transonic Speeds of NACA 65-009 Airfoils Mounted on a Freely Falling Body To Determine the Effects of Sweepback and Aspect Ratio. NACA RM L6K08c, 1947.

7. Thompson, Jim Rogers, and Mathews, Charles W.: Measurements of the Effects of Thickness Ratio and Aspect Ratio on the Drag of Rectangular-Plan-Form Airfoils at Transonic Speeds. NACA RM L7E08, 1947.

8. Wilson, Homer B., Jr., and Horton, Elmer A.: Aerodynamic Characteristics at High and Low Subsonic Mach Numbers of Four NACA 6-Series Airfoil Sections at Angles of Attack From -2° to 31°. NACA RM L53C20, 1953.

9. Stack, John, and Lindsey, W. F.: Characteristics of Low-Aspect-Ratio Wings at Supercritical Mach Numbers. NACA Rep. 922, 1949. (Supersedes NACA TN 1665.)

10. Loftin, Laurence K., Jr.: Theoretical and Experimental Data for a Number of NACA 6A-Series Airfoil Sections. NACA Rep. 903, 1948. (Supersedes NACA TN 1368.)

11. Helfer, Arleigh P.: Electrical Pressure Integrator. NACA TN 2607, 1952.

12. Baals, Donald D., and Mourhess, Mary J.: Numerical Evaluation of the Wake-Survey Equations for Subsonic Flow Including the Effect of Energy Addition. NACA WR L-5, 1945. (Formerly NACA ARR L5H27.)

13. Lindsey, W. F., Stevenson, D. B., and Daley, Bernard N.: Aerodynamic Characteristics of 24 NACA 16-Series Airfoils at Mach Numbers Between 0.3 and 0.8. NACA TN 1546, 1948.

14. Lock, C. N. H.: Examples of the Application of Busemann's Formula To Evaluate the Aerodynamic Force Coefficients on Supersonic Aerofoils. R. & M. No. 2101, British A.R.C., 1944.

15. Harder, Keith C.: Transonic Similarity Rules for Lifting Wings. NACA TN 2724, 1952.

16. Lindsey, W. F., Daley, Bernard N., and Humphreys, Milton D.: The Flow and Force Characteristics of Supersonic Airfoils at High Subsonic Speeds. NACA TN 1211, 1947.

17. Czarnecki, K. R., and Mueller, James N.: Investigation at Mach Number 1.62 of the Pressure Distribution Over a Rectangular Wing With Symmetrical Circular-Arc Section and 30-Percent-Chord Trailing-Edge Flap. NACA RM L9J05, 1950.

TABLE I.- AIRFOIL ORDINATES

[Stations and ordinates given in percent of airfoil chord]

Station	Ordinate for NACA airfoil						
	64A004	64A006	64A009	64A012	63A009	65A009	16-009
0	0	0	0	0	0	0	0
.5	.323	.485	.725	.961	.737	.690	-----
.75	.390	.585	.873	1.158	.887	.837	-----
1.25	.493	.739	1.104	1.464	1.127	1.068	.969
2.50	.678	1.016	1.521	2.018	1.564	1.463	1.354
5.0	.932	1.399	2.095	2.788	2.171	1.965	1.882
7.5	1.122	1.634	2.525	3.364	2.624	2.385	2.274
10.0	1.278	1.919	2.879	3.839	2.990	2.736	2.593
15	1.520	2.283	3.430	4.580	3.552	3.292	3.101
20	1.702	2.557	3.844	5.132	3.956	3.714	3.498
25	1.836	2.757	4.144	5.534	4.240	4.034	3.812
30	1.929	2.896	4.351	5.809	4.419	4.266	4.063
35	1.983	2.977	4.469	5.965	4.495	4.420	-----
40	1.999	2.999	4.497	5.993	4.473	4.495	4.391
45	1.966	2.945	4.408	5.863	4.359	4.486	-----
50	1.889	2.825	4.221	5.605	4.161	4.379	4.500
55	1.776	2.653	3.956	5.244	3.891	4.174	-----
60	1.634	2.438	3.629	4.801	3.560	3.881	4.376
65	1.469	2.188	3.248	4.289	3.177	3.519	-----
70	1.282	1.907	2.825	3.721	2.751	3.099	3.952
75	1.078	1.602	2.371	3.118	2.301	2.631	-----
80	.866	1.285	1.901	2.500	1.845	2.127	3.149
85	.652	.967	1.431	1.882	1.389	1.602	-----
90	.438	.649	.961	1.263	.932	1.075	1.888
95	.223	.331	.490	.644	.475	.547	1.061
100	.008	.013	.018	.025	.019	.020	.090
L.E. radius:	.106	.246	.556	.994	.601	.516	.397
T.E. radius:	.010	.014	.019	.028	.022	.021	-----

NACA 64A206 airfoil			
Upper surface		Lower surface	
Station	Ordinate	Station	Ordinate
0	0	0	0
.454	.539	.546	-.427
.699	.622	.801	-.504
1.192	.858	1.308	-.616
2.432	1.225	2.568	-.803
4.924	1.758	5.076	-1.036
7.421	2.168	7.579	-1.196
9.921	2.513	10.079	-1.321
14.924	3.063	15.076	-1.501
19.931	3.486	20.069	-1.626
24.940	3.807	25.060	-1.705
29.950	4.044	30.050	-1.748
34.961	4.201	35.039	-1.753
39.973	4.278	40.027	-1.720
44.985	4.259	45.015	-1.631
49.997	4.155	50.003	-1.495
55.007	3.979	54.993	-1.327
60.017	3.740	59.983	-1.136
65.026	3.443	64.974	-.933
70.033	3.090	69.967	-.724
75.039	2.682	74.961	-.522
80.046	2.219	79.954	-.349
85.045	1.637	84.955	-.245
90.032	1.138	89.968	-.158
95.016	.576	94.984	-.086
100.000	.013	100.000	-.013

L.E. radius: 0.246
T.E. radius: 0.014
Slope of radius through L.E.: 0.095

NACA 64A506 airfoil			
Upper surface		Lower surface	
Station	Ordinate	Station	Ordinate
0	0	0	0
.388	.613	.612	-.331
.624	.769	.876	-.373
1.107	1.027	1.393	-.423
2.333	1.530	2.667	-.474
4.812	2.288	5.188	-.484
7.304	2.889	7.696	-.457
9.803	3.400	10.197	-.418
14.812	4.227	15.188	-.323
19.828	4.877	20.172	-.225
24.850	5.382	25.150	-.124
29.876	5.764	30.124	-.022
34.903	6.035	35.097	.085
39.932	6.195	40.068	.199
44.962	6.231	45.038	.341
49.991	6.151	50,009	.501
55.019	5.969	54.981	.663
60.043	5.692	59.957	.816
65.064	5.324	64.936	.950
70.082	4.862	69.918	1.052
75.096	4.300	74.904	1.102
80.115	3.617	79.885	1.057
85.113	2.764	84.887	.844
90.079	1.870	89.921	.582
95.040	.942	94.960	.284
100.000	.013	100.000	-.013

L.E. radius: 0.246
T.E. radius: 0.014
Slope of radius through L.E.: 0.238

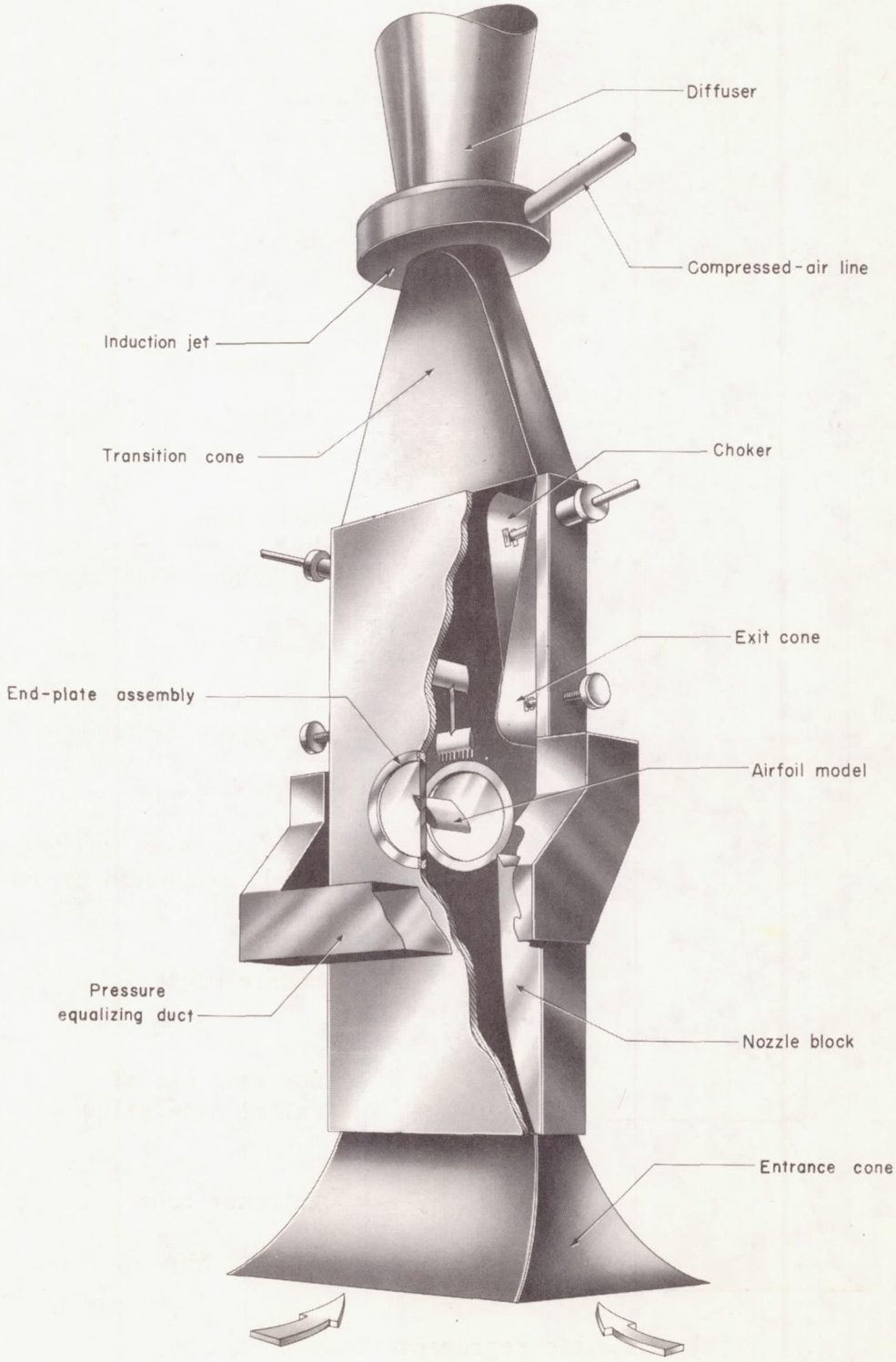

(a) Pictorial representation.

Figure 1.- Langley 4- by 19-inch semiopen tunnel.

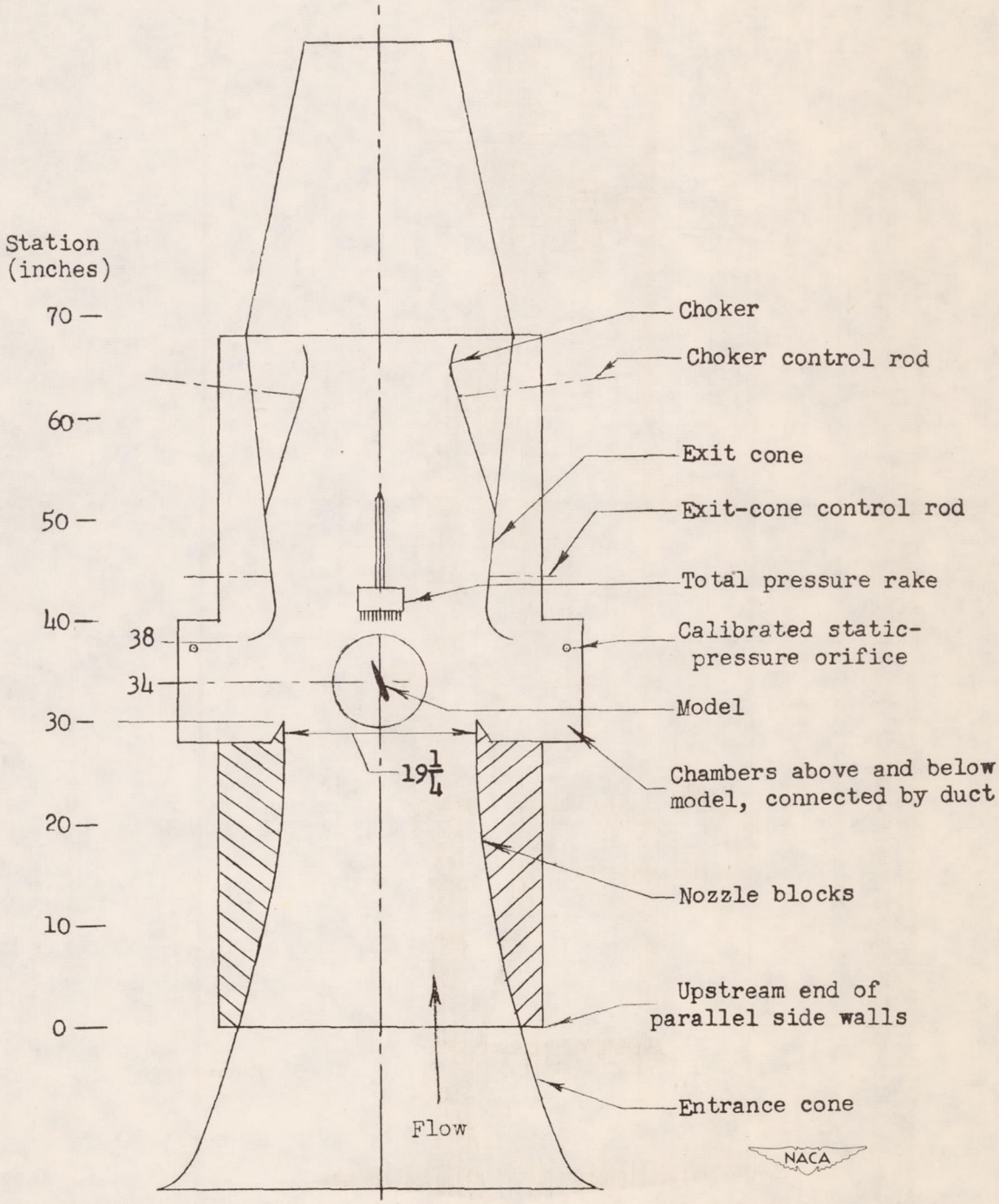

(b) Schematic representation.

Figure 1.- Concluded.

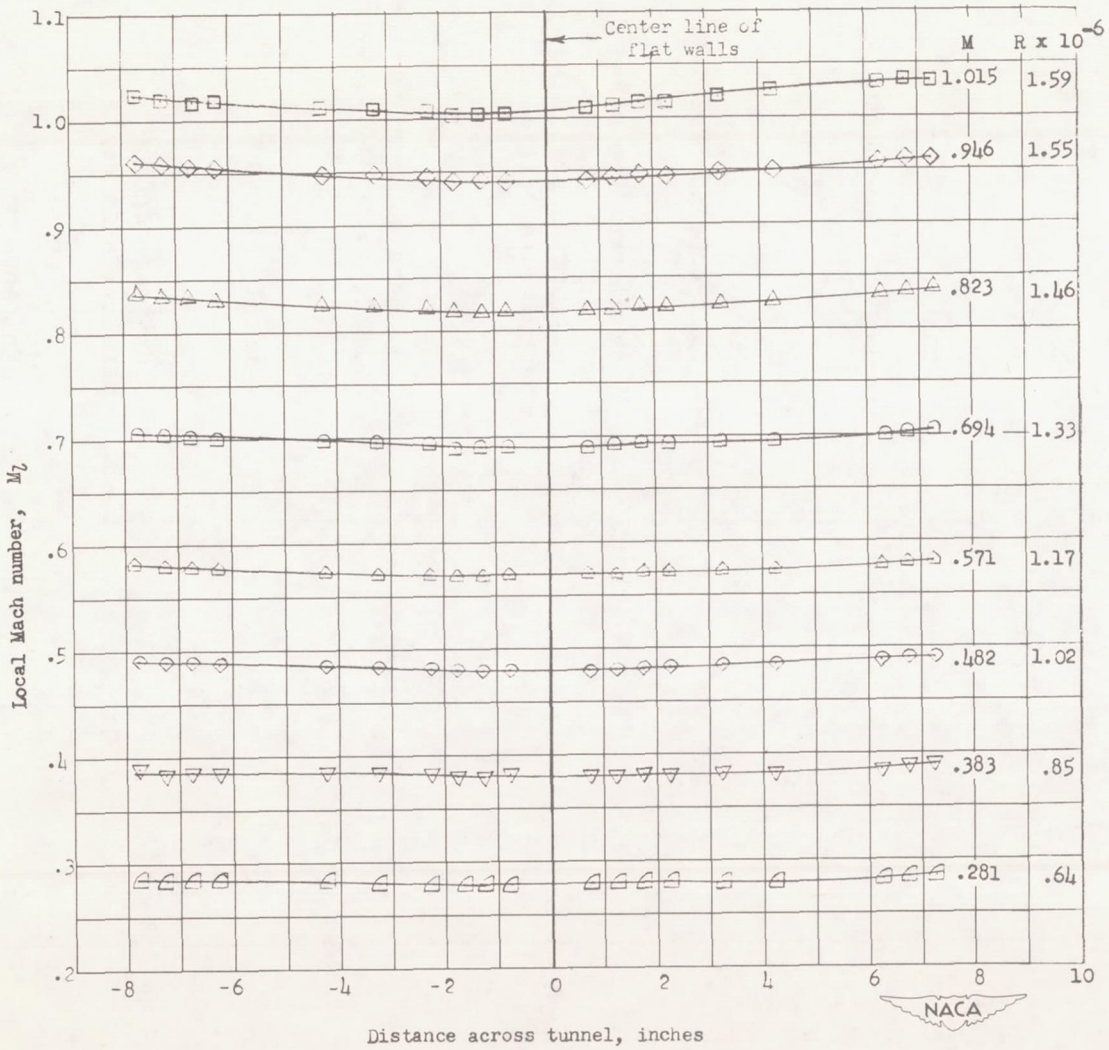

Figure 2.- Representative Mach number distributions across the 19-inch dimension at the 34-inch station of the tunnel.

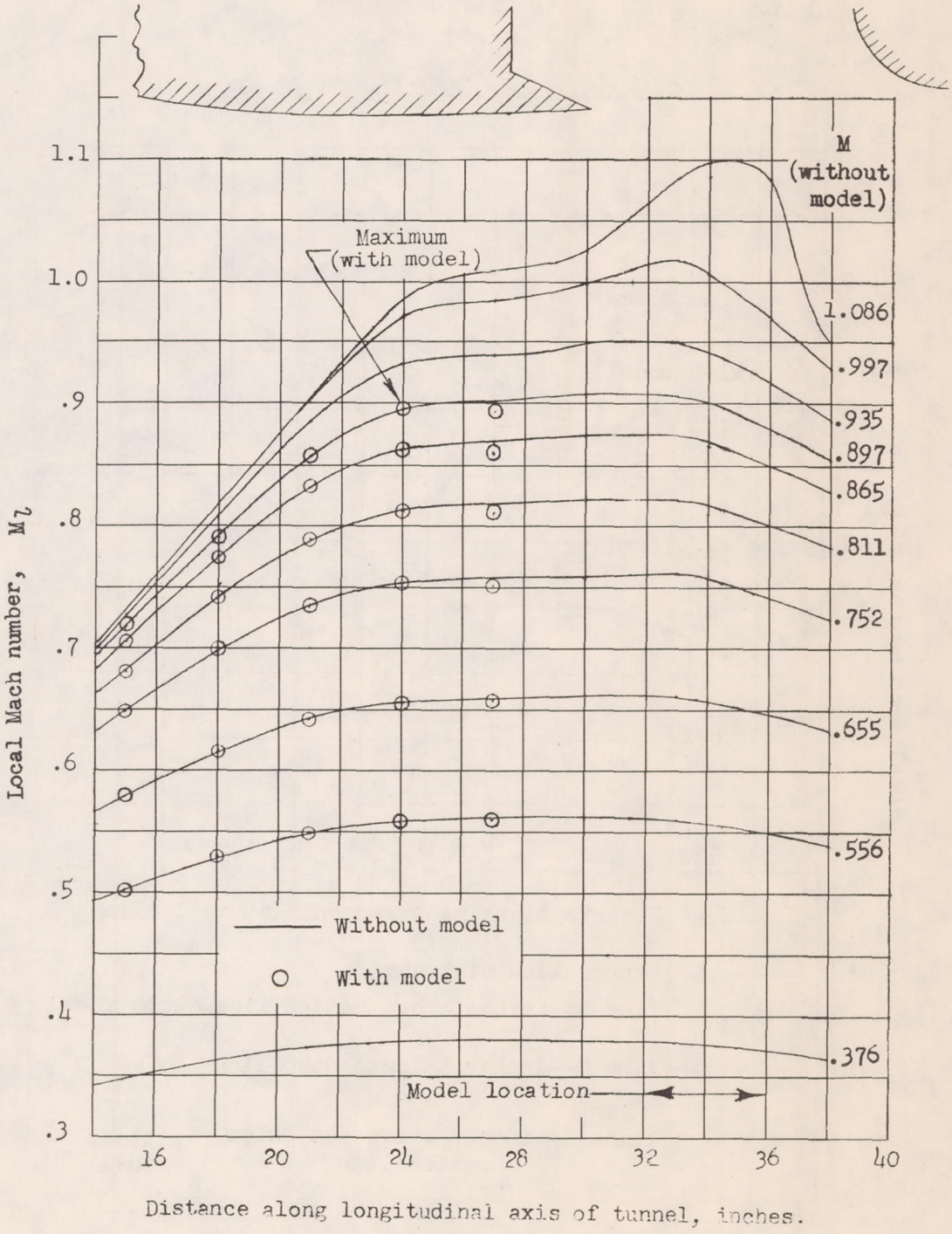

(a) Distributions along center line.

Figure 3.- Local Mach number distributions along center line of the flat side walls of the Langley 4- by 19-inch semiopen tunnel, with and without model. NACA 64A012 airfoil, $\alpha_{test} = 8^{\circ}$.

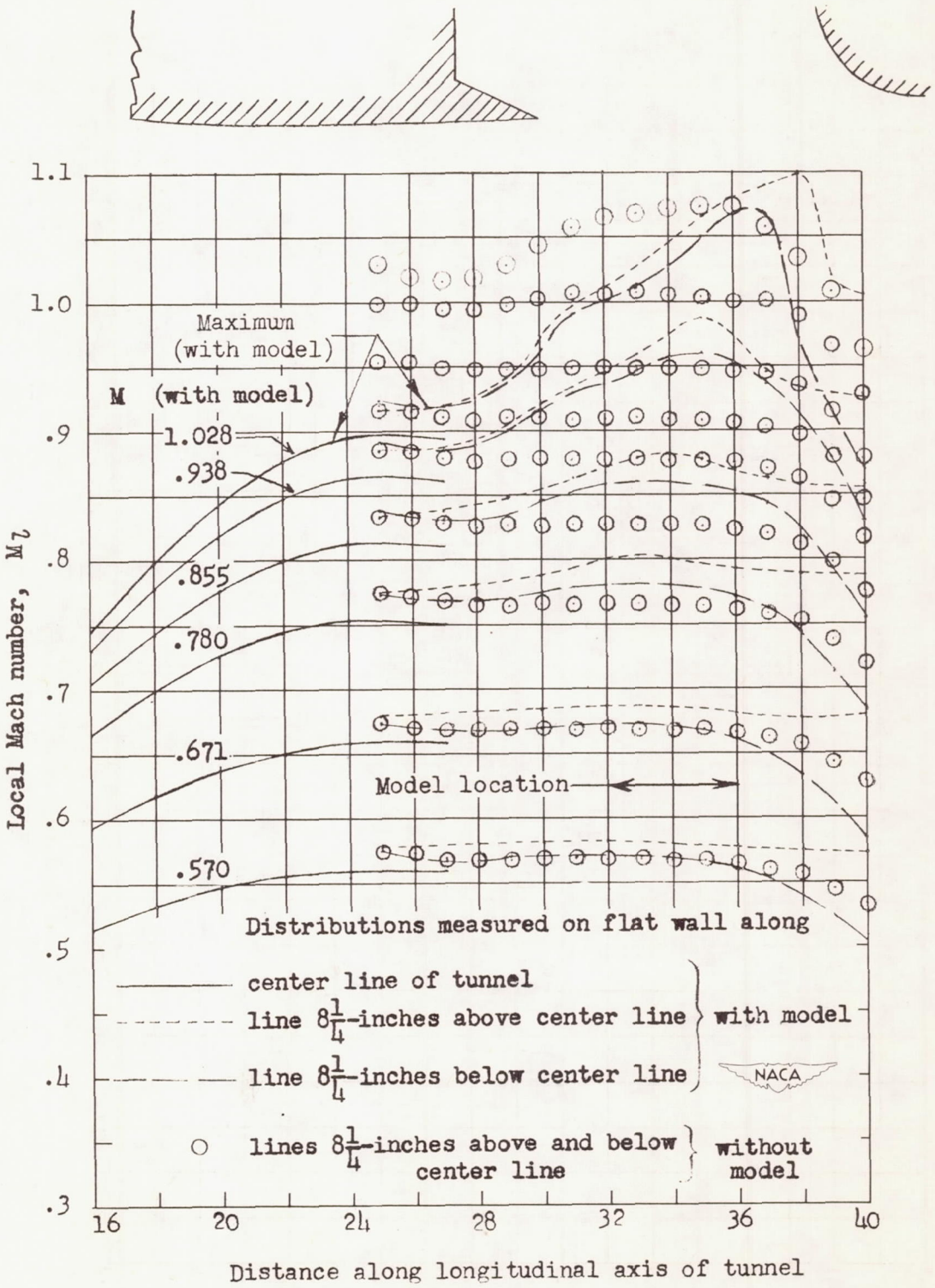

(b) Distributions near free boundaries.

Figure 3.- Concluded.

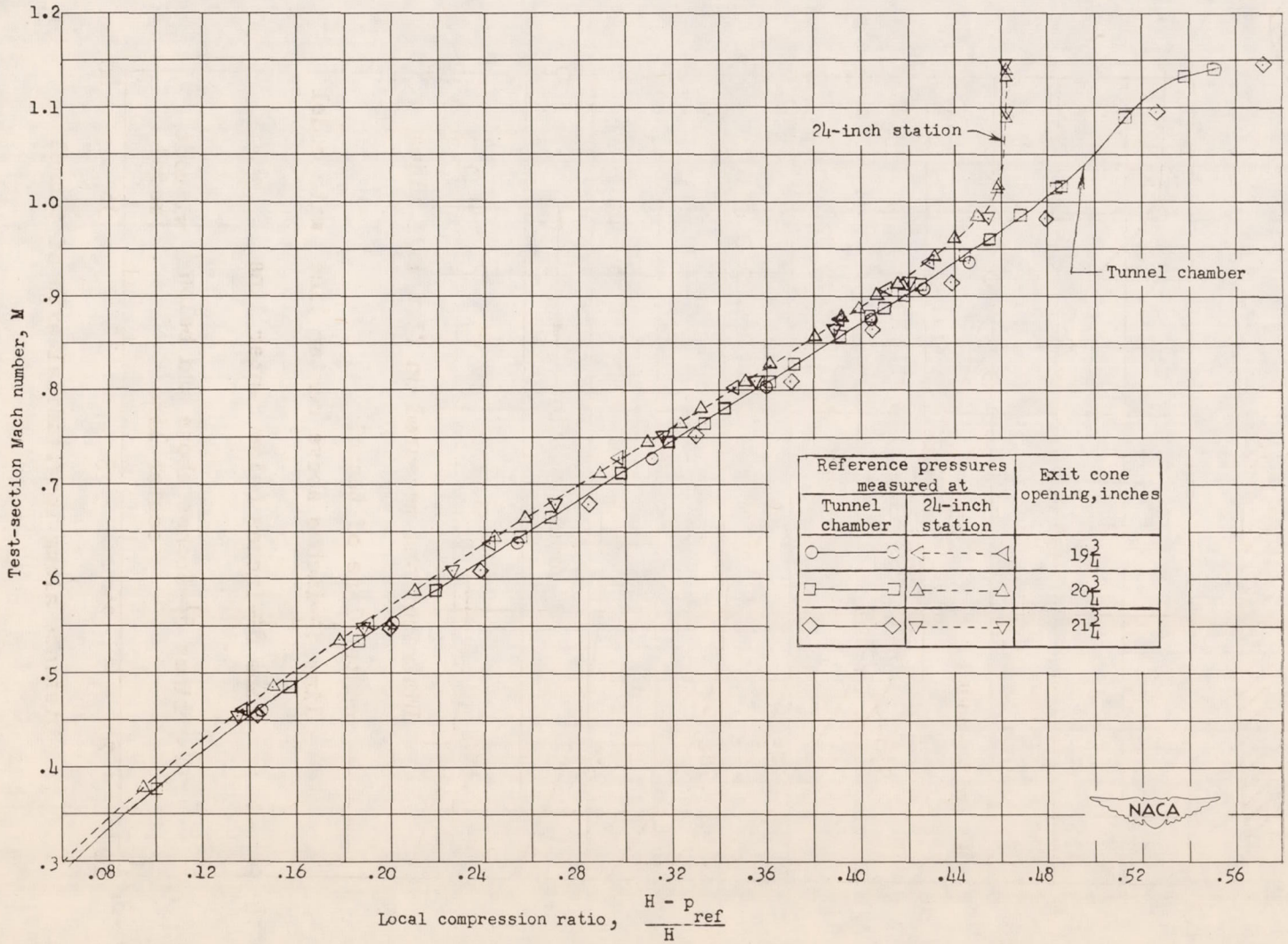

Figure 4.- Representative calibrations of the Langley 4- by 19-inch semiopen tunnel for several exit-cone openings (tunnel empty).

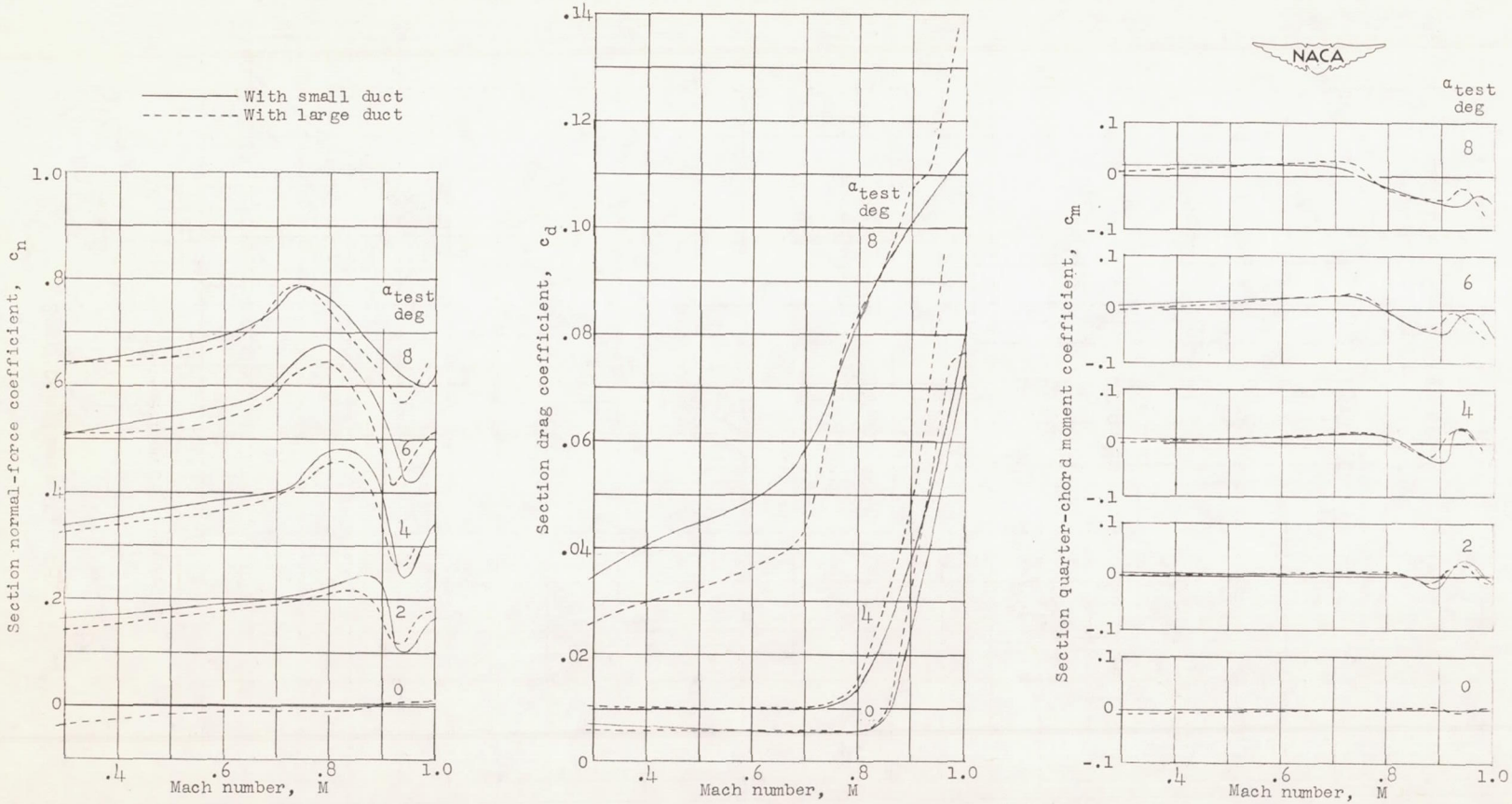

Figure 5.- Effect of duct size on airfoil section characteristics. NACA 64A009 airfoil.

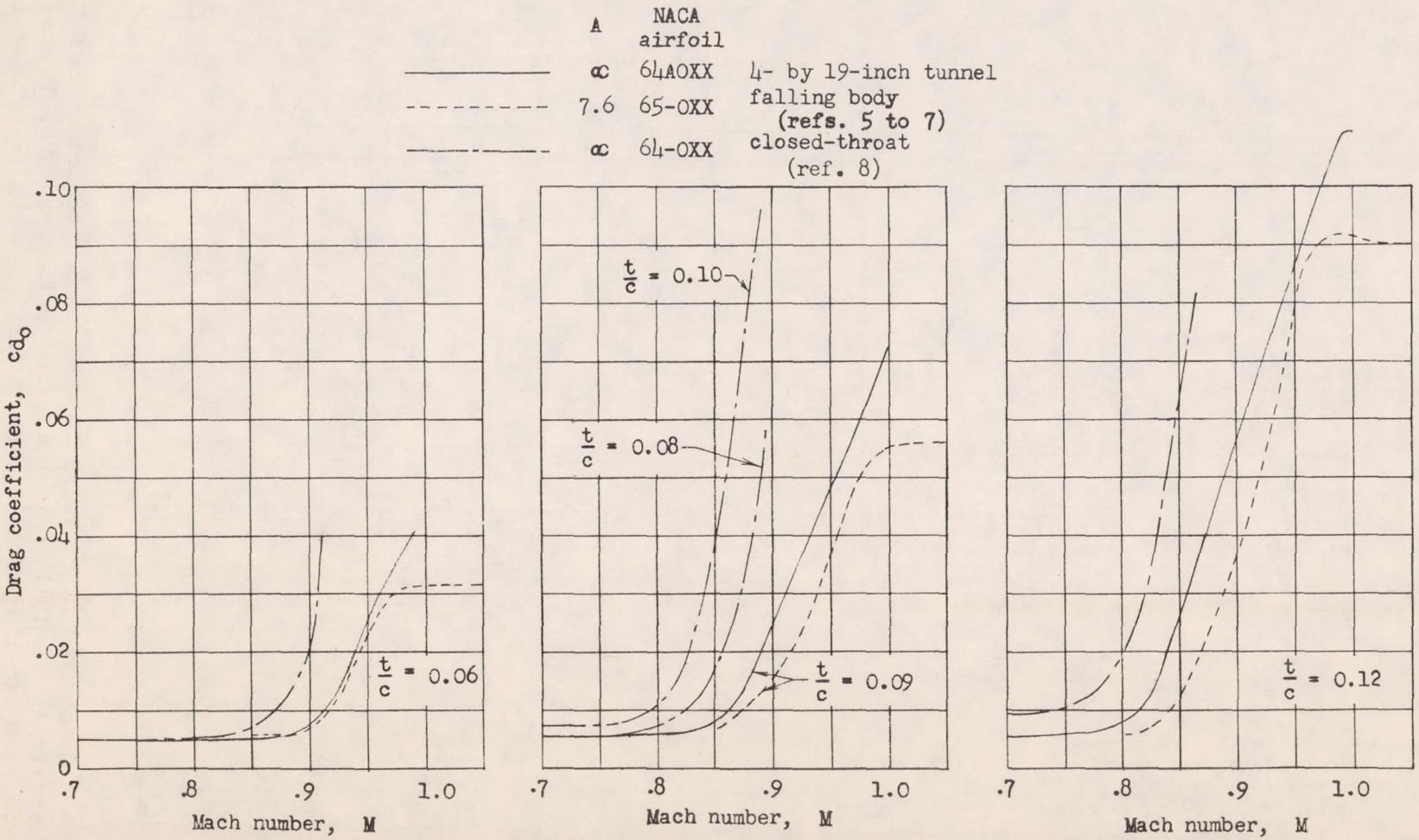

Figure 6.- Comparison of zero-lift drag coefficients obtained from tests in the Langley 4- by 19-inch semiopen tunnel with those obtained from tests by other methods.

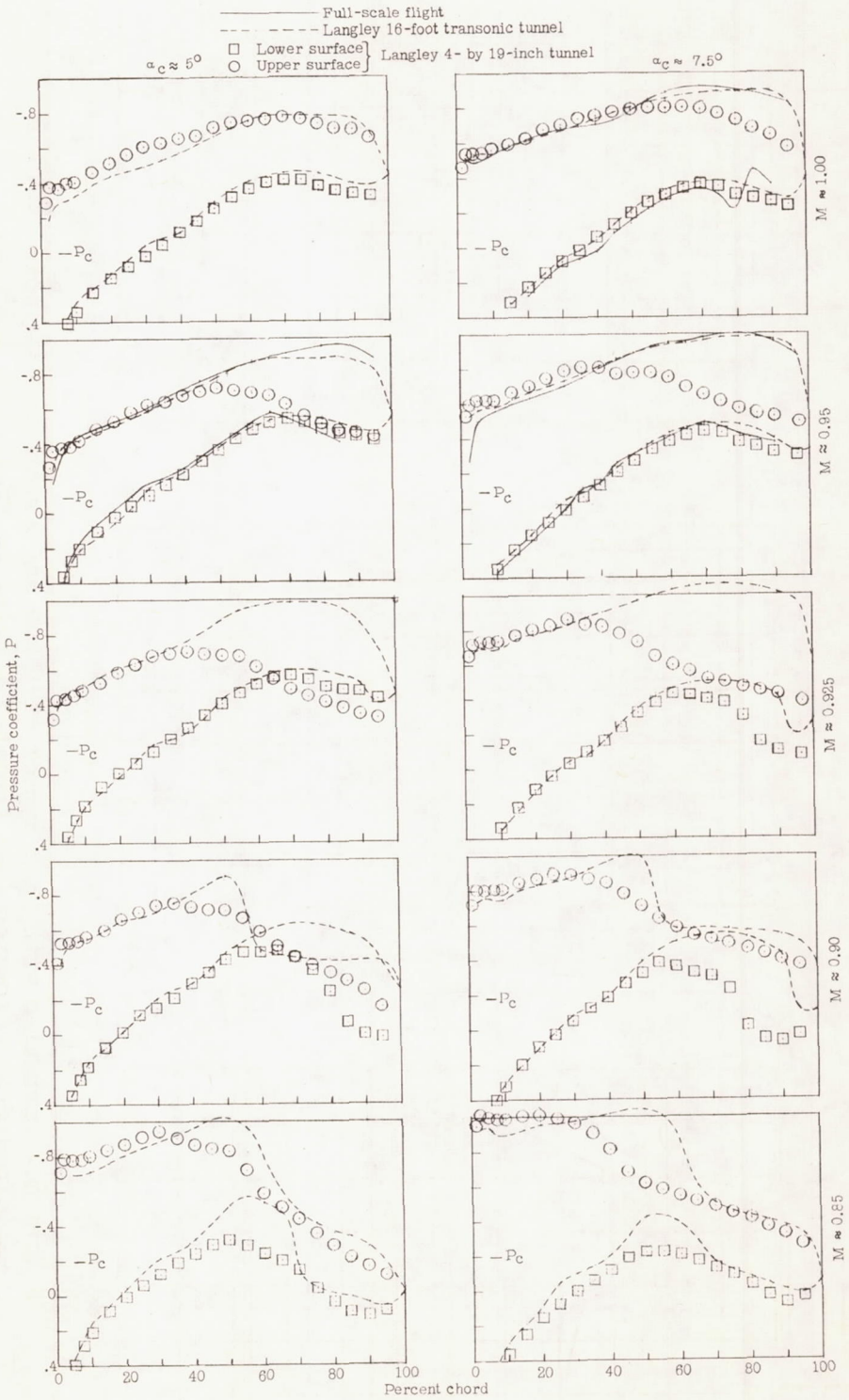

Figure 7.- A comparison of pressure distributions obtained on an NACA 65-110 airfoil from full scale and model tests of a three-dimensional wing and from two-dimensional tests in Langley 4- by 19-inch semiopen tunnel.

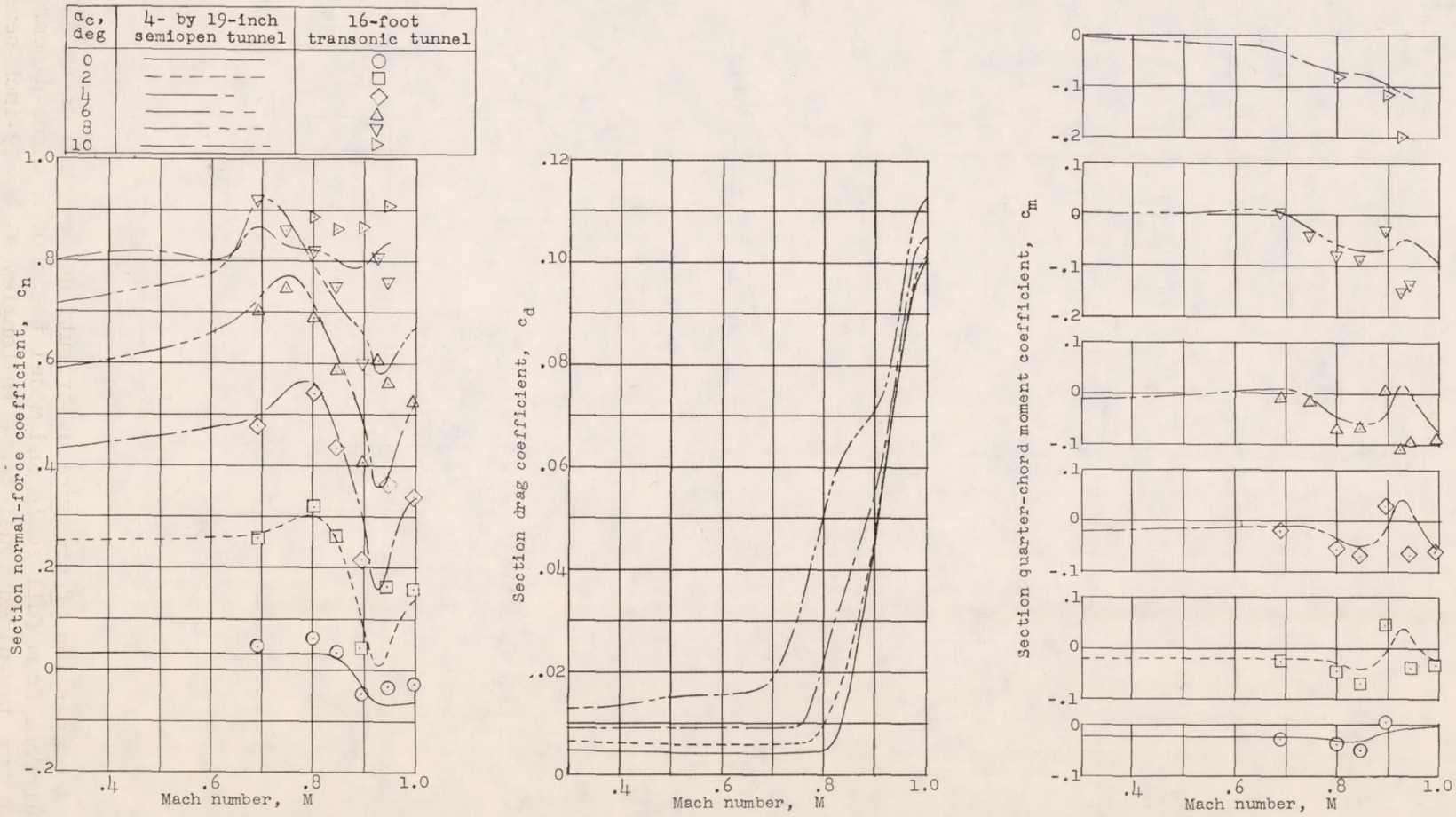

Figure 8.- Variation with Mach number of force and moment coefficients obtained from corrected data from the Langley 4- by 19-inch semiopen tunnel compared with data at corresponding angles of attack obtained at the midsemispan station of a wing on a one-quarter-size model of the X-1 airplane (NACA 65-110 airfoil section).

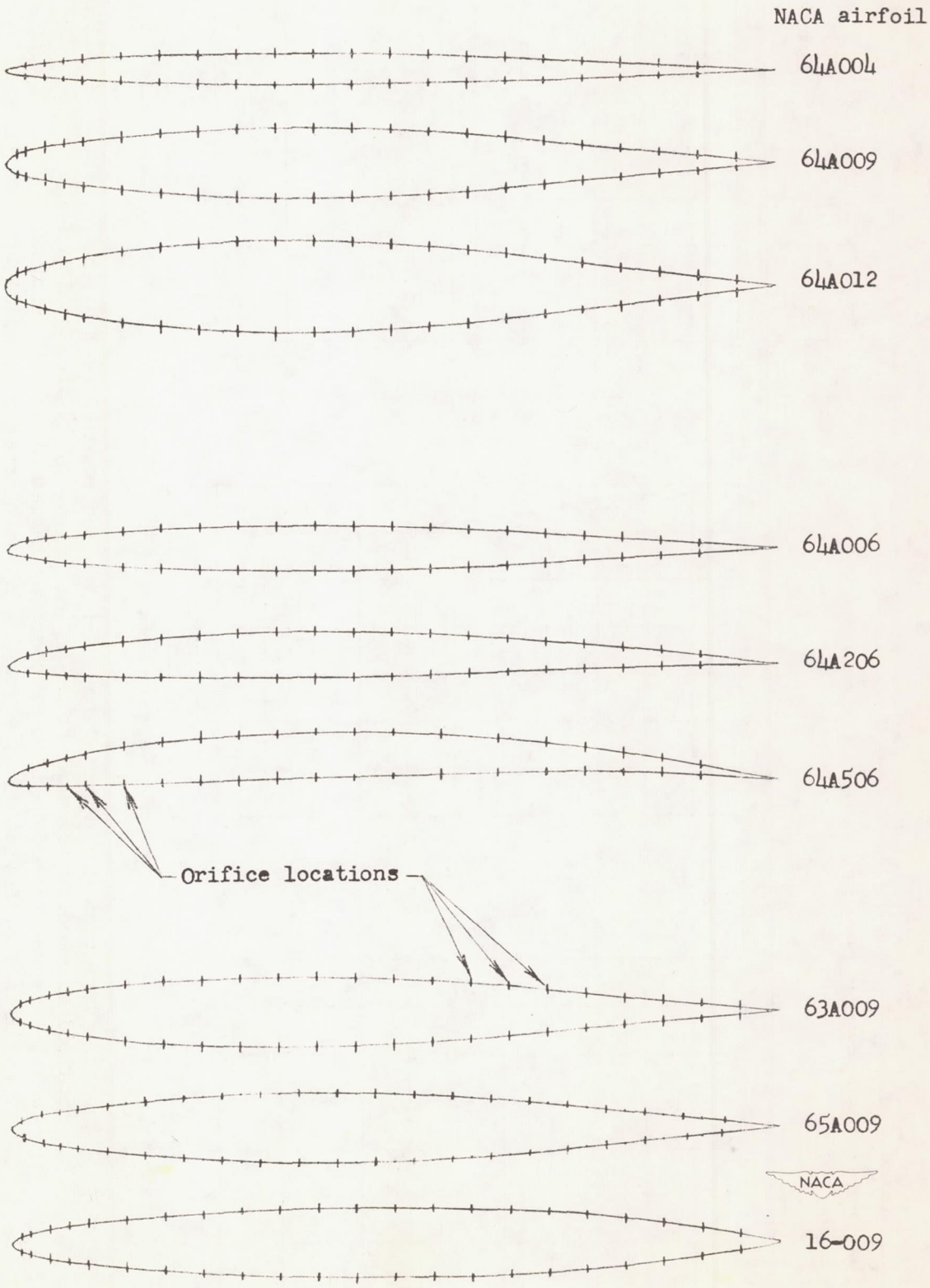

Figure 9.- Airfoil profiles and static-pressure orifice locations.

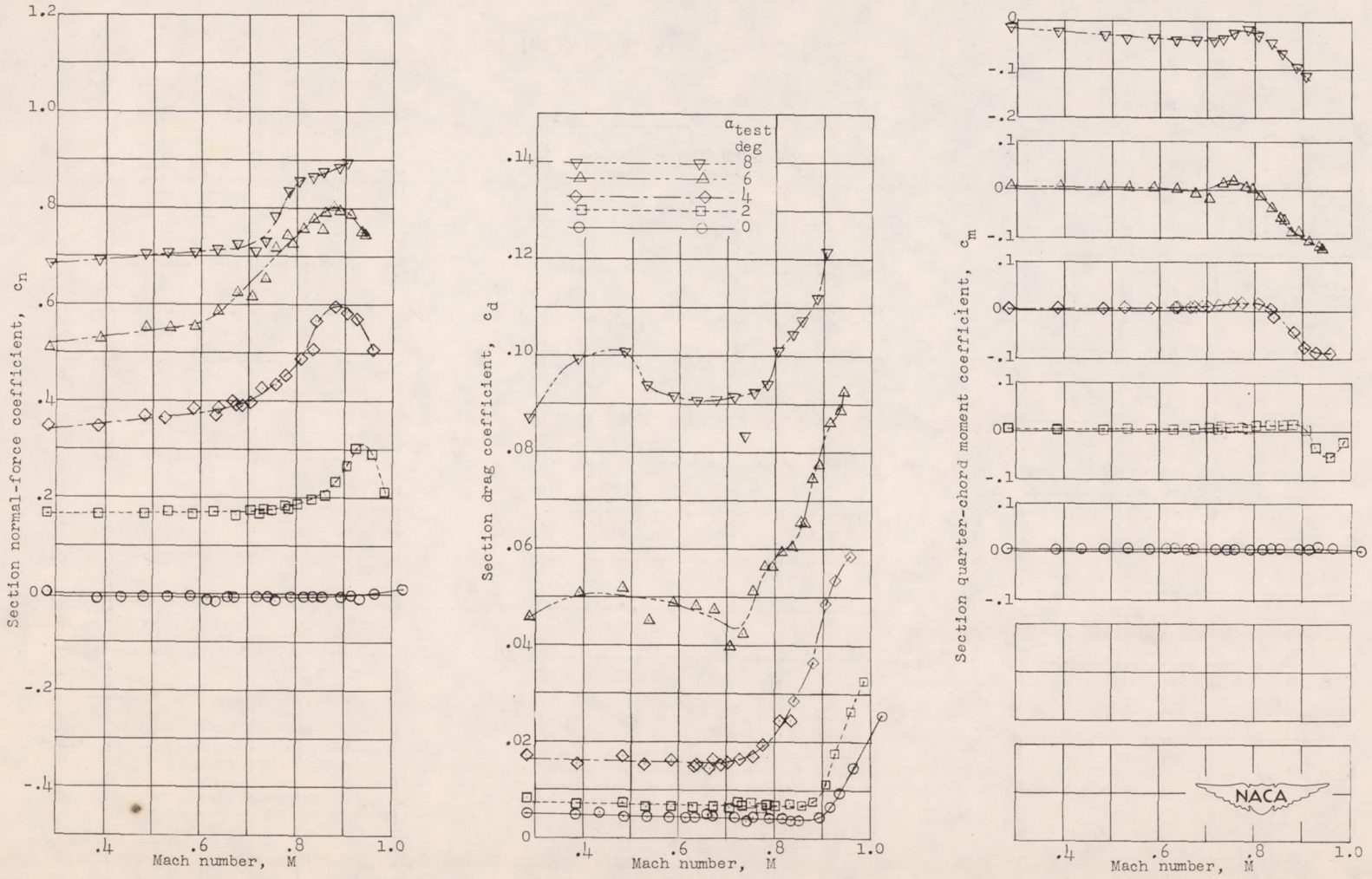

(a) NACA 64A004 airfoil (small duct).

Figure 10.- Variation of airfoil section characteristics with Mach number.

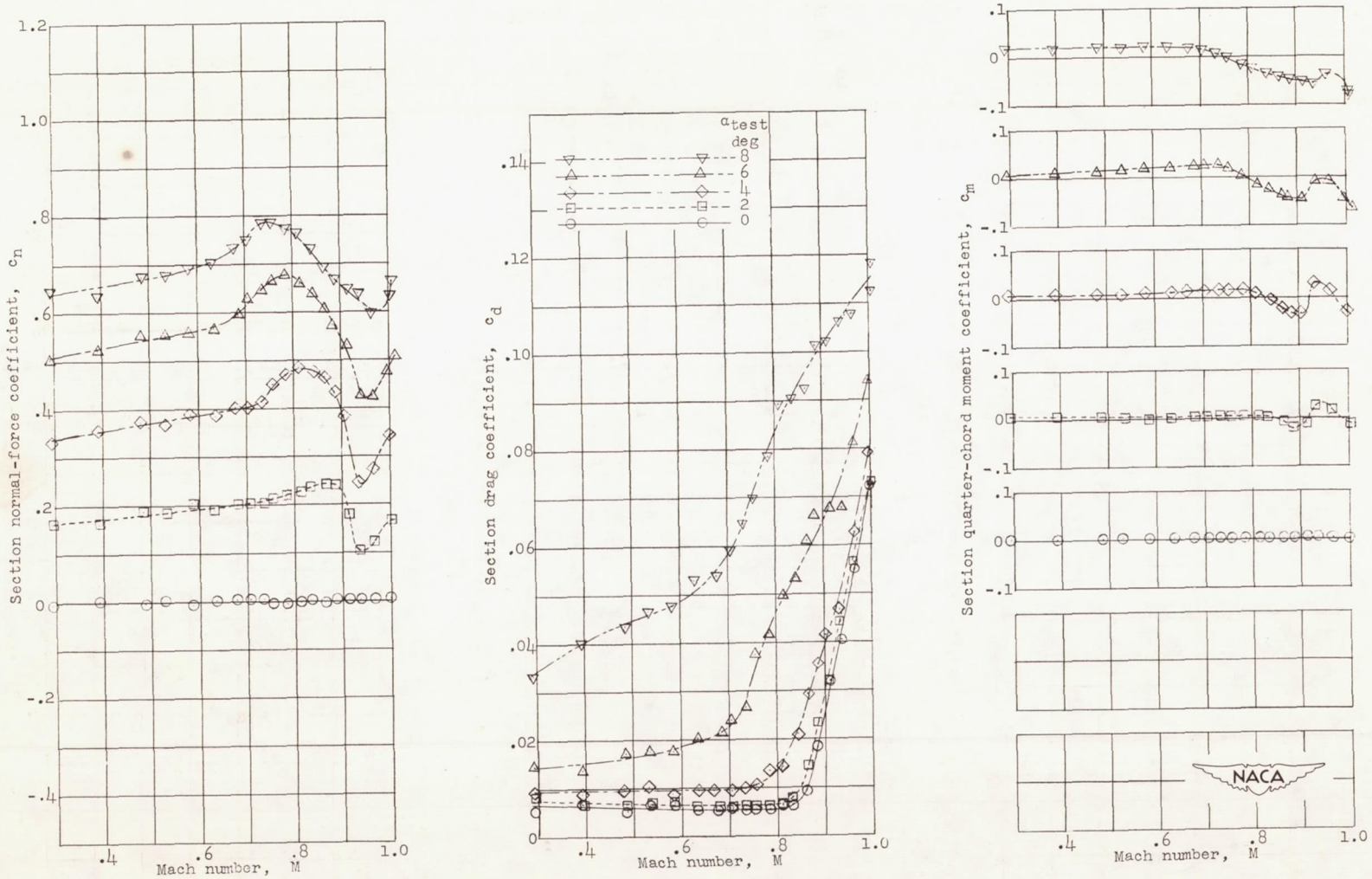

(b) NACA 64A009 airfoil (small duct).

Figure 10.- Continued.

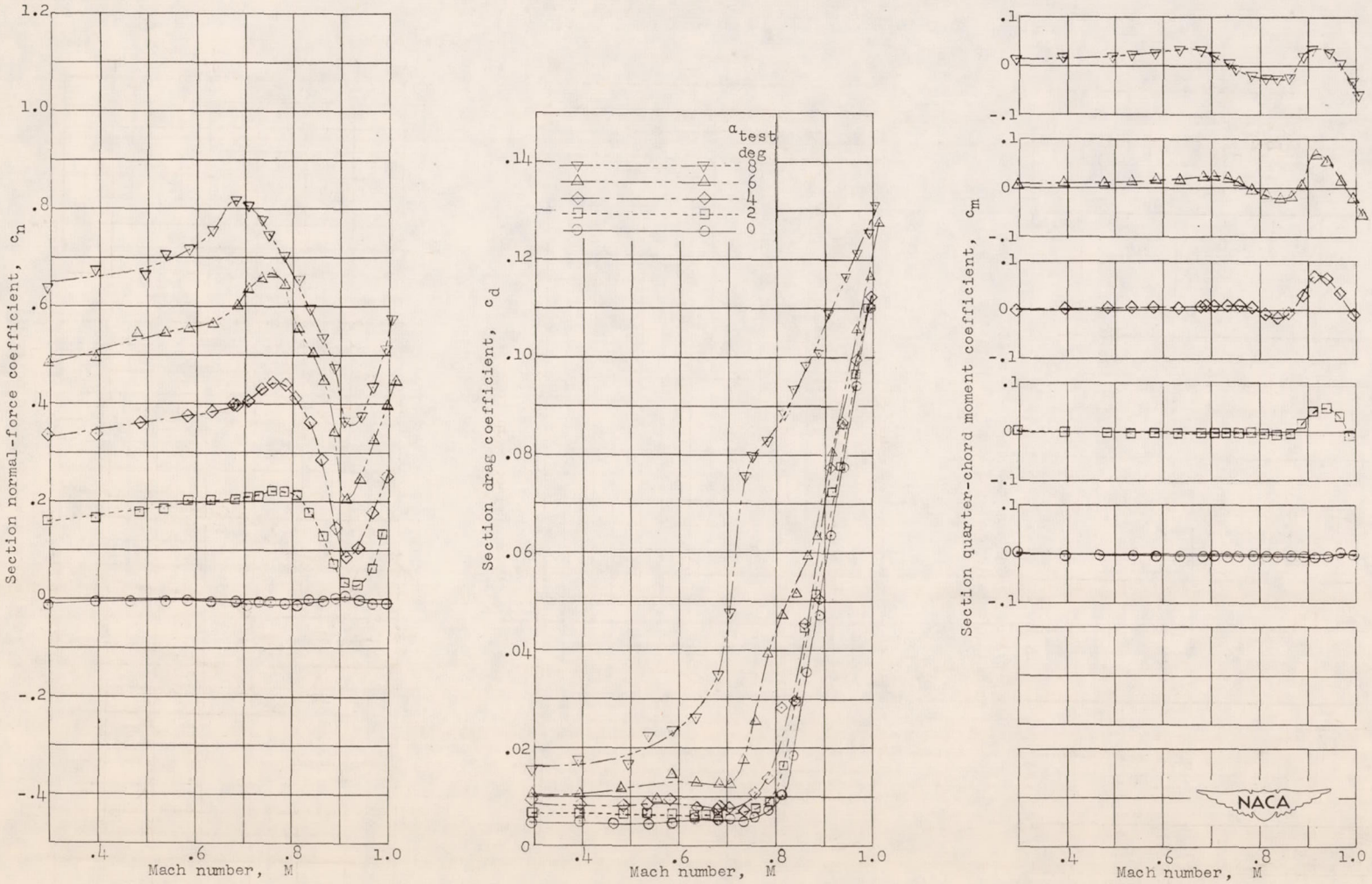

(c) NACA 64A012 airfoil (small duct).

Figure 10.- Continued.

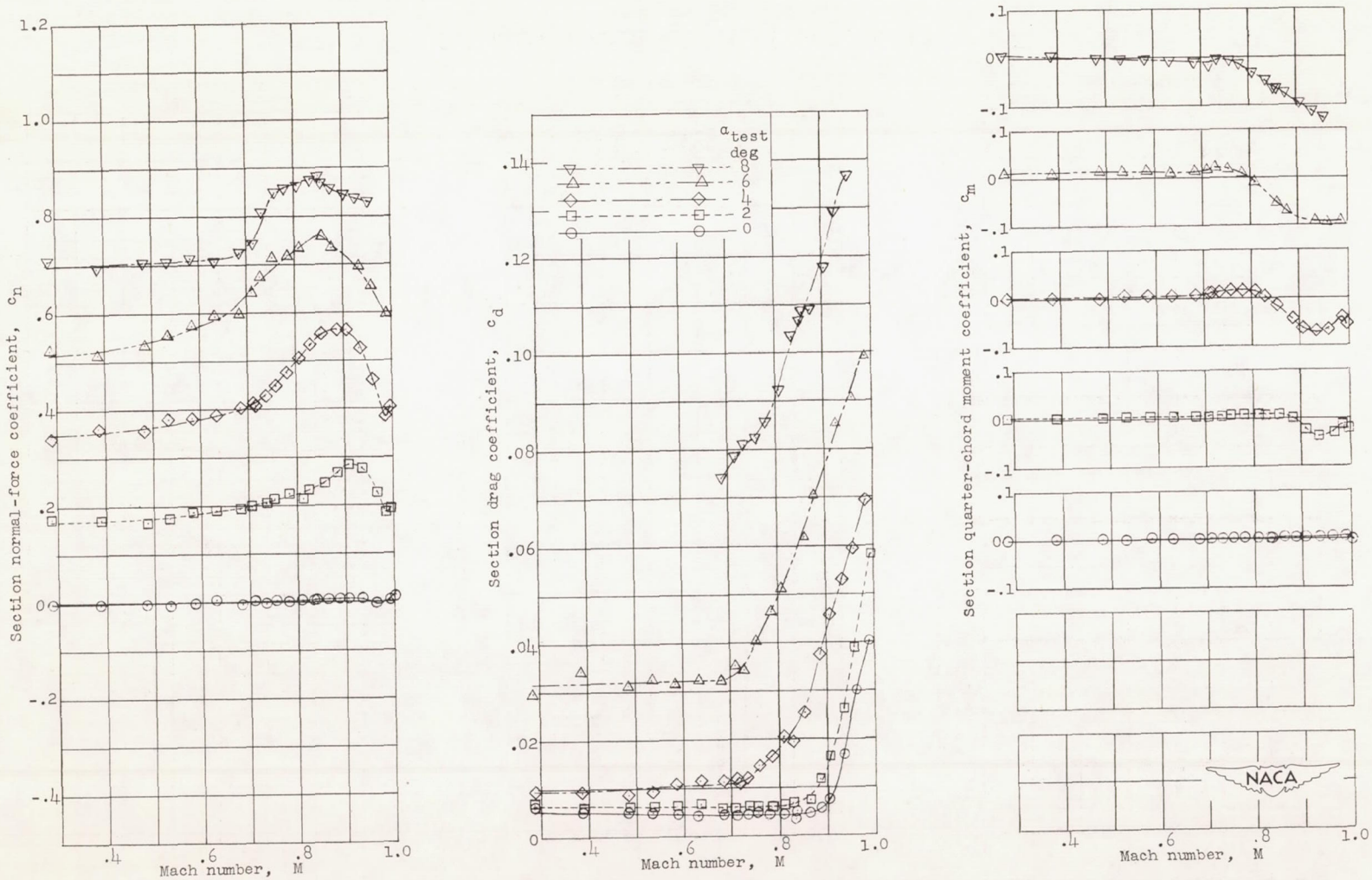

(d) NACA 64A006 airfoil (small duct).

Figure 10.- Continued.

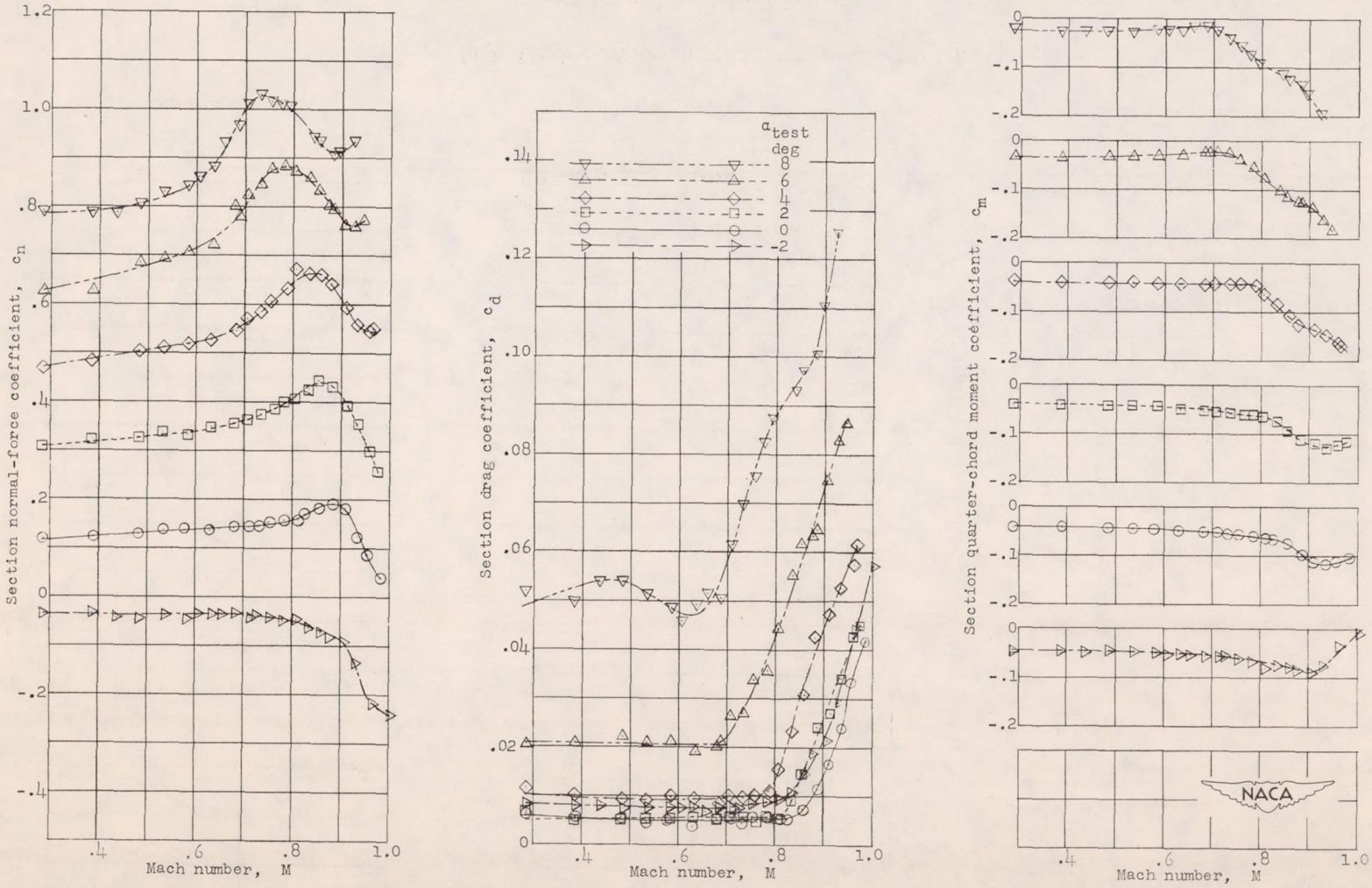

(e) NACA 64A206 airfoil (small duct).

Figure 10.- Continued.

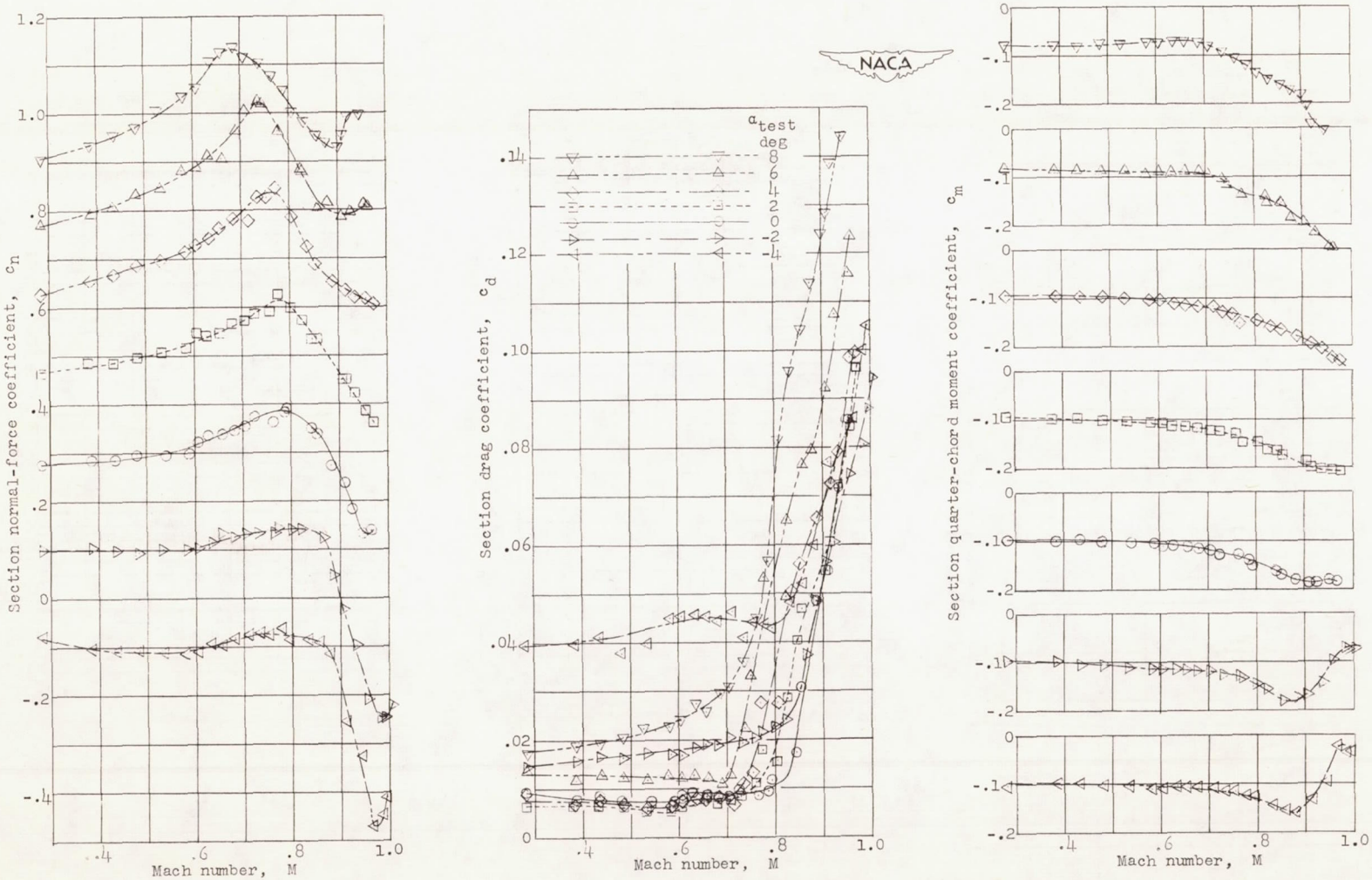

(f) NACA 64A506 airfoil (small duct).

Figure 10.- Continued.

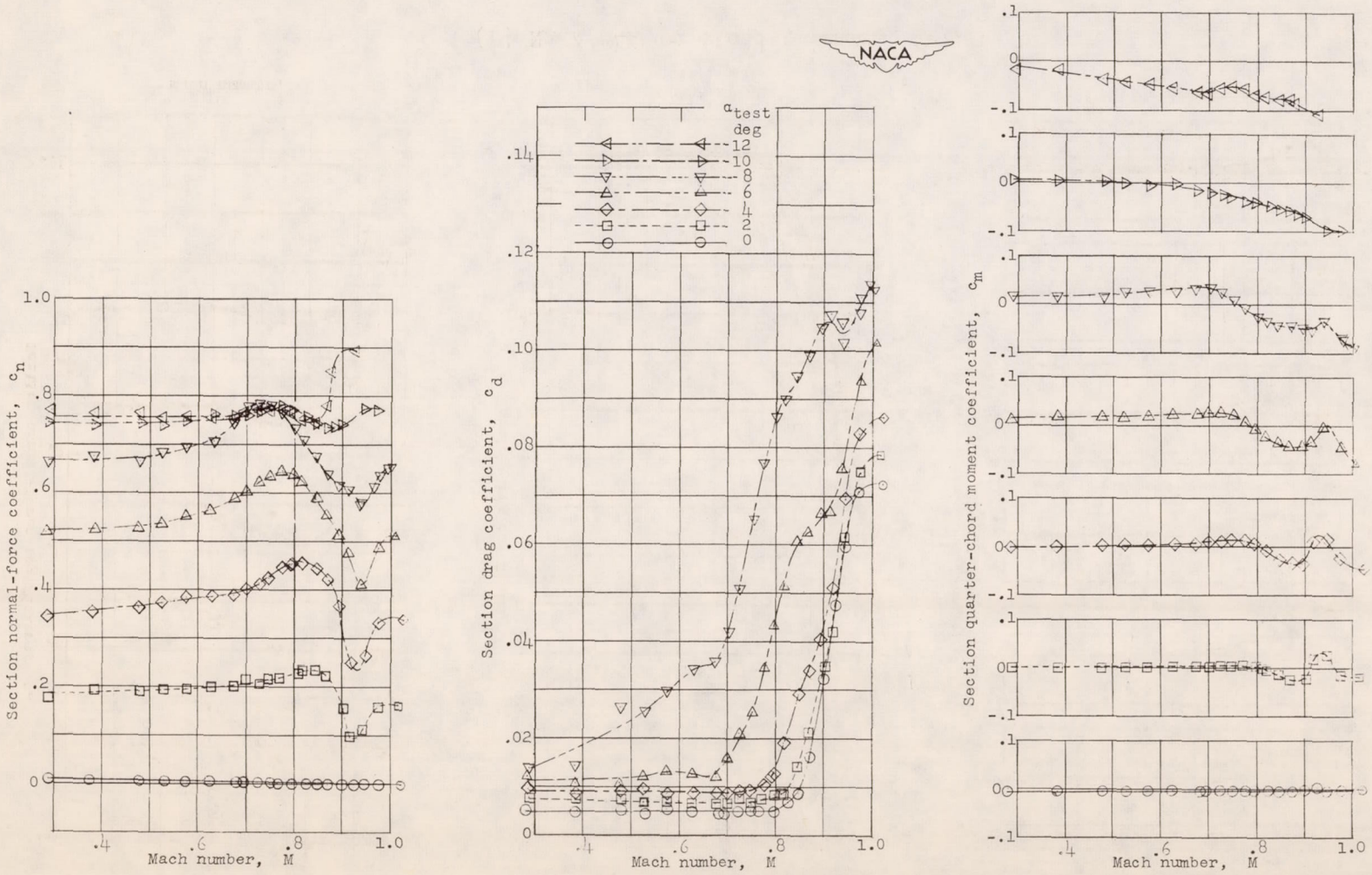

(g) NACA 63A009 airfoil (large duct).

Figure 10.- Continued.

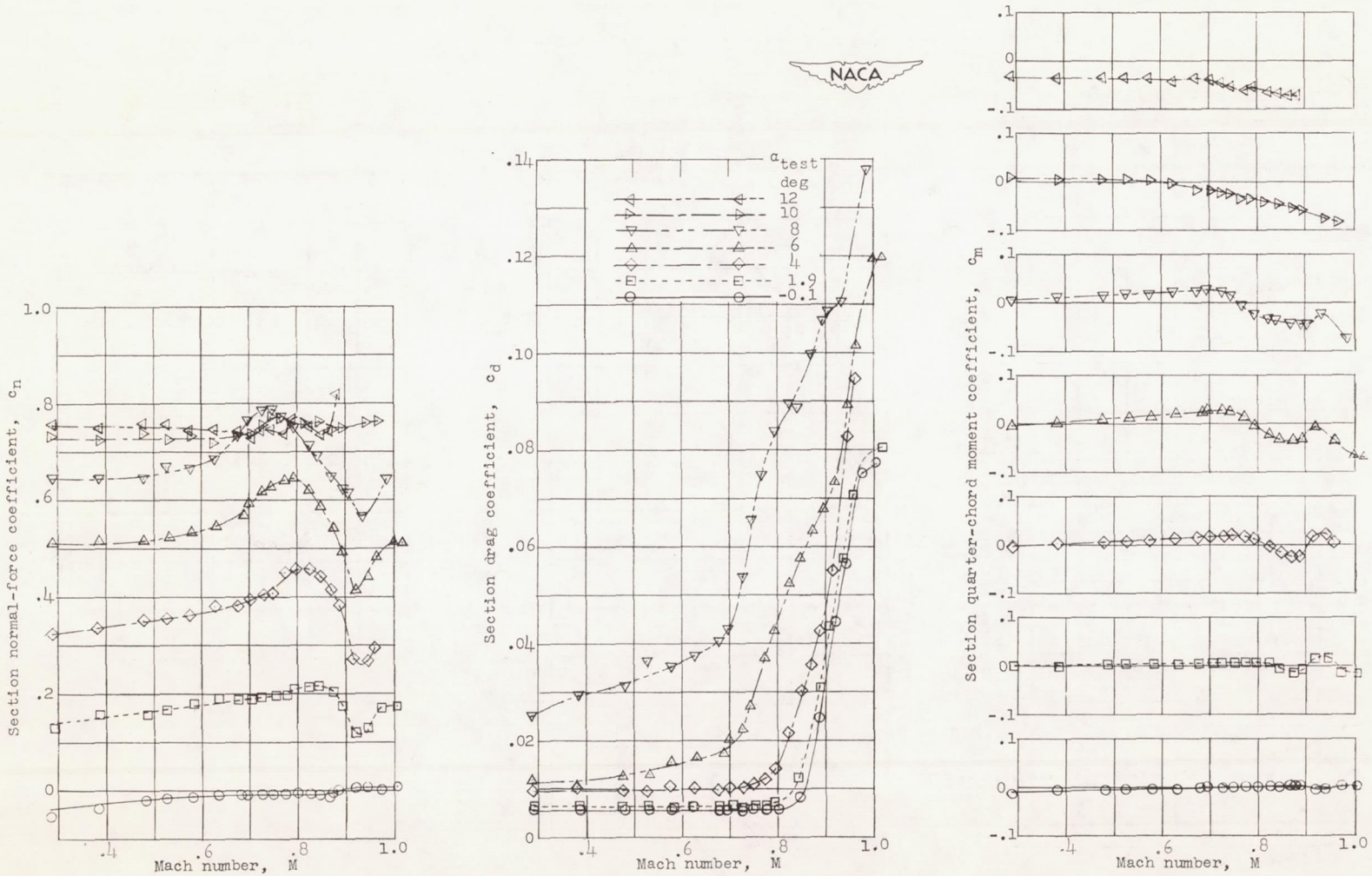

(h) NACA 64A009 airfoil (large duct).

Figure 10.- Continued.

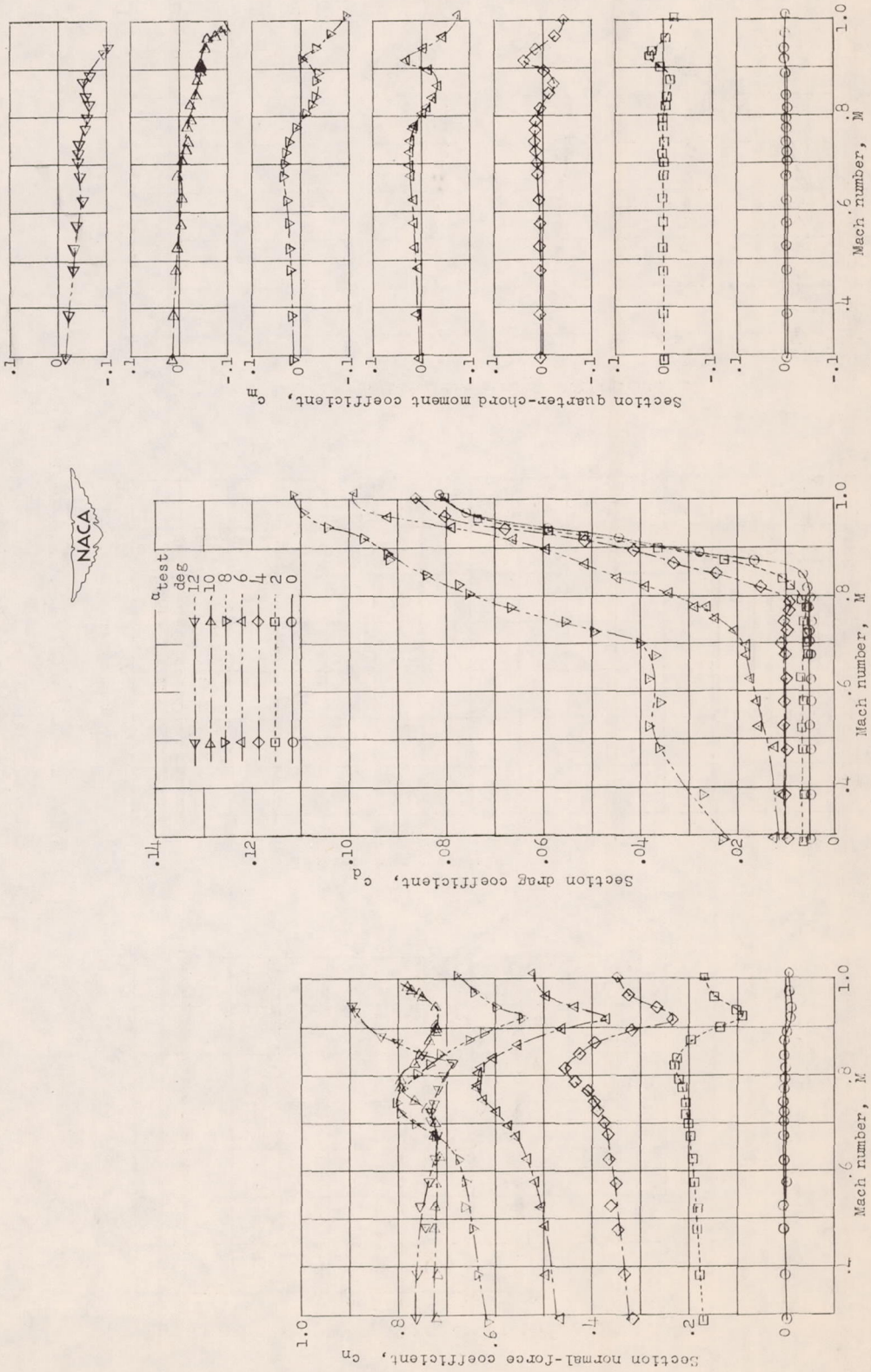

(i) NACA 65A009 airfoil (large duct).

Figure 10.- Continued.

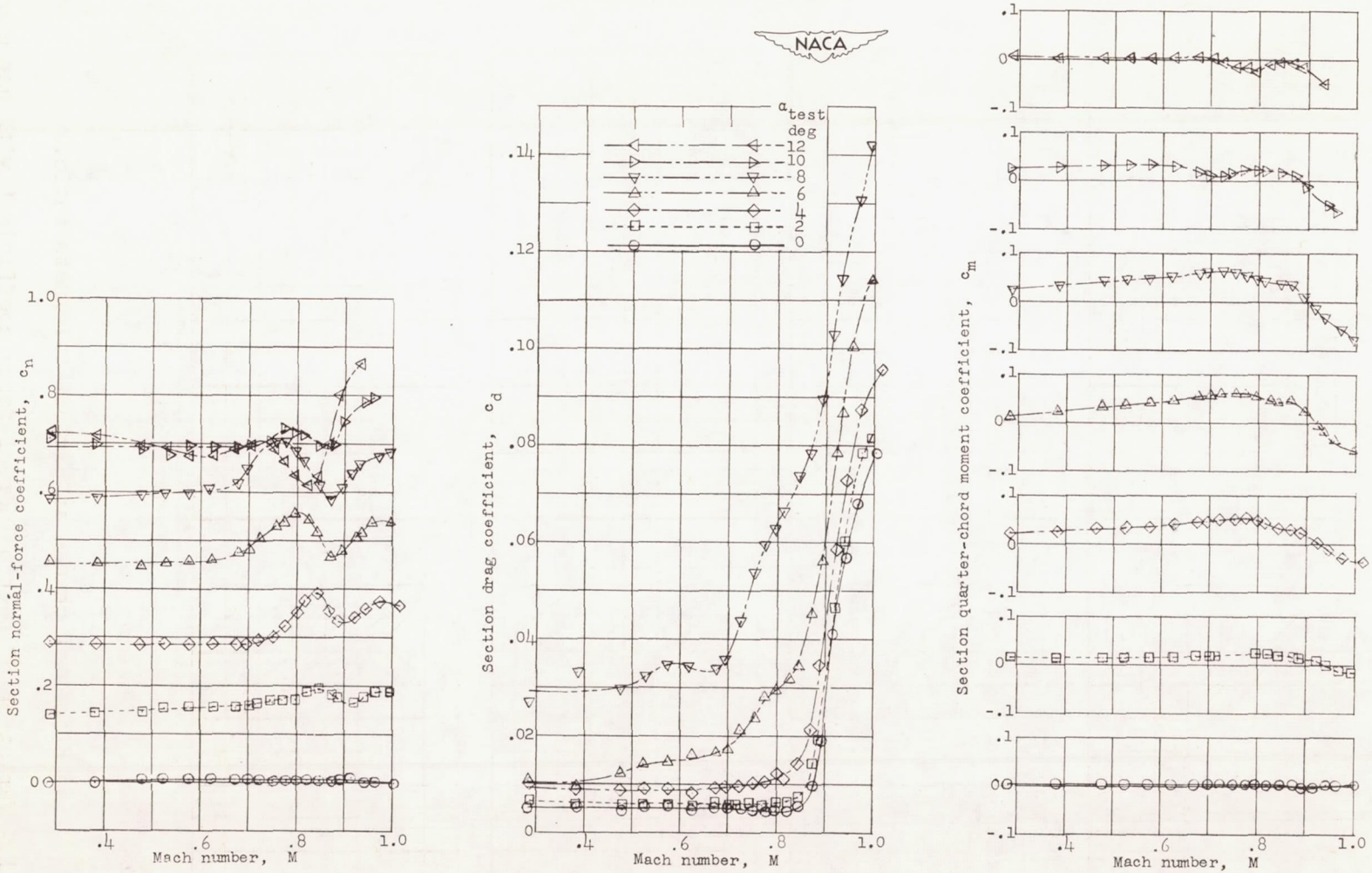

(j) NACA 16-009 airfoil (large duct).

Figure 10.- Concluded.

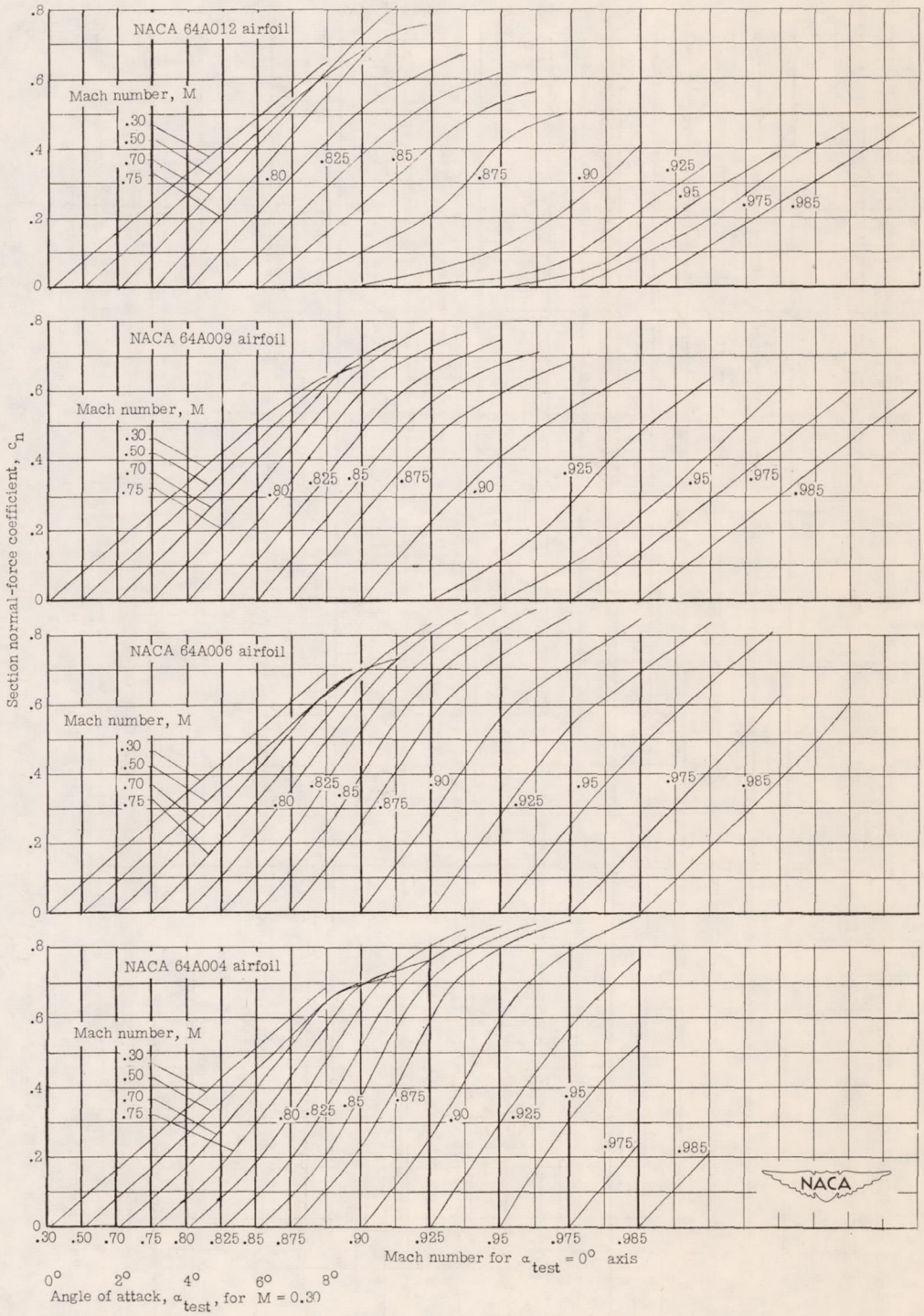

(a) Effect of change in airfoil thickness ratio.

Figure 11.- Variation of section normal-force coefficient with angle of attack at various Mach numbers.

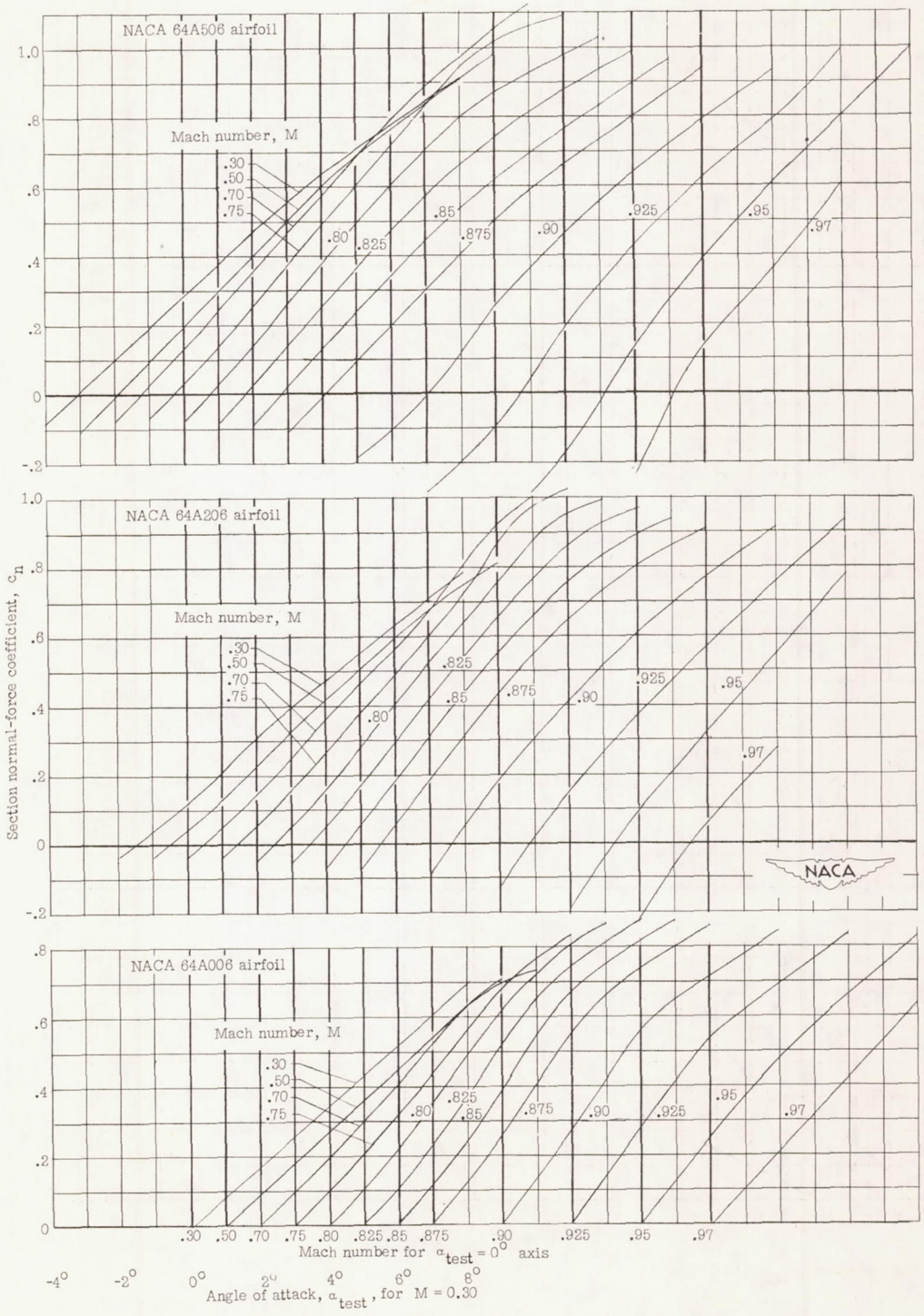

(b) Effect of change in airfoil design lift coefficient.

Figure 11.- Continued.

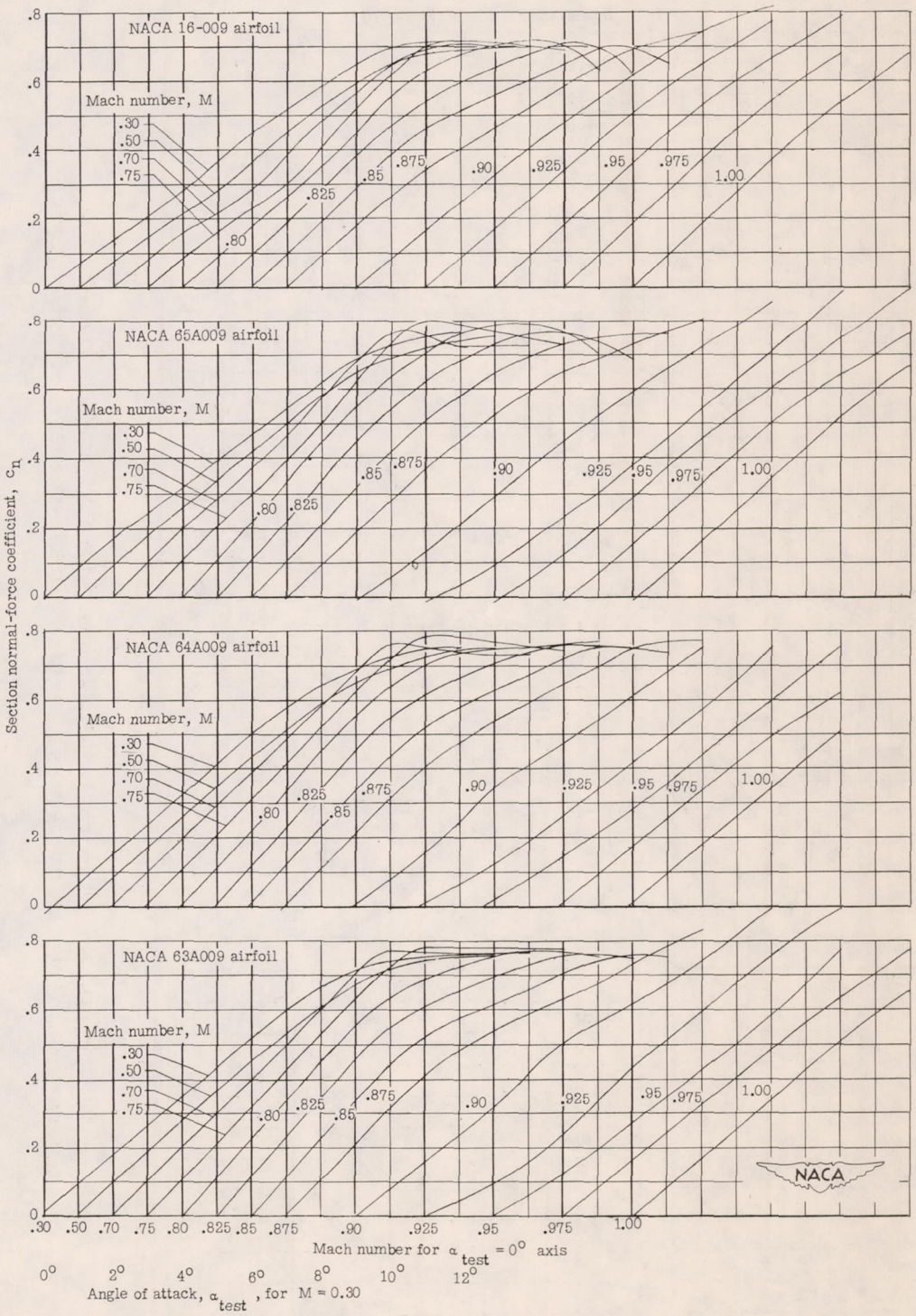

(c) Effect of change in airfoil thickness distribution.

Figure 11.- Concluded.

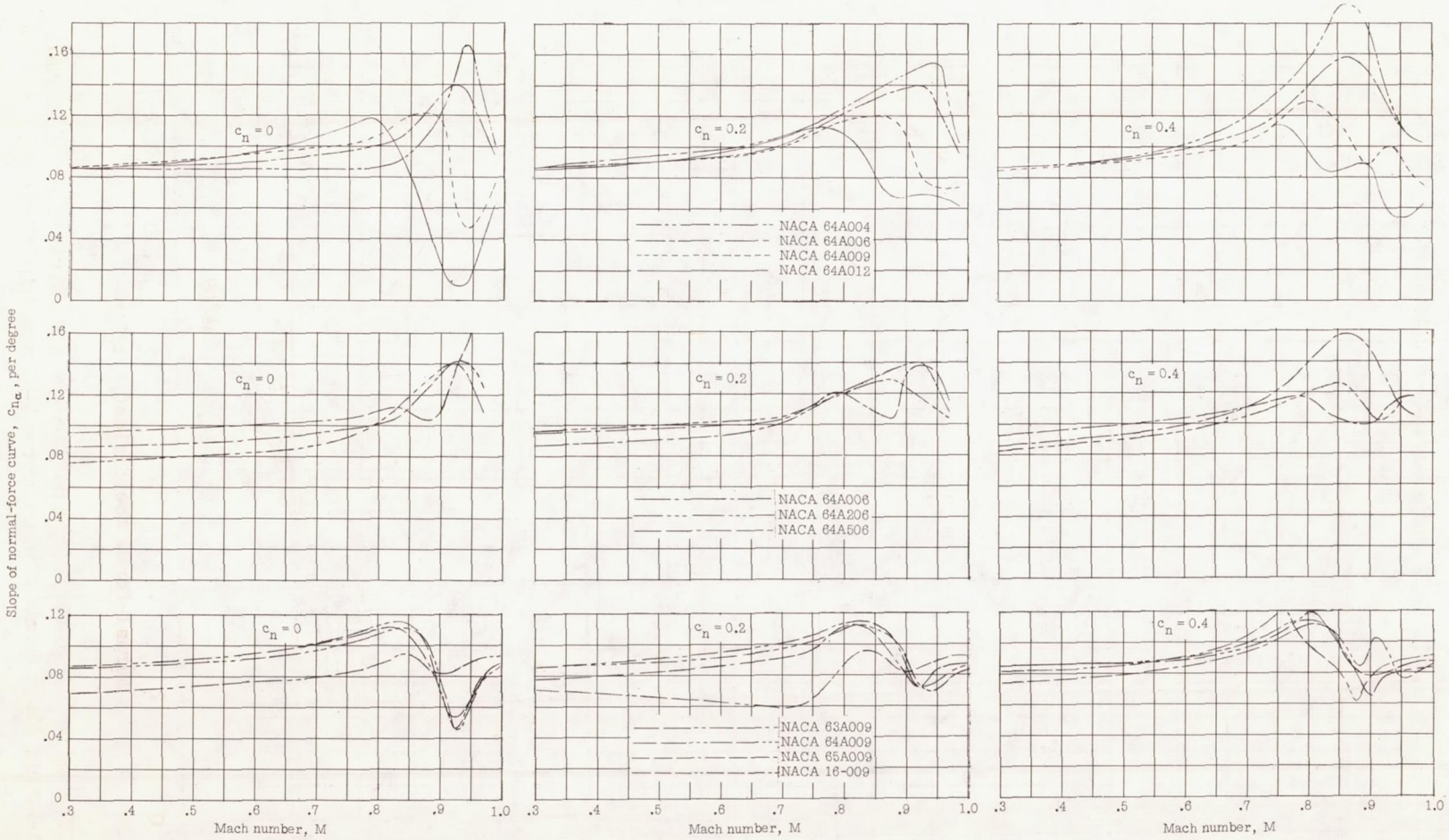

Figure 12.- Variation of normal-force-curve slope with Mach number for the various airfoils at several section normal-force coefficients.

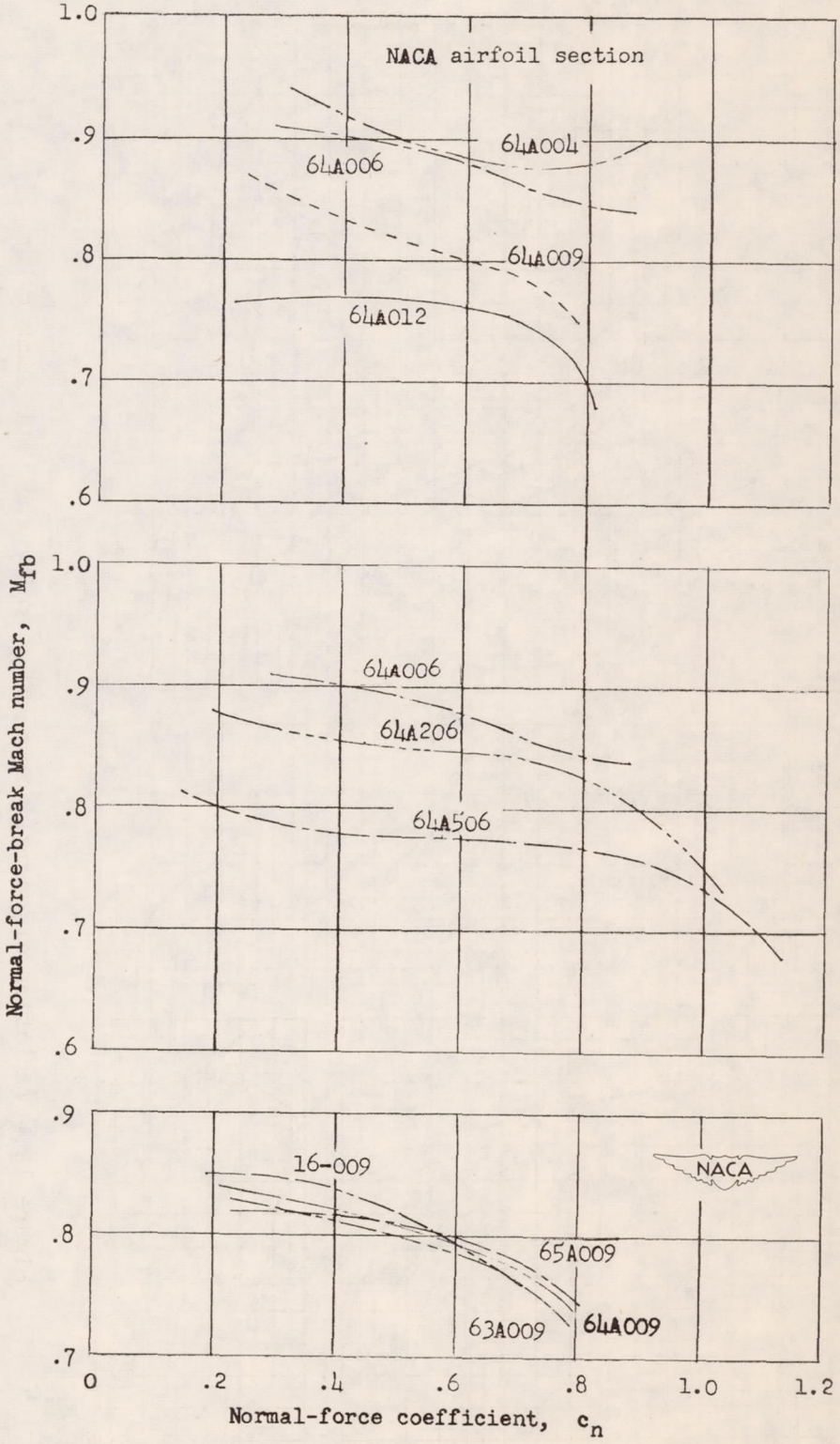

Figure 13.- The effect of airfoil profile on the variation of normal-force-break Mach number with normal-force coefficient.

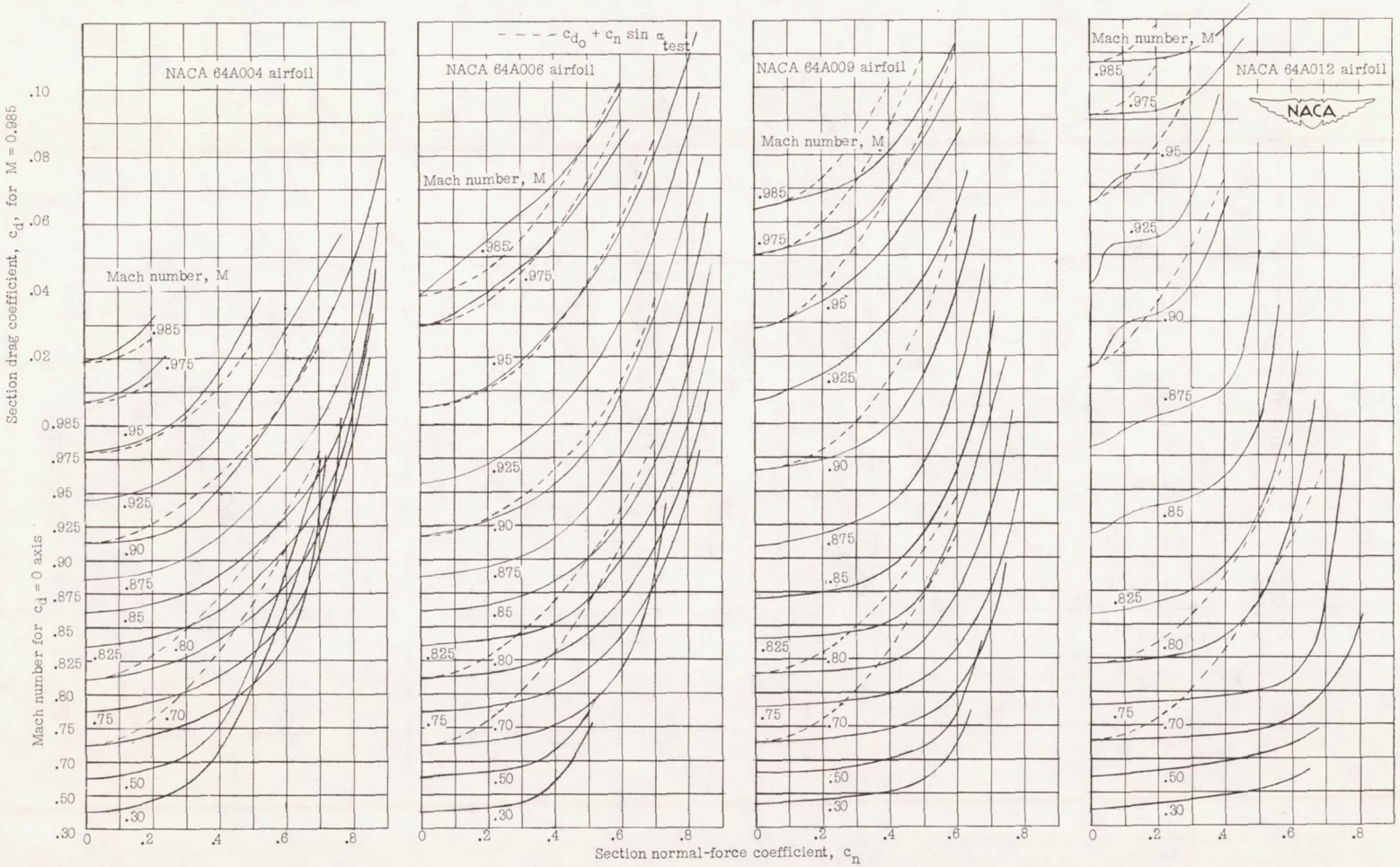

(a) Effect of change in airfoil thickness ratio.

Figure 14.- Variation of section drag coefficient with section normal-force coefficient at various Mach numbers.

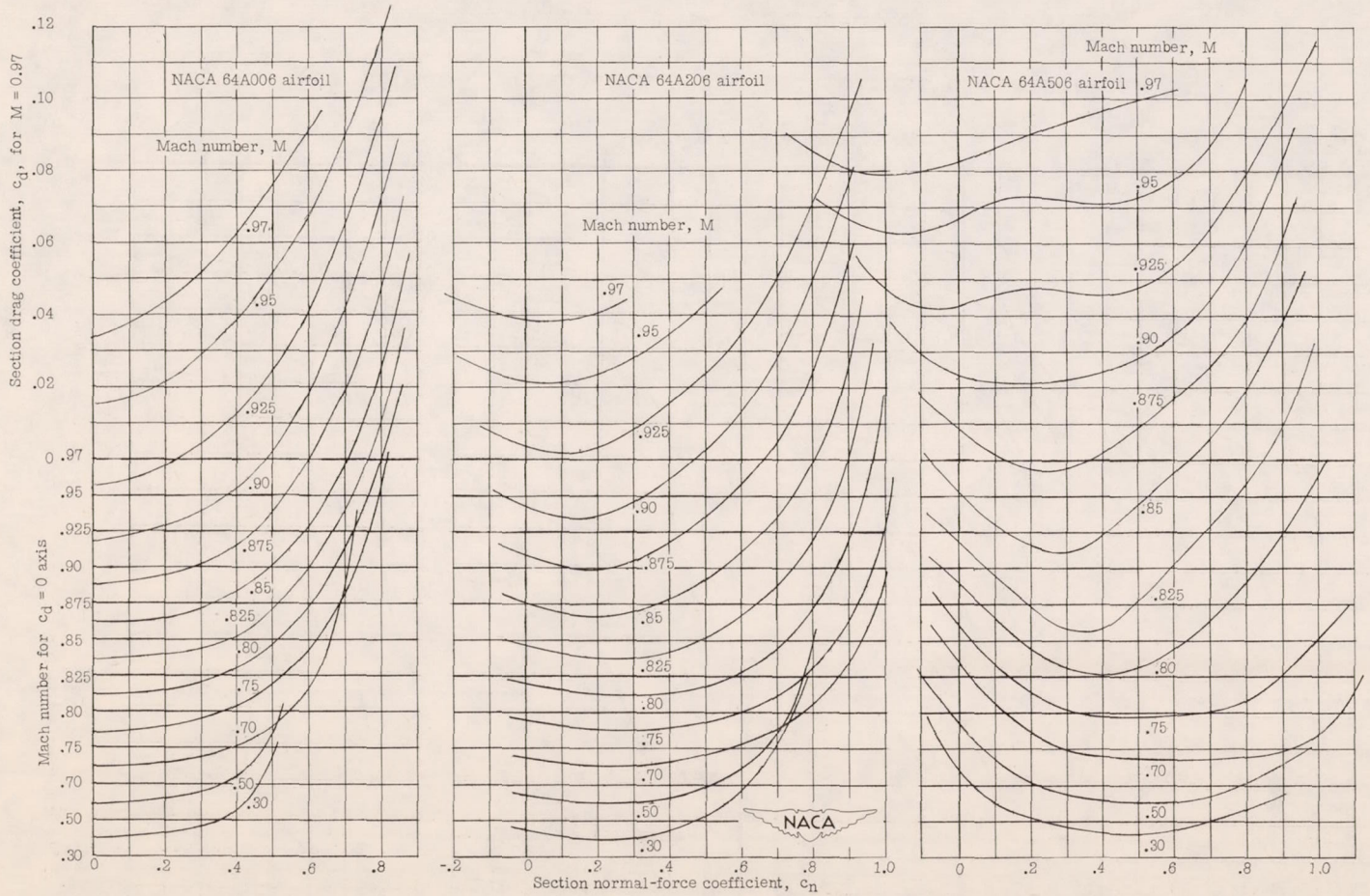

(b) Effect of change in airfoil design lift coefficient.

Figure 14.- Continued.

(c) Effect of change in airfoil thickness distribution.

Figure 14.- Concluded.

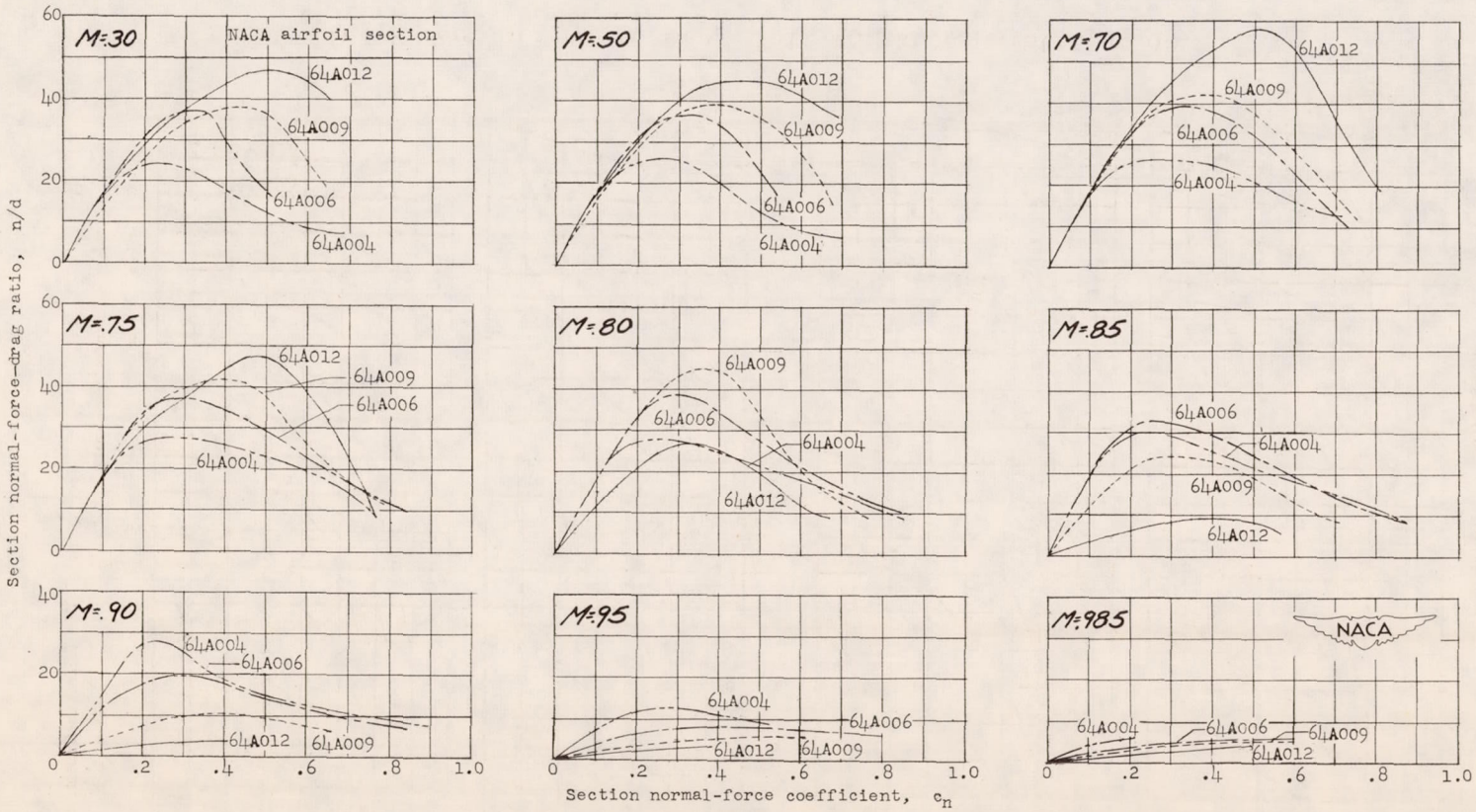

(a) Effect of change in airfoil thickness ratio.

Figure 15.- Variation with section normal-force coefficient of the section normal-force—drag ratio at various Mach numbers.

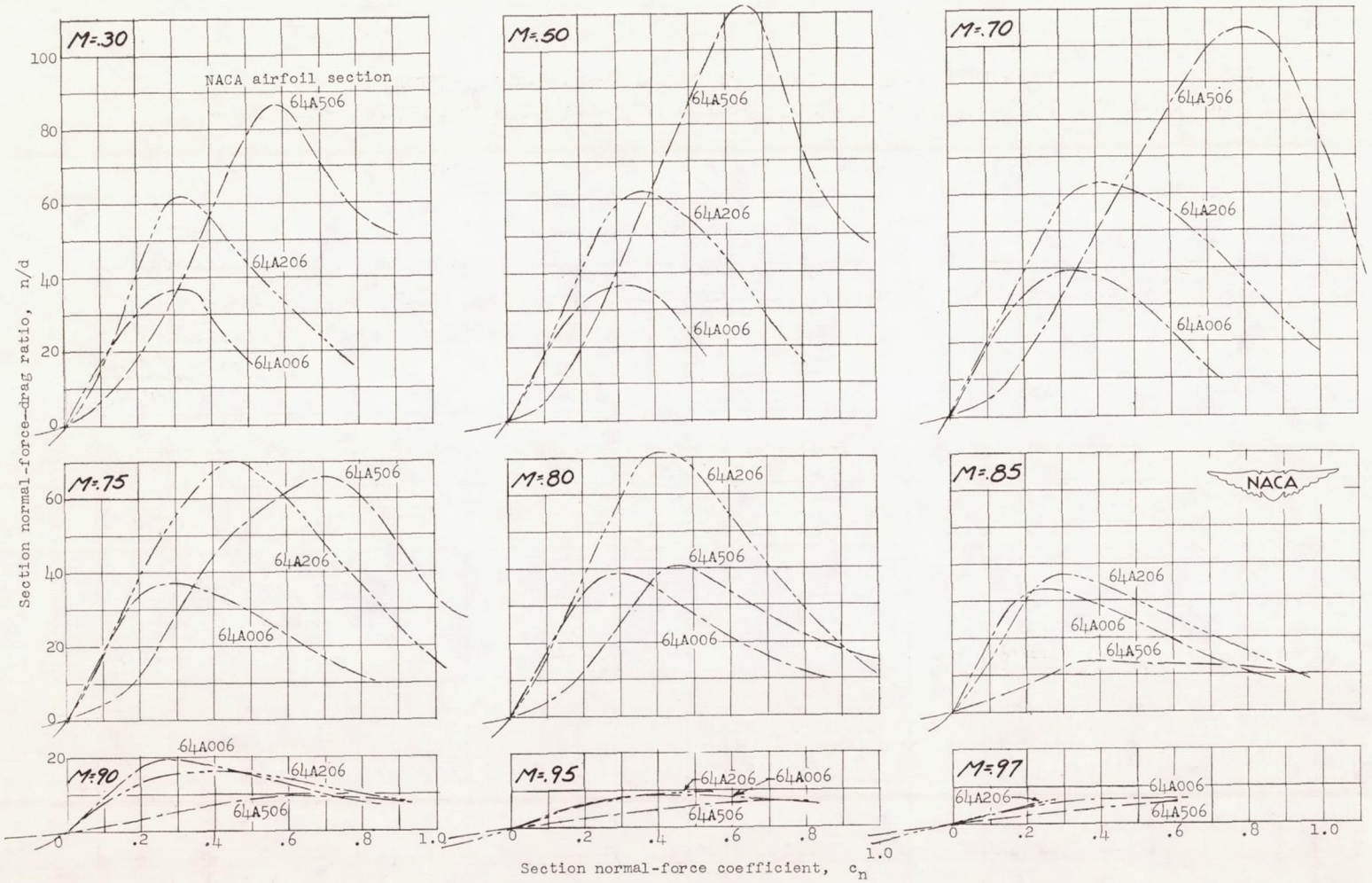

(b) Effect of change in airfoil design lift coefficient.

Figure 15.- Continued.

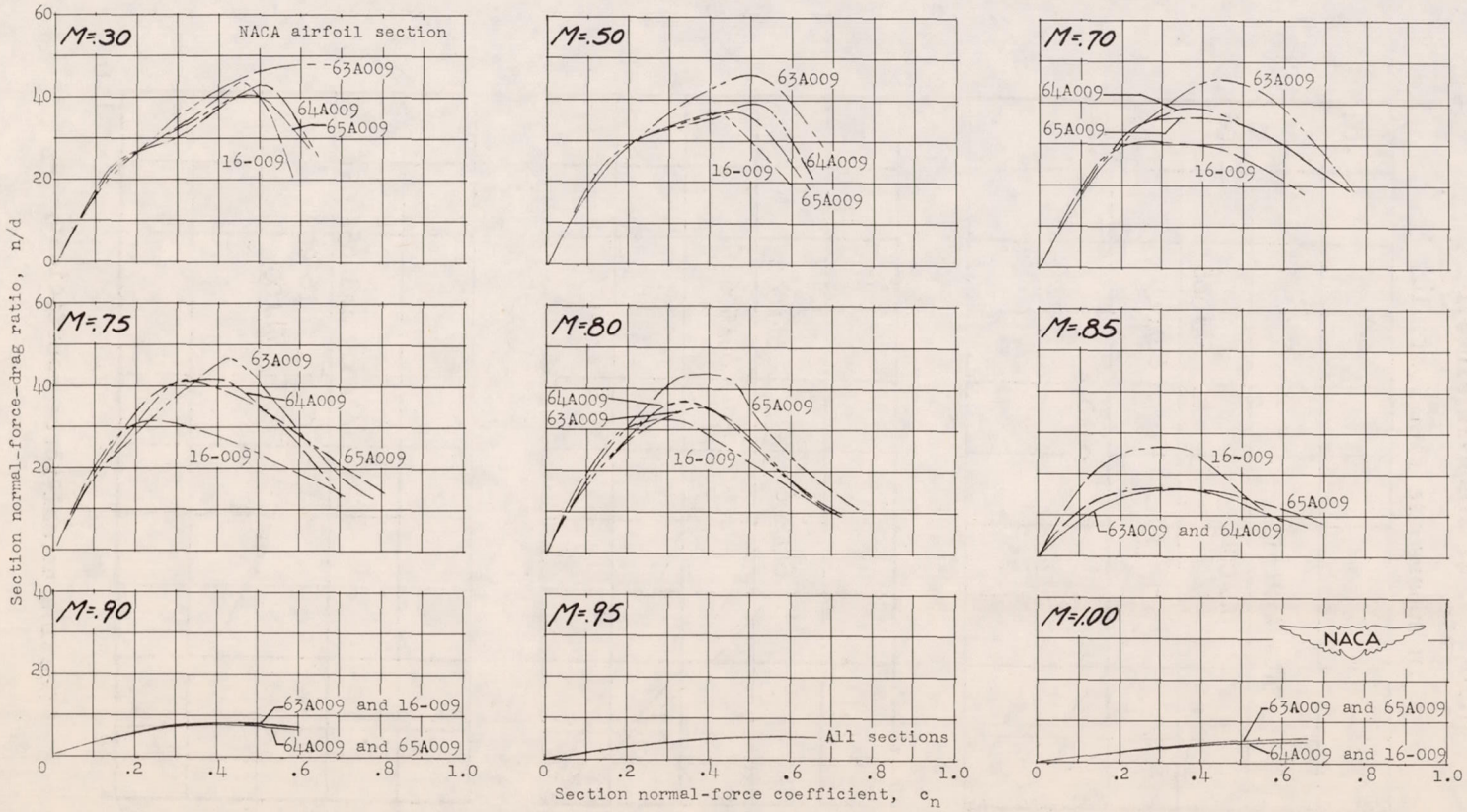

(c) Effect of change in airfoil thickness distribution.

Figure 15.- Continued.

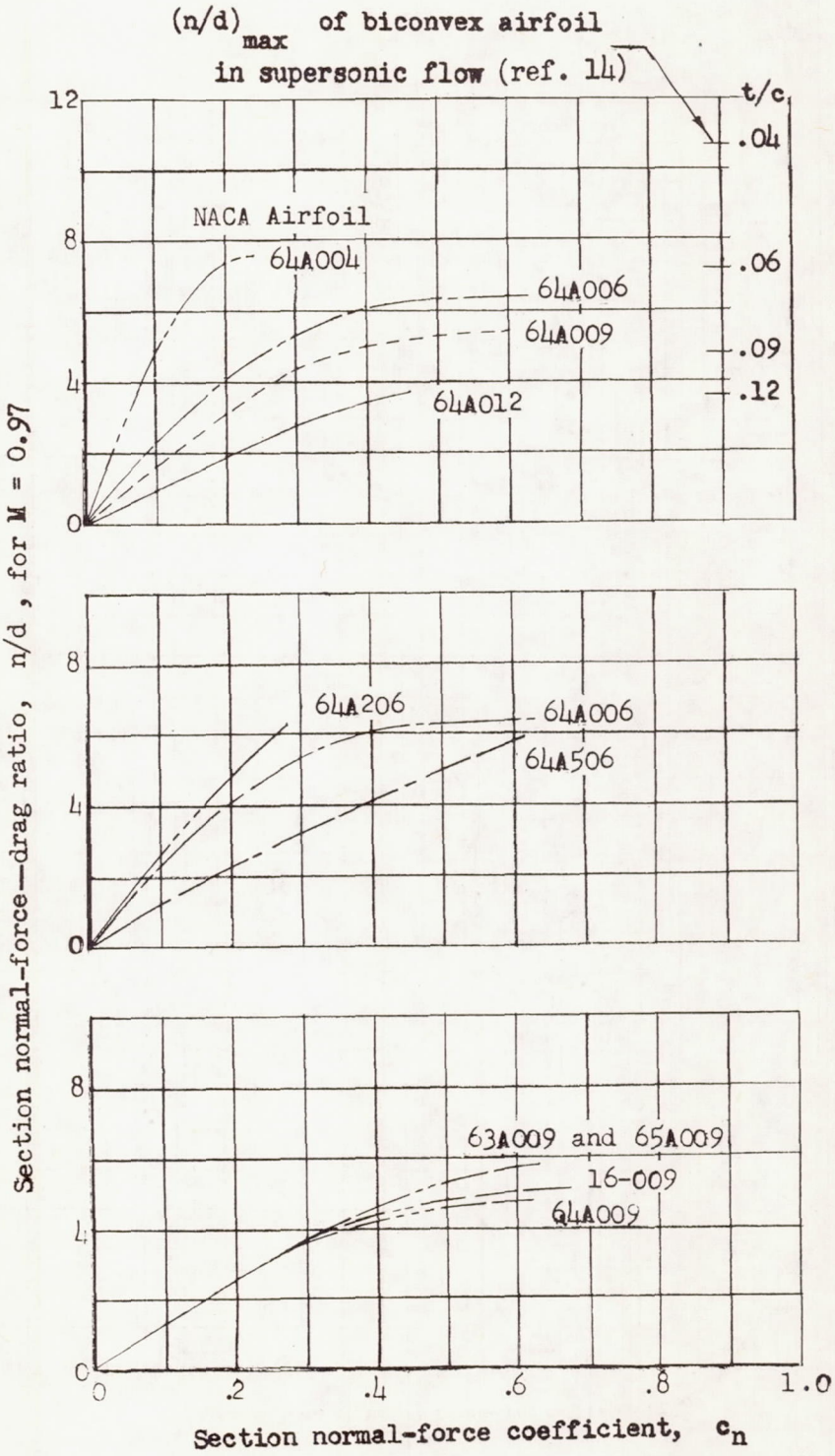

(d) Effect of profile at M = 0.97.

Figure 15.- Concluded.

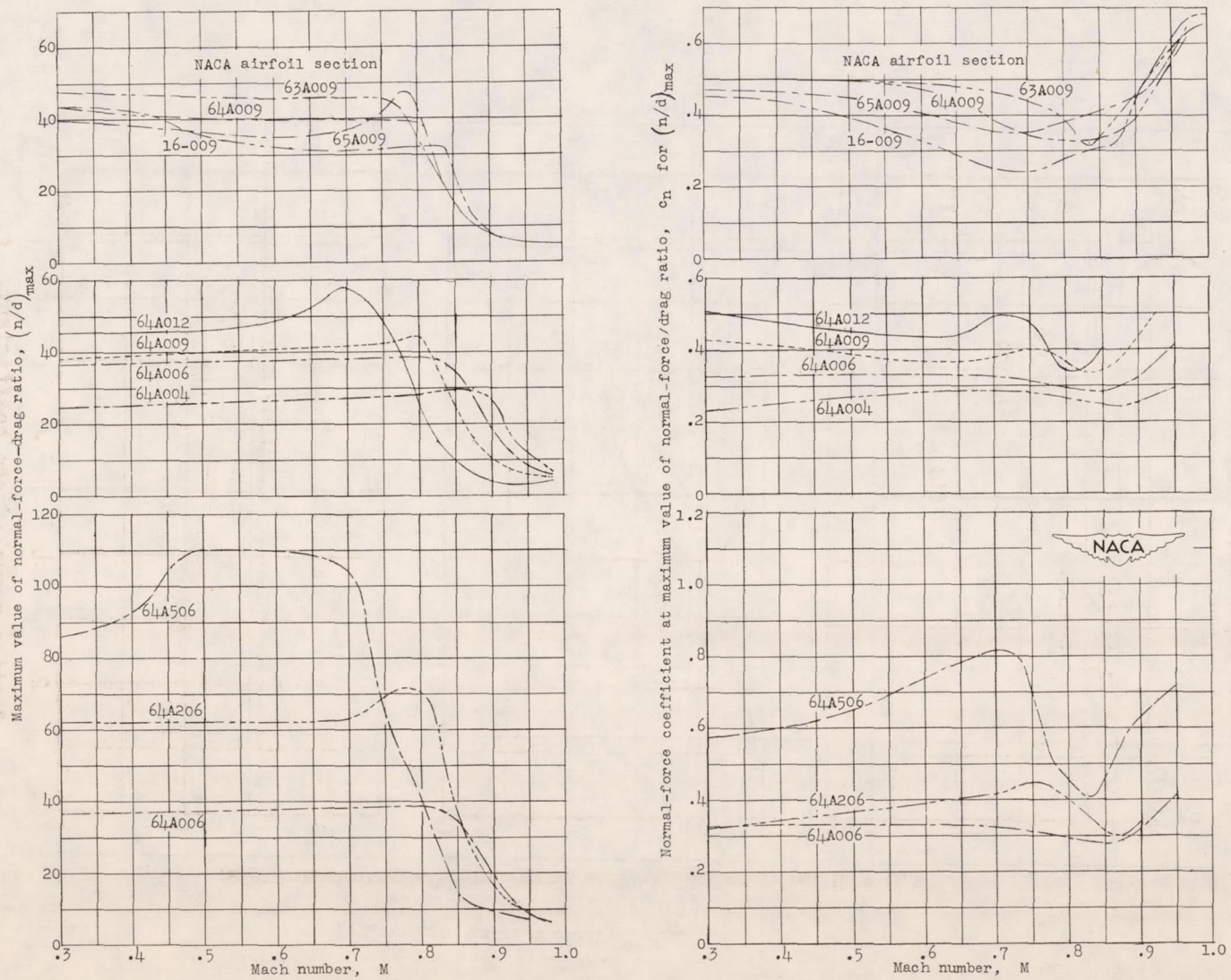

Figure 16.- Conditions pertaining to maximum normal-force—drag ratio.

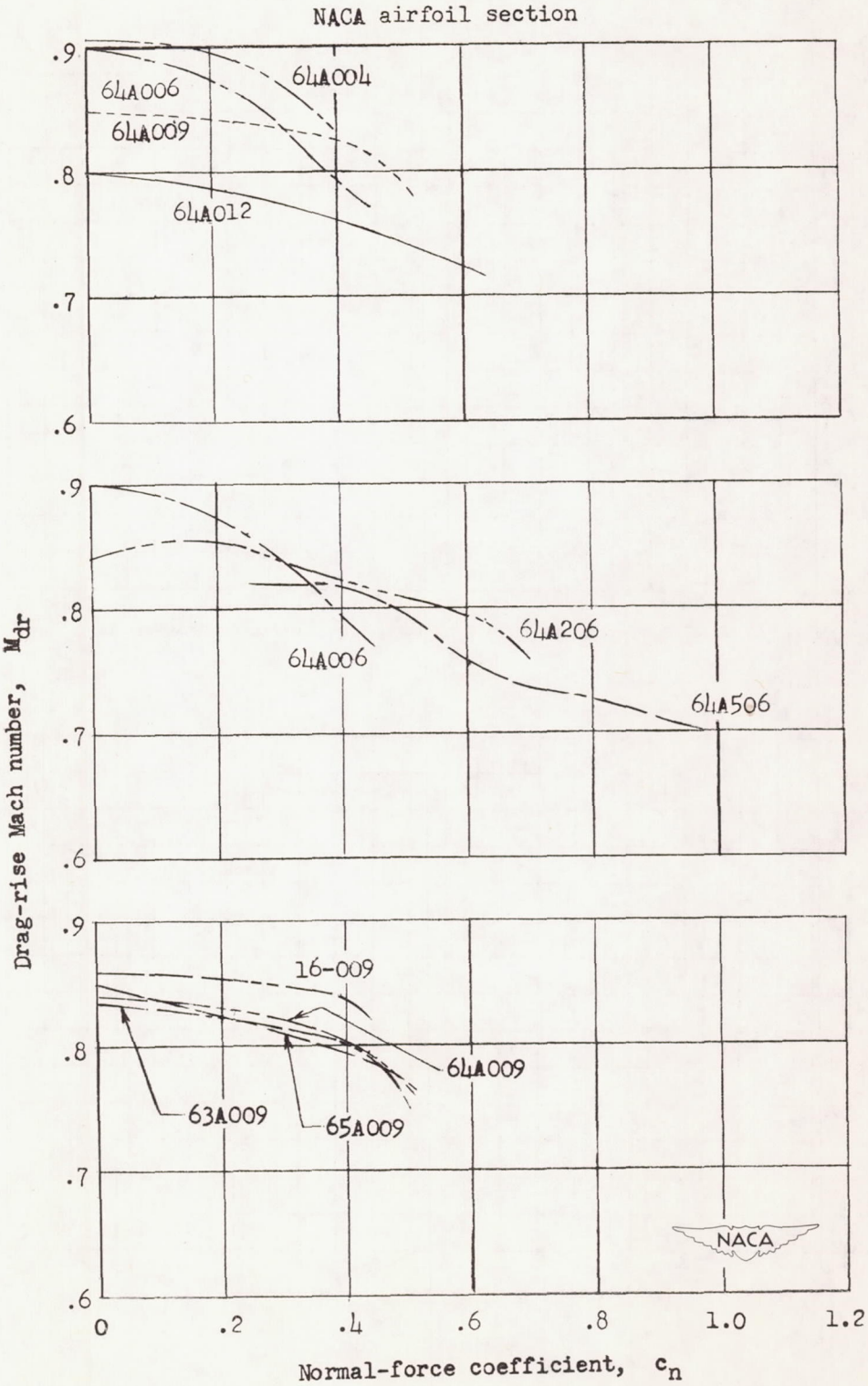

Figure 17.- The effect of airfoil profile on the variation of drag-rise Mach number with normal-force coefficient.

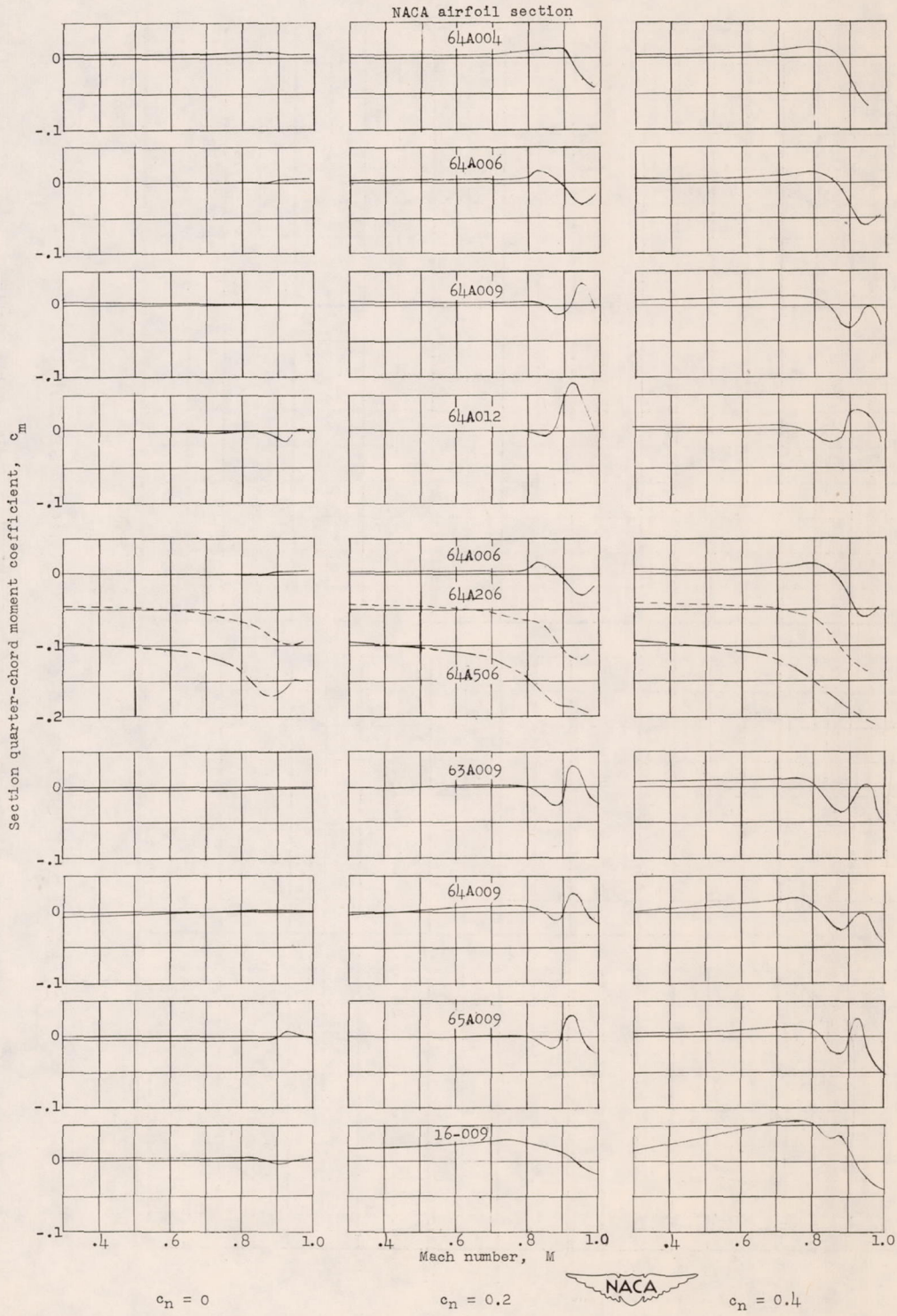

Figure 18.- The variation of section quarter-chord moment coefficient with Mach number for several normal-force coefficients for all the airfoils tested.

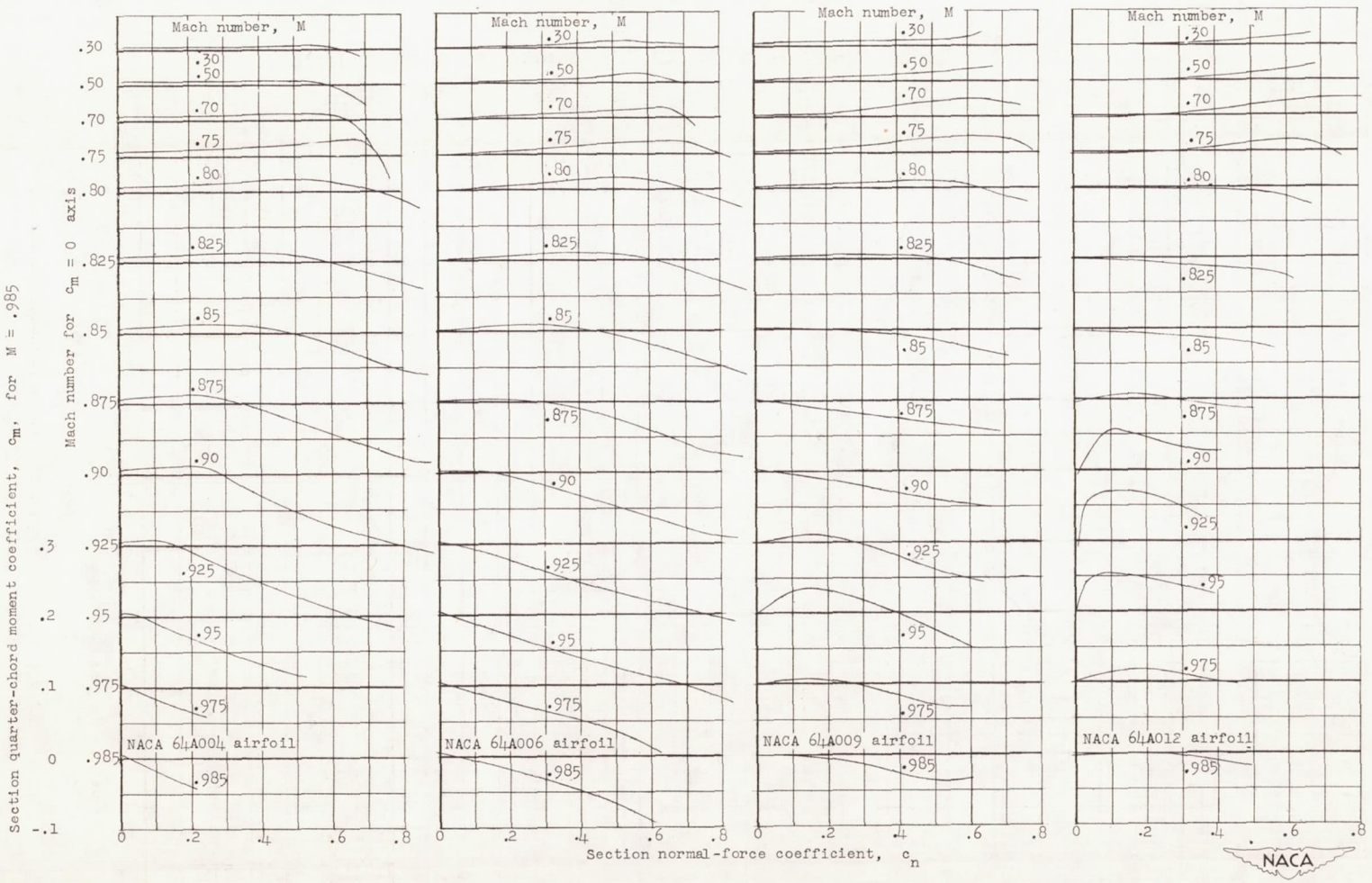

(a) Effect of change in airfoil thickness ratio.

Figure 19.- Variation of section quarter-chord moment coefficient with section normal-force coefficient at various Mach numbers.

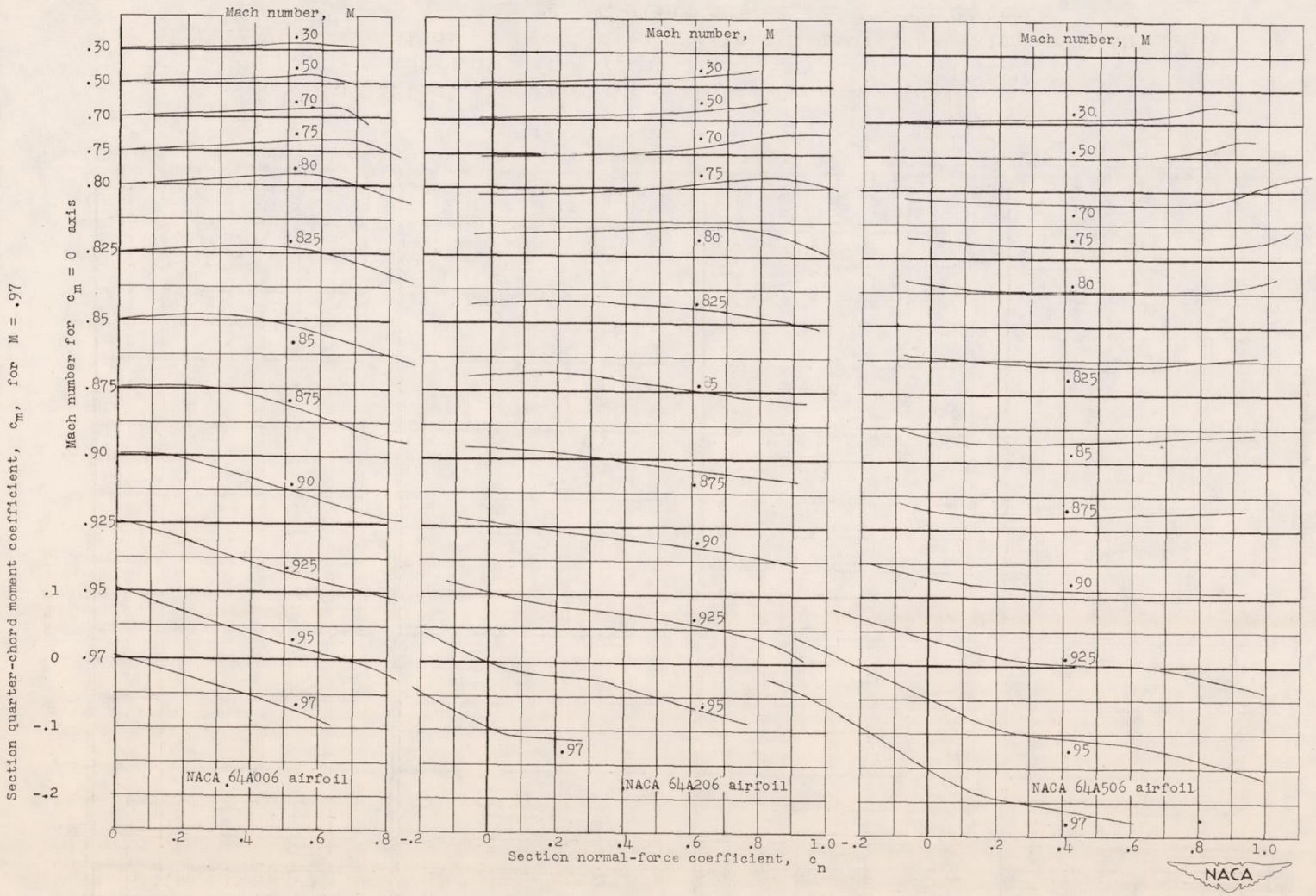

(b) Effect of change in airfoil design lift coefficient.

Figure 19.- Continued.

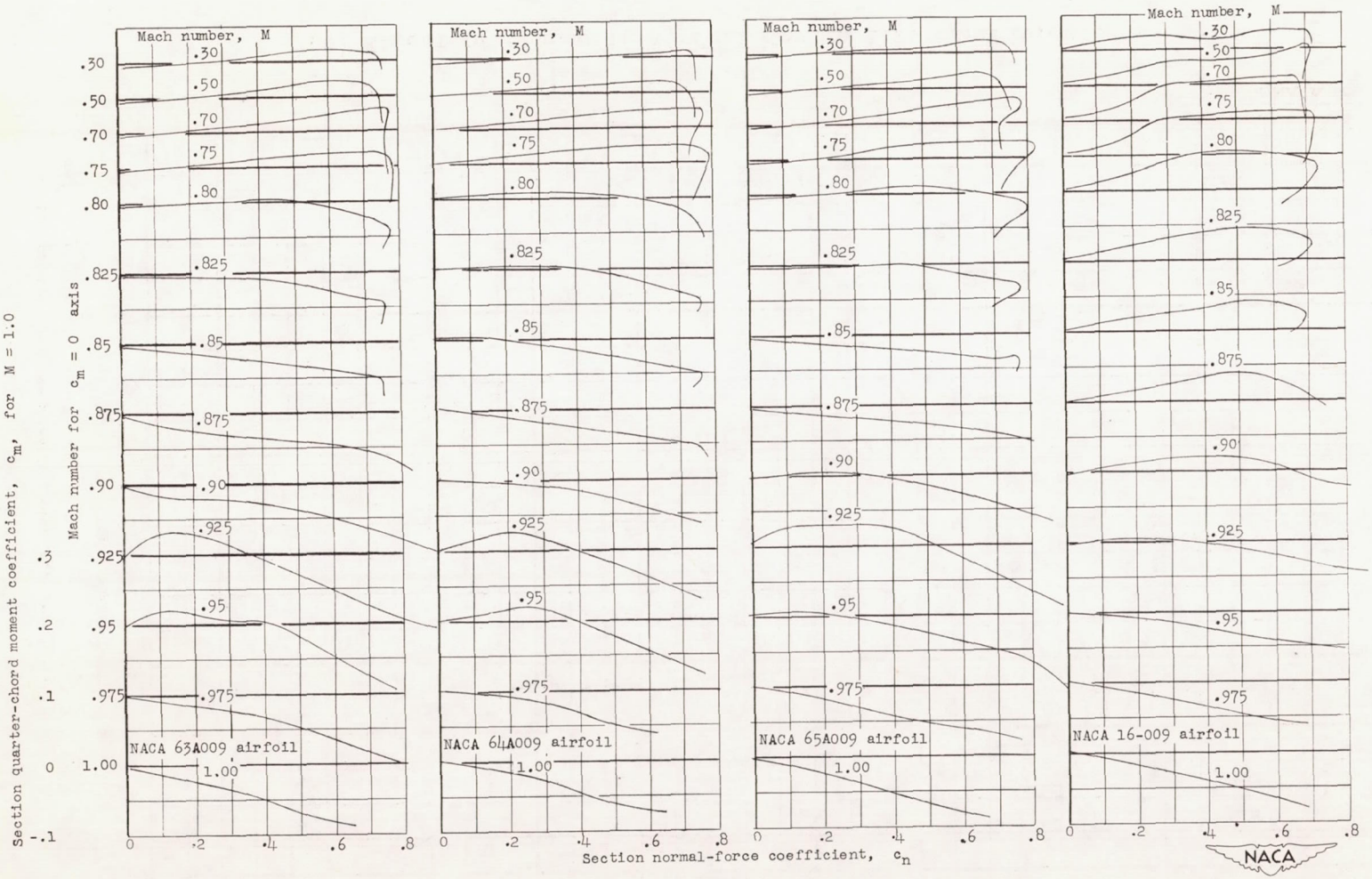

(c) Effect of change in airfoil thickness distribution.

Figure 19.- Concluded.

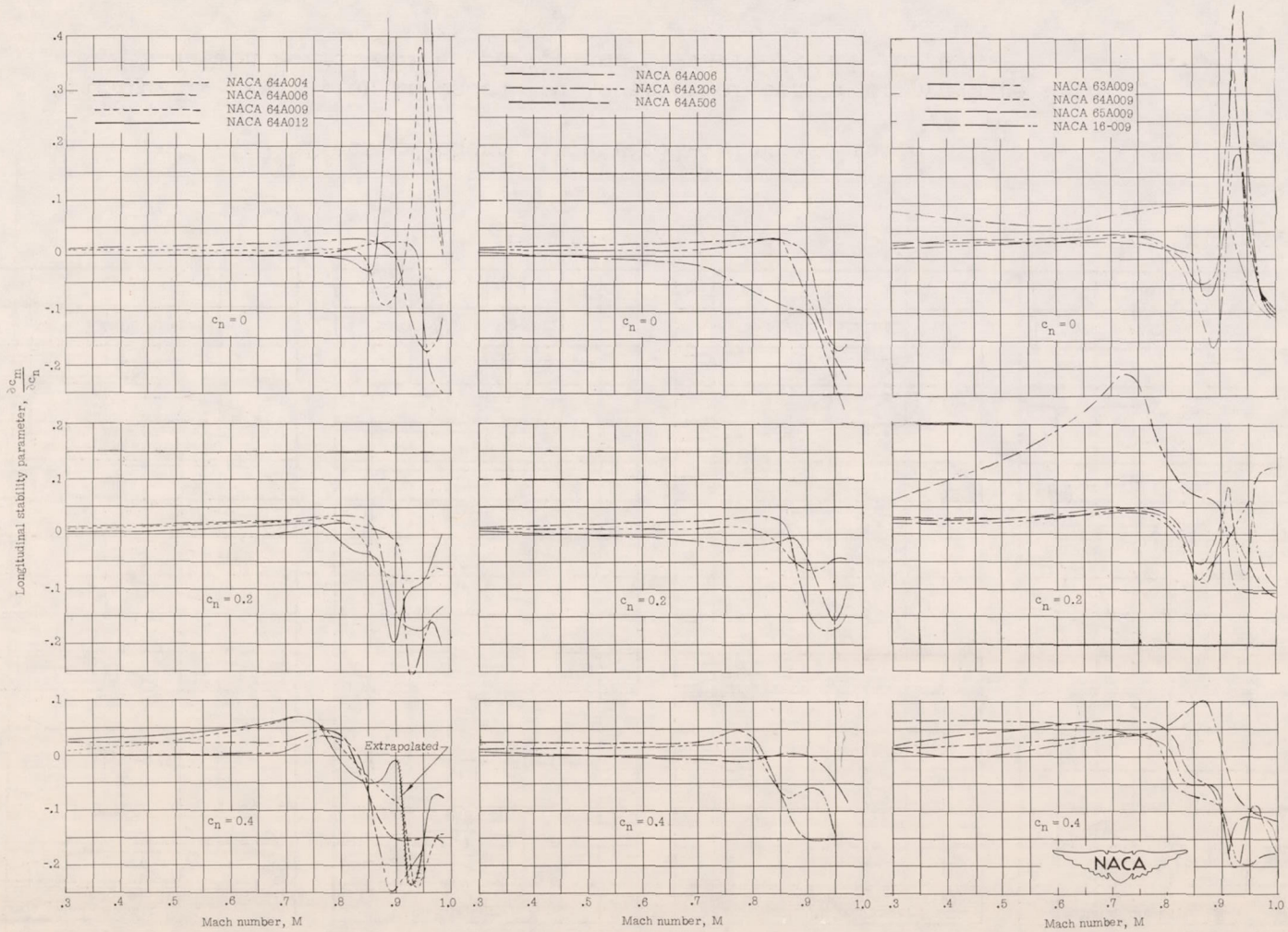

Figure 20.- Variation of a longitudinal stability parameter with Mach number for the various airfoils at several section normal-force coefficients.

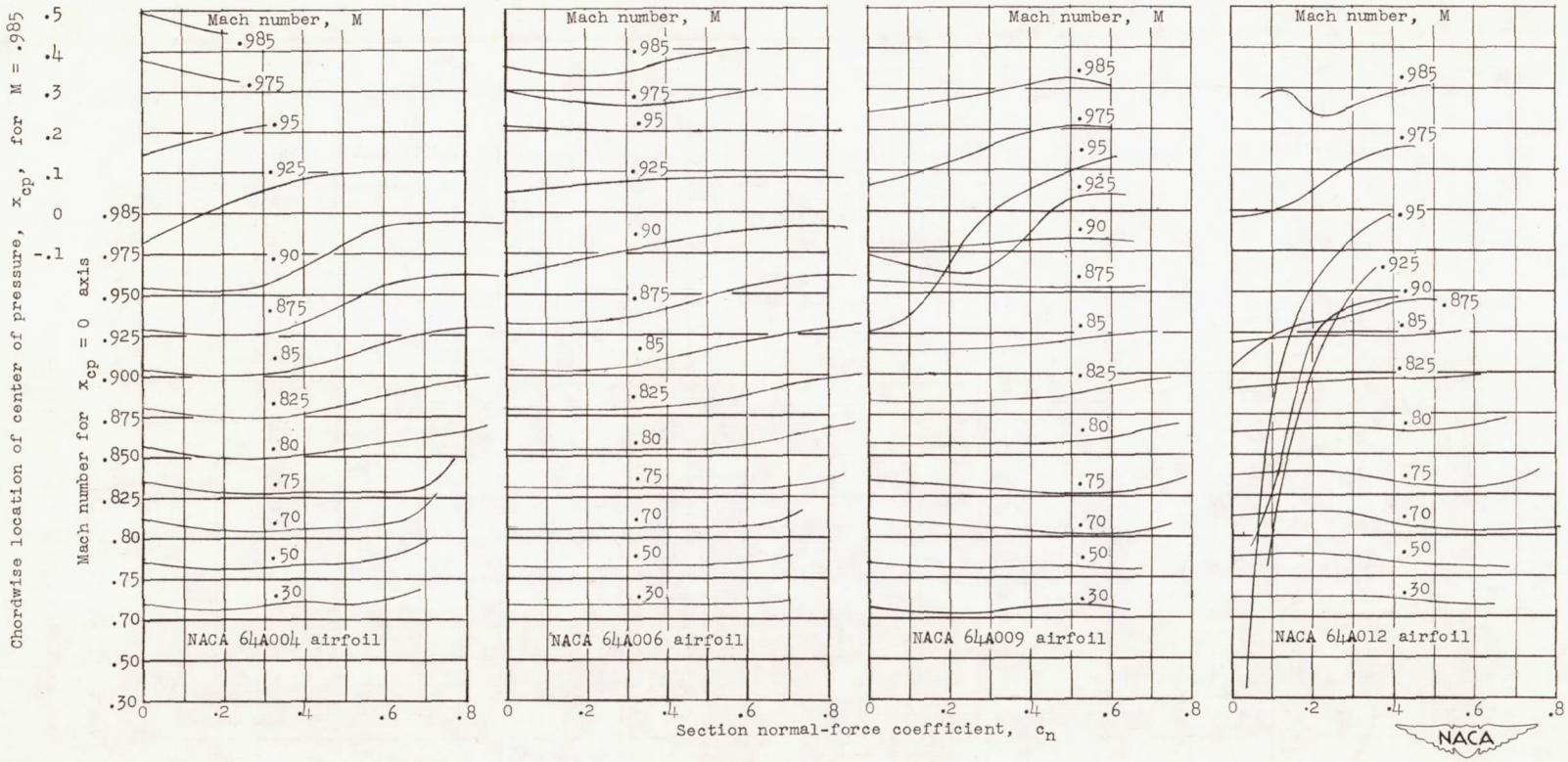

(a) Effect of change in airfoil-thickness ratio.

Figure 21.- Variation in chordwise location of center of pressure with section normal-force coefficient at various Mach numbers.

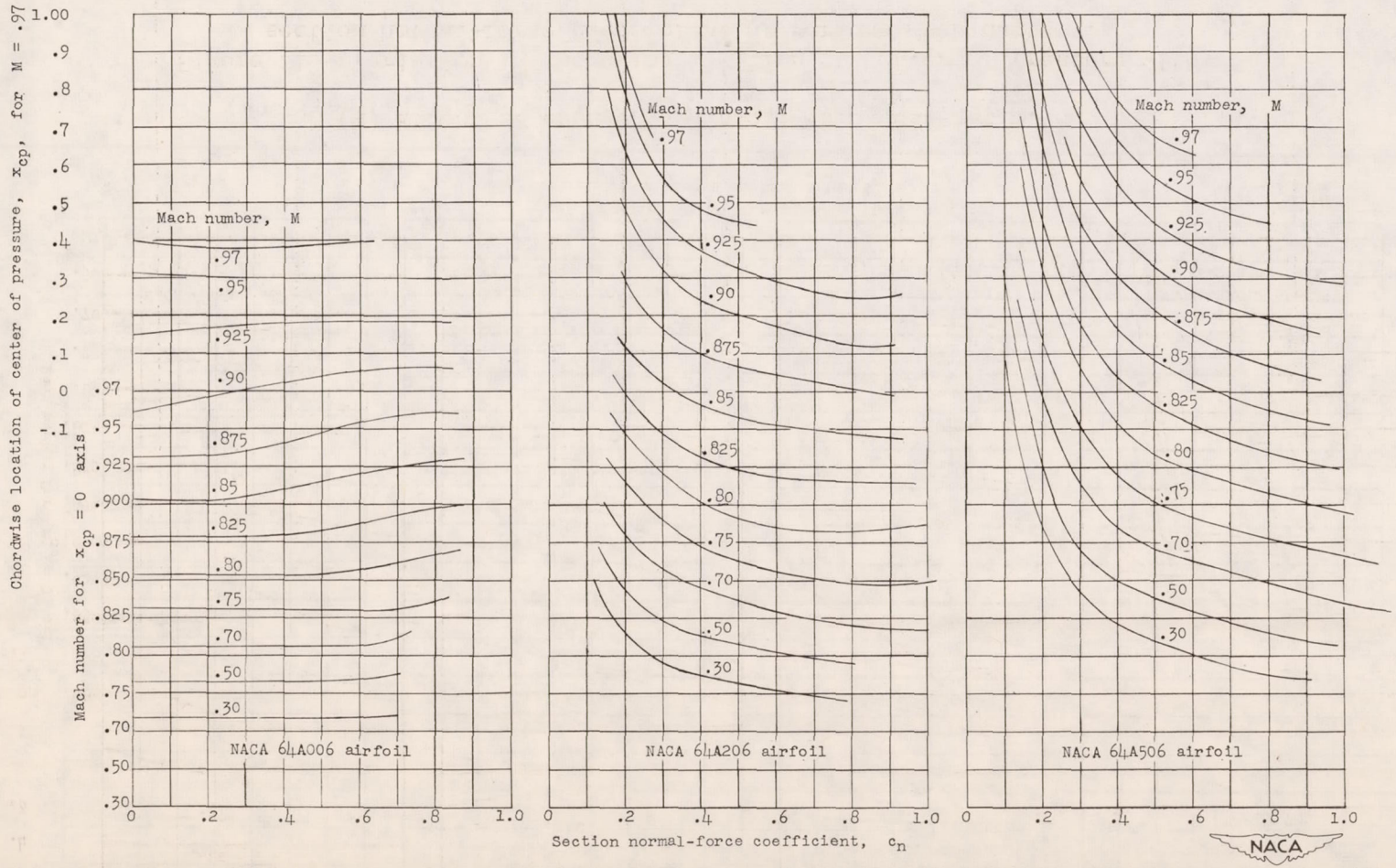

(b) Effect of change in airfoil design lift coefficient.

Figure 21.- Continued.

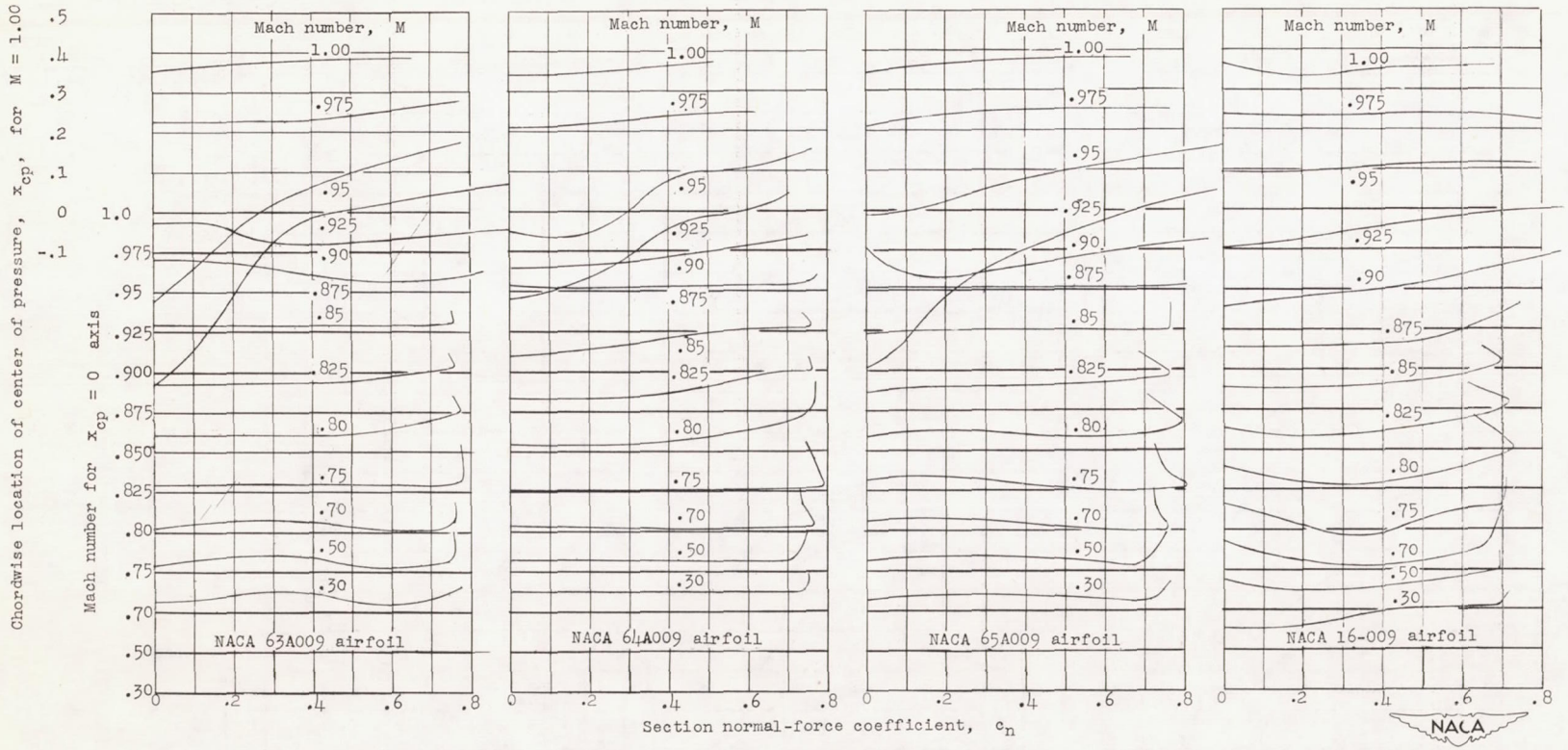

(c) Effect of change in airfoil thickness distribution.

Figure 21.- Concluded.

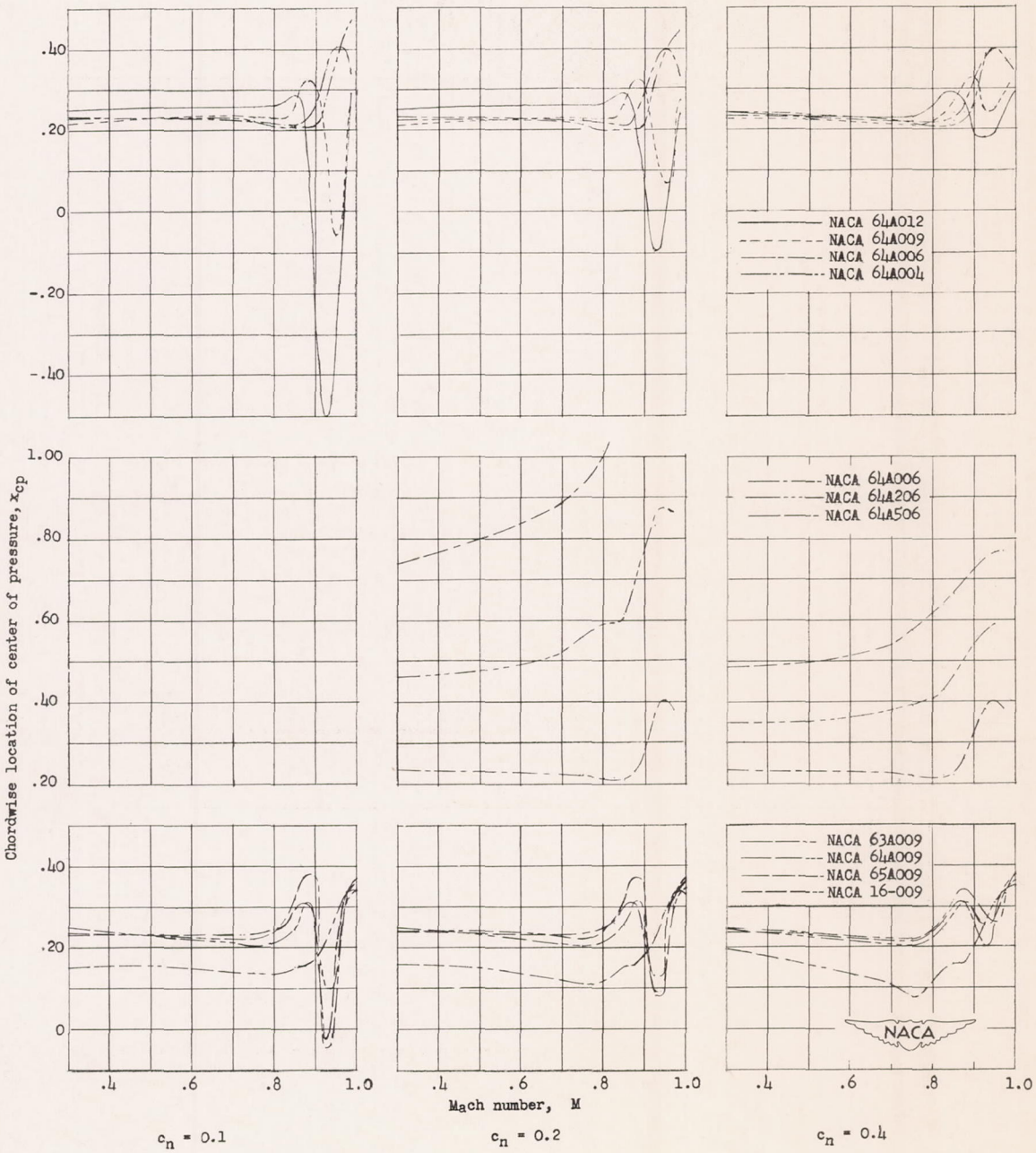

Figure 22.- The variation of chordwise location of center of pressure with Mach number for several normal-force coefficients for all the airfoils tested.

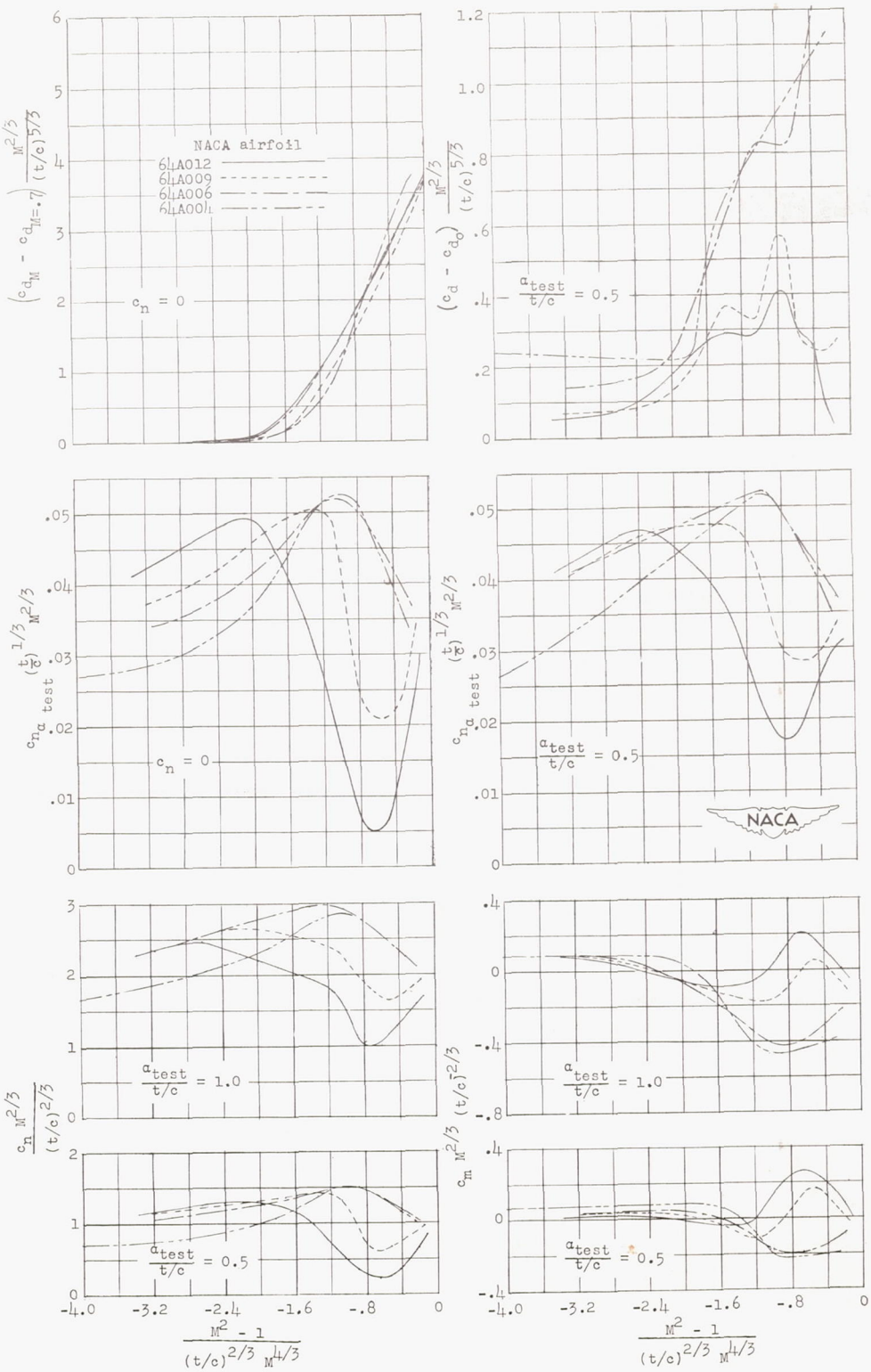

Figure 23.- Correlation of experimental data of the NACA 64AOXX airfoils using the transonic similarity law.

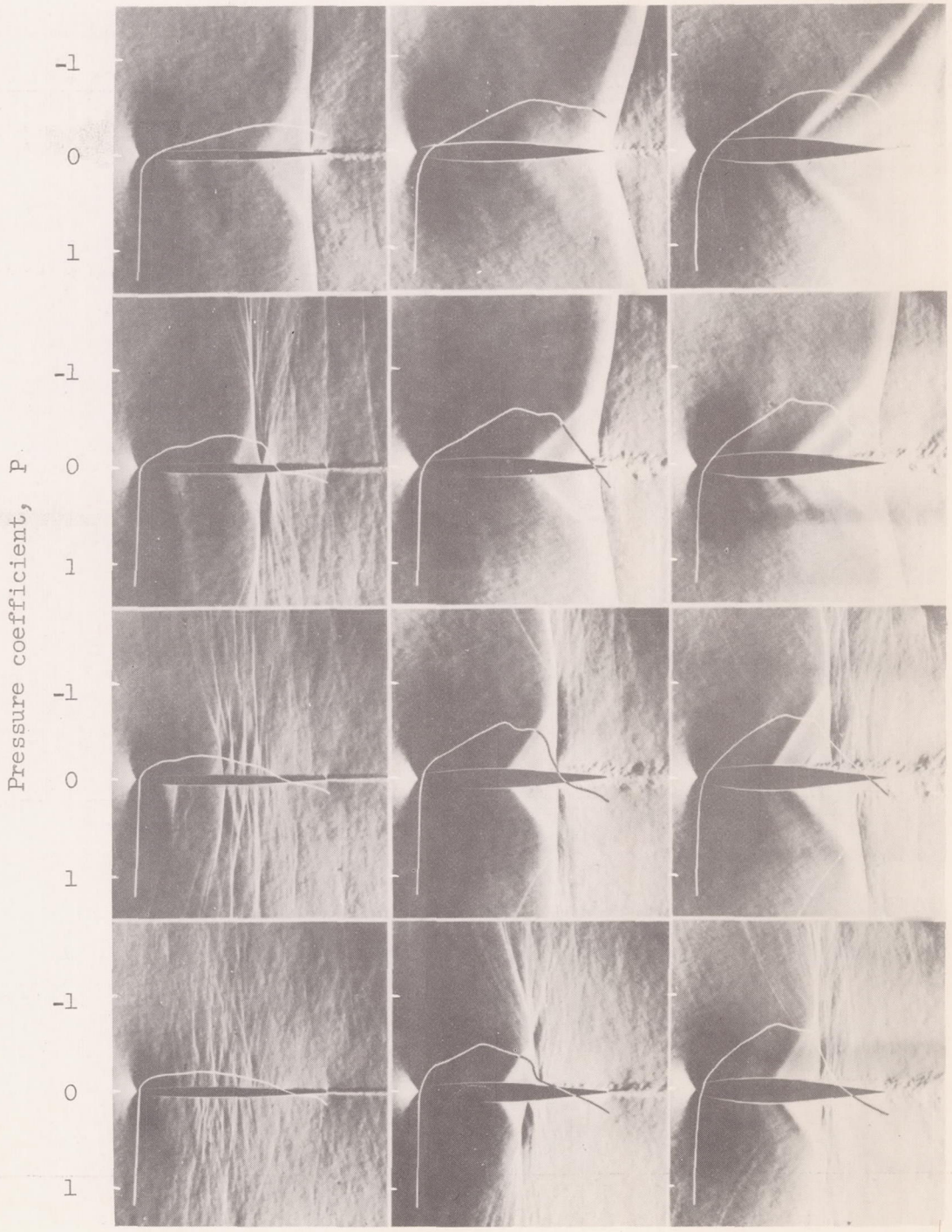

(a) $\alpha_{test} = 0^{\circ}$.

NACA
L-73042

Figure 24.- Effect of change of airfoil thickness ratio on flow.

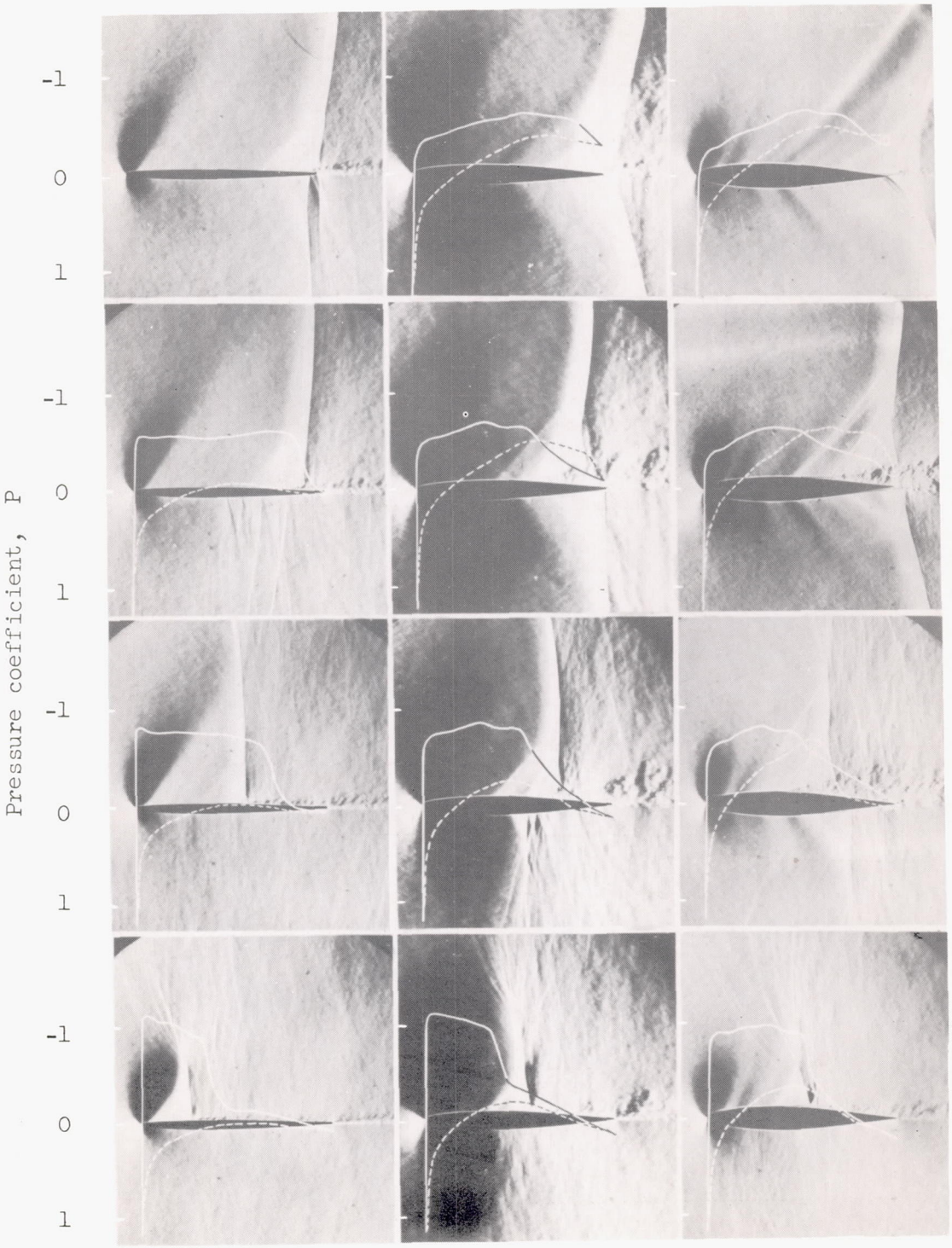

(b) $\alpha_{test} = 4^{\circ}$.

Figure 24.- Continued.

NACA
L-73041

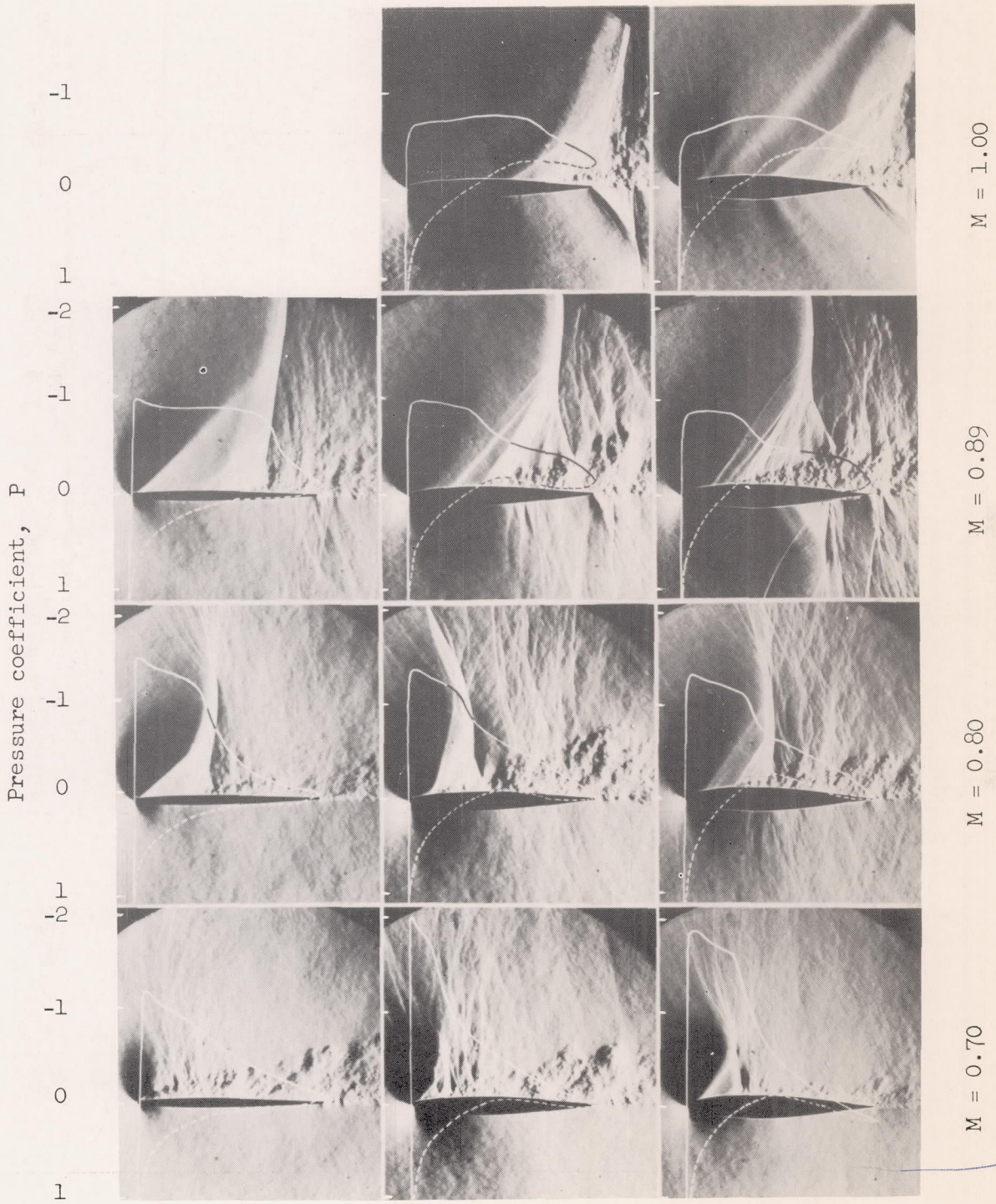

NACA 64A004 NACA 64A009 NACA 64A012

(c) $\alpha_{test} = 8^{\circ}$.

NACA
L-73046

Figure 24.- Concluded.

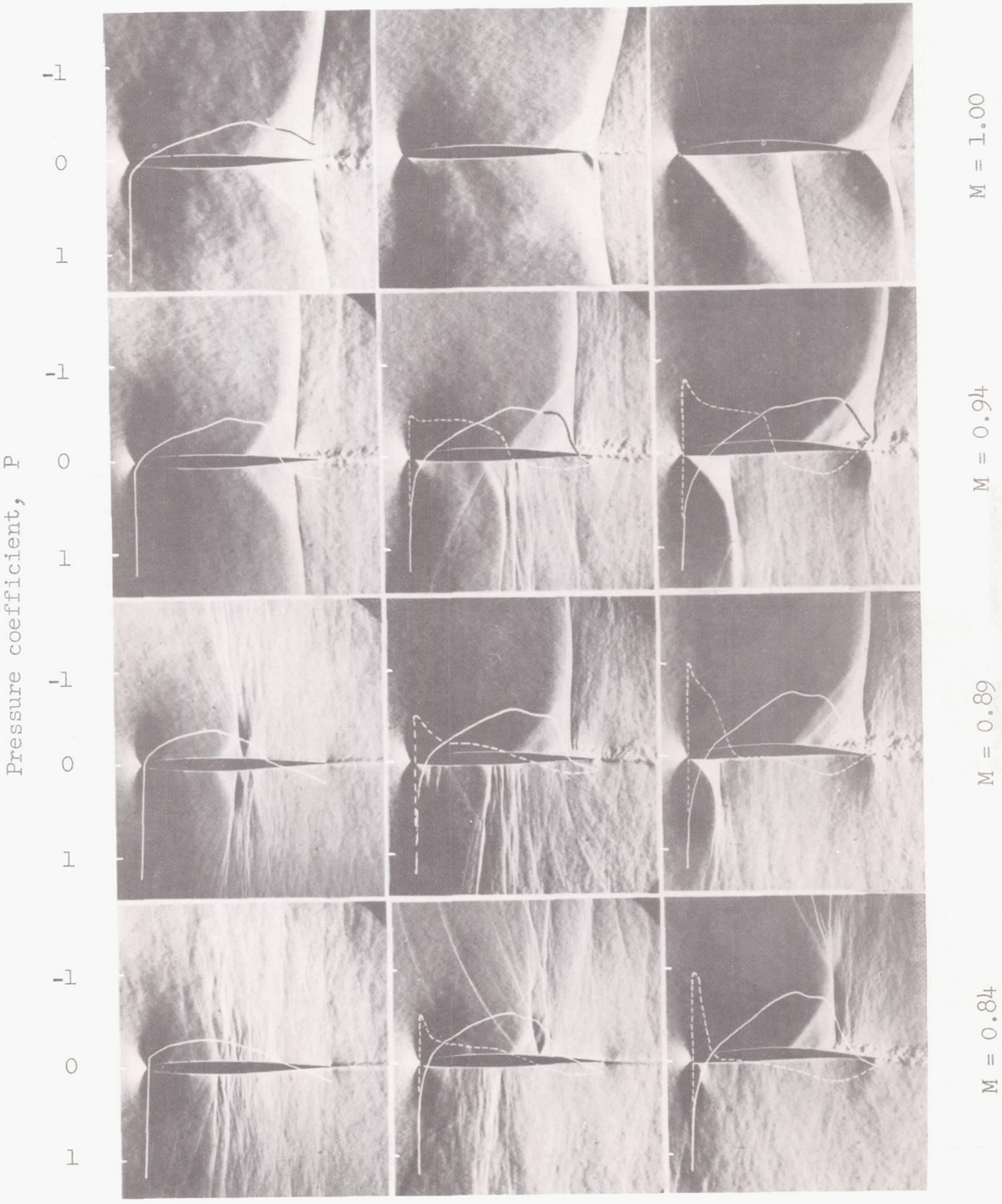

(a) $\alpha_{test} = 0^{\circ}$.

NACA L-73049

Figure 25.- Effect of change of airfoil design lift coefficient on flow.

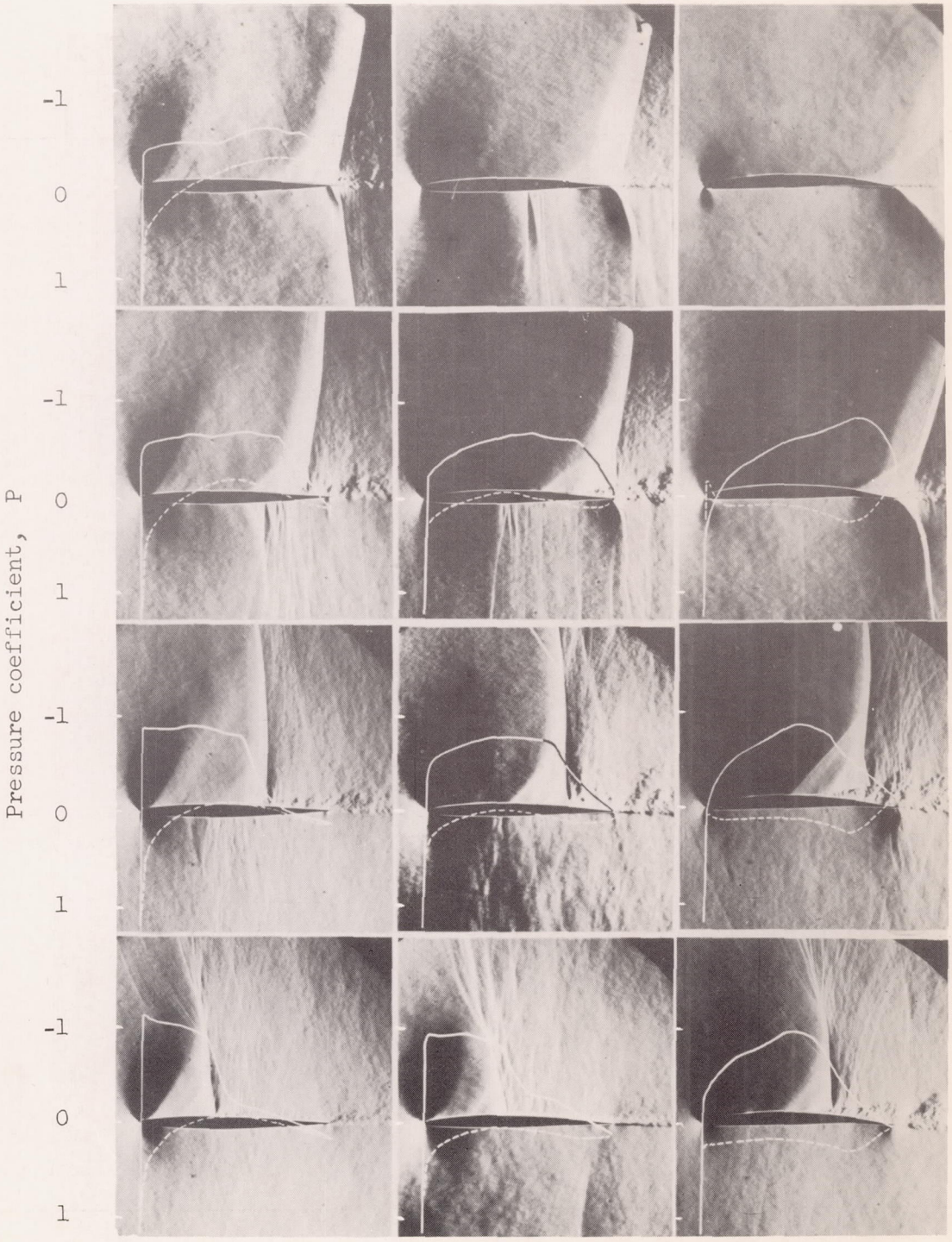

NACA 64A006 NACA 64A206 NACA 64A506

(b) $\alpha_{test} = 4^{\circ}$.

L-73045

Figure 25.- Continued.

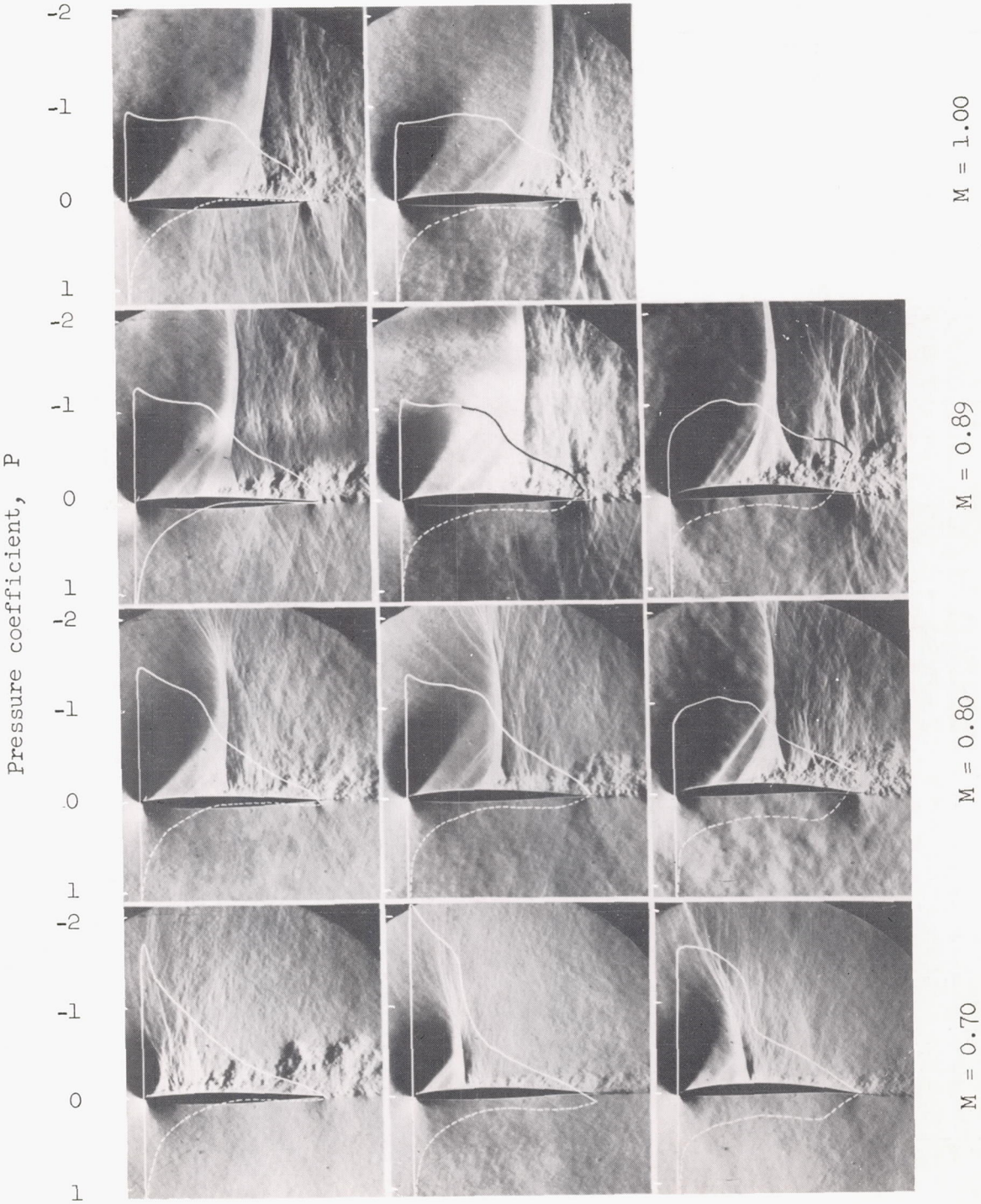

(c) $\alpha_{test} = 8^{\circ}$.

NACA L-73044

Figure 25.- Concluded.

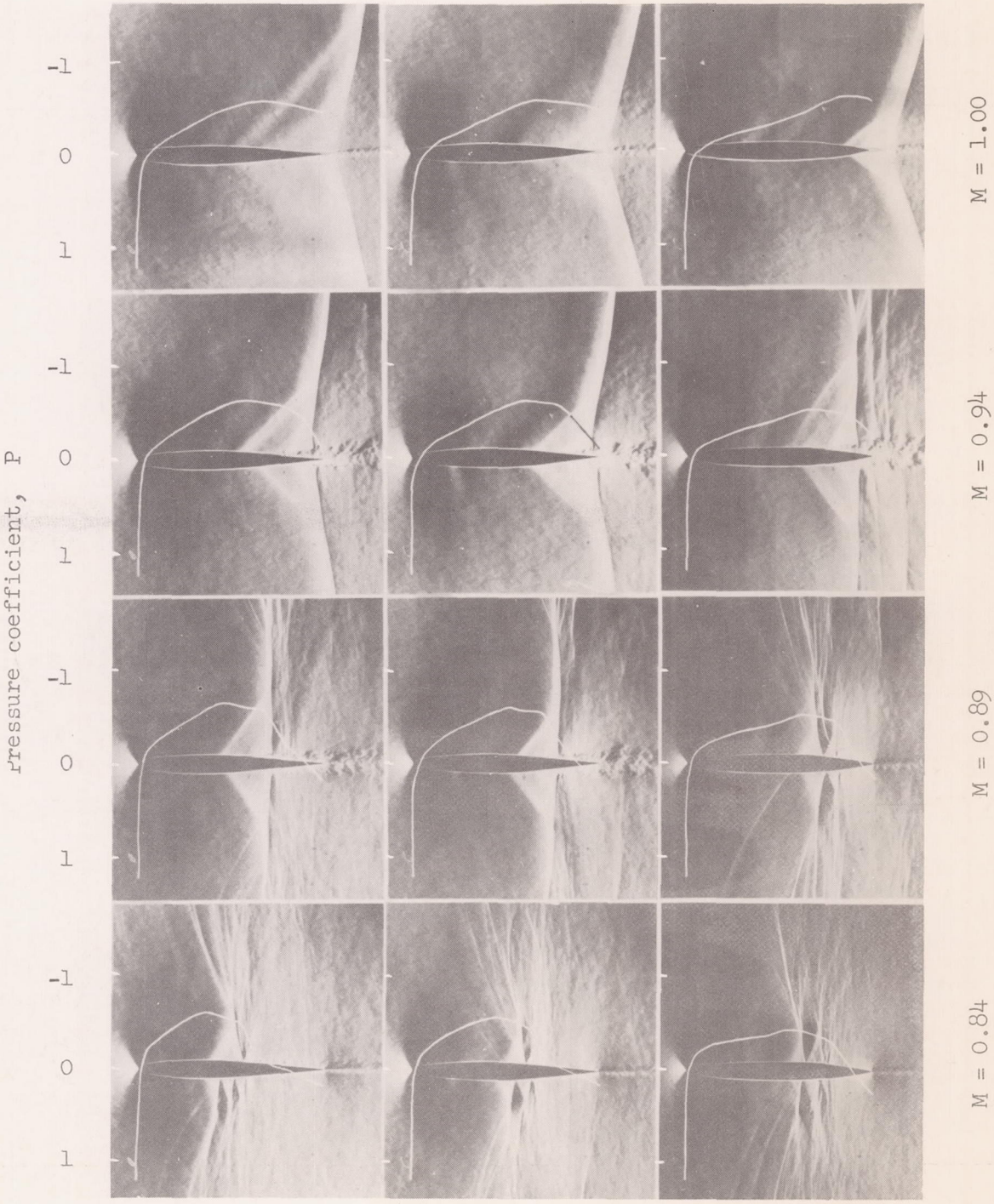

NACA 63A009 NACA 65A009 NACA 16-009

(a) $\alpha_{test} = 0^{\circ}$.

NACA
L-73047

Figure 26.- Effect of change of airfoil thickness distribution on flow.

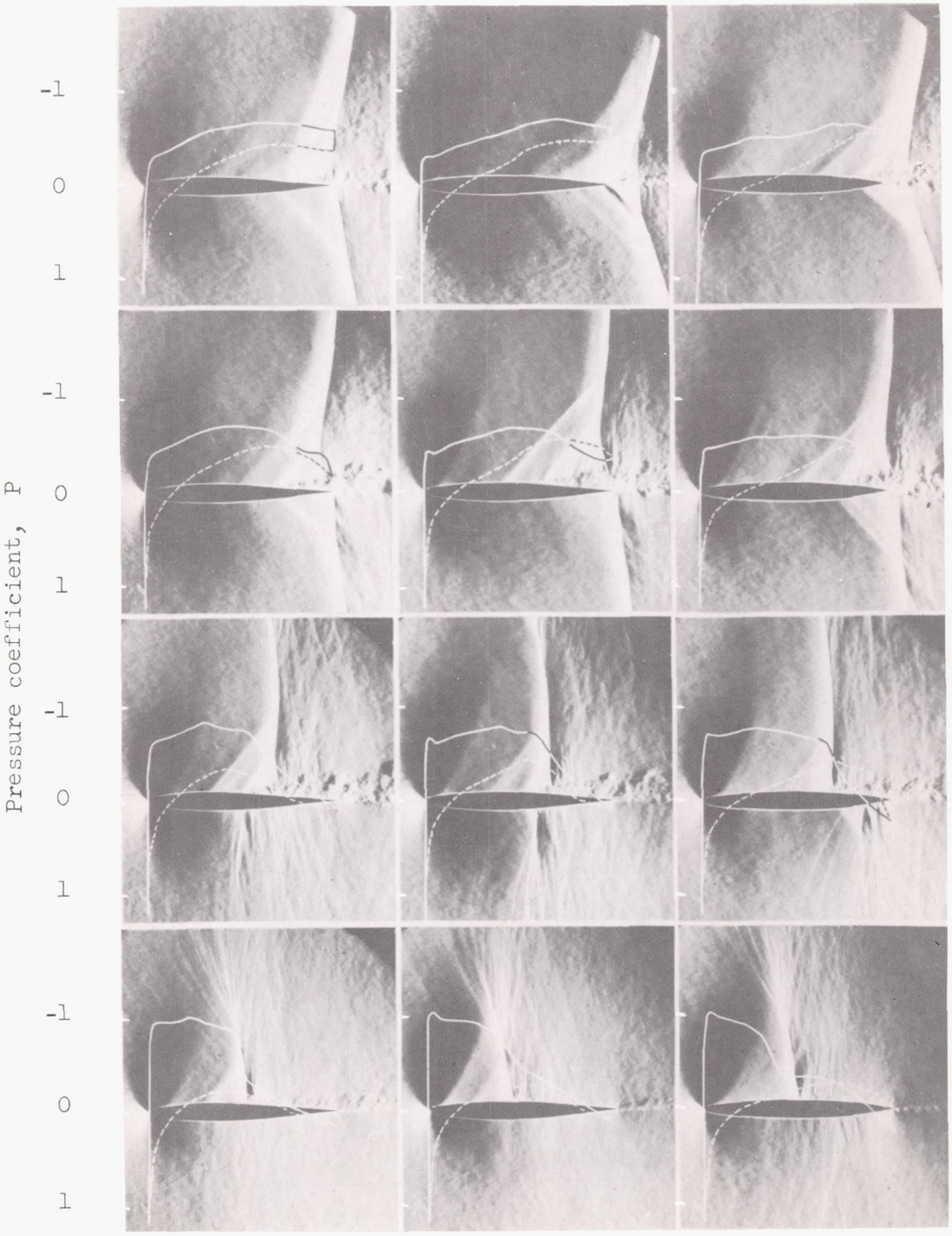

NACA 63A009 NACA 65A009 NACA 16-009

(b) $\alpha_{test} = 4^{\circ}$.

Figure 26.- Continued.

NACA
L-73043

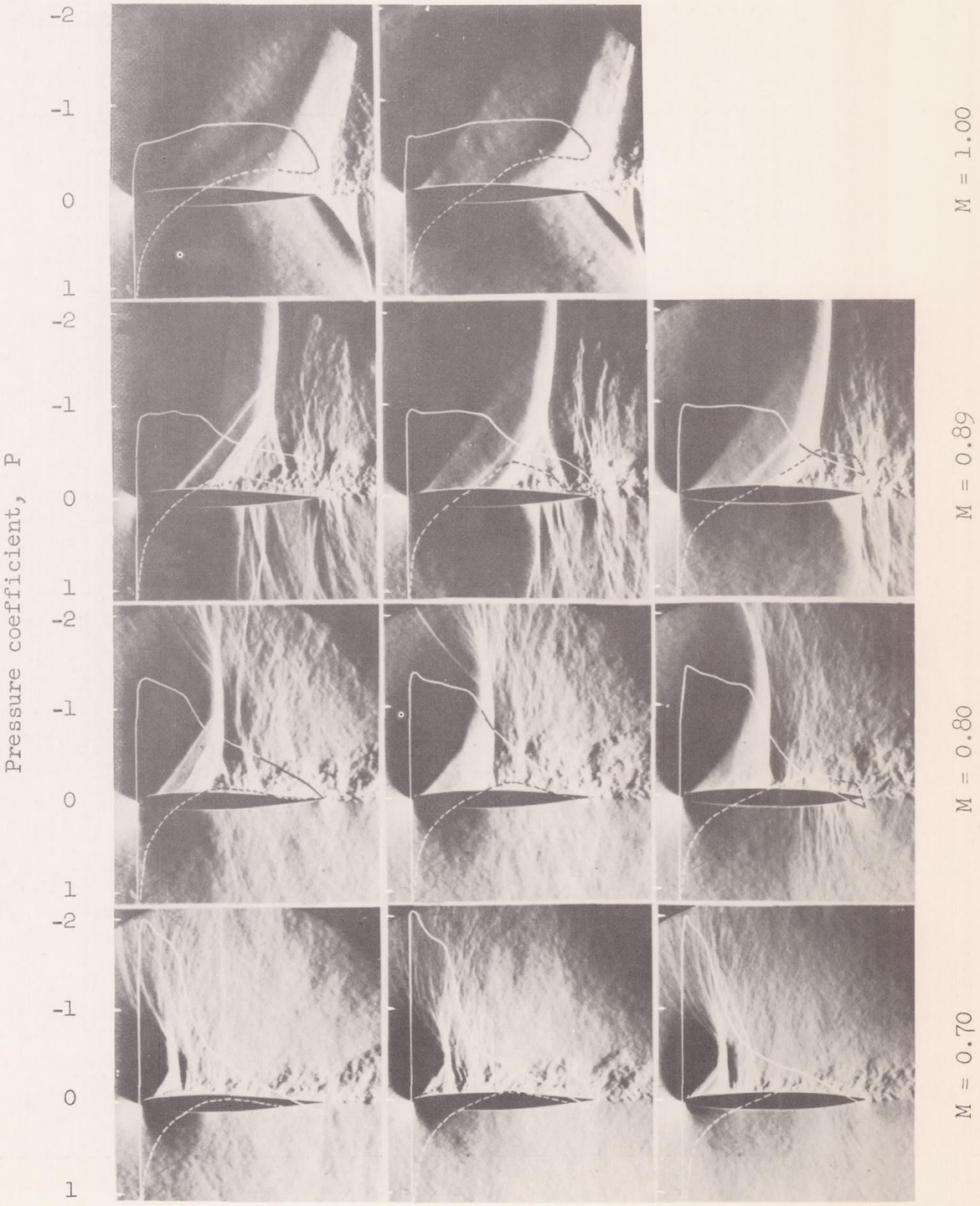

(c) $\alpha_{test} = 8^{\circ}$.

L-73048

Figure 26.- Concluded.